POLITECNICO DI TORINO

MASTER's Degree in Biomedical Engineering

MASTER's Degree Thesis

Single-channel Read-out Device for Extracellular Signal Detection of Neuronal Cell Cultures

Supervisors

Prof. Danilo DEMARCHI

Dr.Eng. Alessandro SANGINARIO

Prof. Valentina CARABELLI

Candidate

Chiara LEMMA

Academic year 2020-2021

Summary

In vitro electroanalytical experiments through multi-electrode arrays (MEAs) are applied to observe the extracellular behaviour of excitable cells and screen the effect of specific chemical modulators and drug injections. MEAs are usually interfaced with an electronic interface consisting of a preamplification stage and a filtering one. In this project, a preamplification stage on a printed circuit board is designed for amplifying a single-channel of the available 16 electrodes of a Micro-Graphitic Single Crystal Diamond Multi-Electrode Array (μG-SCD MEA) chip, realized by the University of Torino. Thus, this read-out device provides essential tools for a future device blending and optimizing the single channel's preamplifier to all the μG-SCD MEA's available electrodes. Specifically, the μG-SCD MEA's system devotes to investigating the extracellular signals from mice's midbrain neurons through two electroanalytical recordings: amperometry and potentiometry. Single-cell amperometry allows the detection of quantal fusion events, while potentiometric measurements, the spontaneous electrical activity. Moreover, specific monophasic or biphasic stimulation patterns can be sent through a NI DAQ to the cell culture, triggering the neurons' activity. To select the experimental configuration (recording and stimulation), post-process, visualize and save the recorded data, a LabVIEW interface is implemented. Overall, in addition to the preamplifier, an active filtering stage for the single-channel and noise analysis of the electronic system are introduced to find the system's critical issues. The simulation's results performed with the MEA's electrodes submerged in a physiological solution demonstrated that the noise bandwidth has to be improved, particularly in the amperometric configuration. In contrast, it should fit in the potentiometric one. However, the device's performances have still to be adequately tested on neuronal cell cultures: just an amperometric application on cell lines (PC12) was performed. Once the main expedients showed in this work are extended to all the available electrodes, the researchers could use the read-out device to screen the midbrain cells' activity, applying both electroanalytical measurements approximately simultaneously from any μG-SCD MEA's electrode.

Acknowledgements

"I would like first to express my deep gratitude to my thesis advisor, Dr. Eng. Alessandro Sanginario. He always supported me and gave me the right guidance in this project. I would sincerely like to highlight the meaningful role of Prof. Danilo Demarchi, whose classes and topics have always fascinated me.
Moreover, I must express my very profound gratitude to my parents and grandparents for providing me with unfailing support throughout my years of study. Finally, to my friends for their continuous encouragement and for the beautiful memories we shared. This accomplishment would not have been possible without all of them."

Chiara

Table of Contents

List of Tables

List of Figures

Chapter 1

Introduction

The health system is currently showing the necessity to support a population increasing ceaselessly, thus requiring more bioengineering applications and devices to optimize and accelerate the diagnoses, drug screening and treatment of pathologies. One of the essential tools used for this purpose is based on the research of cellular biochemical parameters through Micro-Electro-Mechanical Systems (MEMS) technology. The primary information used to support this research is obtained by analyzing the extracellular recordings of excitable cultured cells. These signals usually contain electroanalytical information such as current, potential, conductivity and impedance. The most common electroanalytical methods involve potentiometry, the study of the spontaneous electrical activity of the cultured cells, and amperometry, the analysis of the small currents released by evoked quantal fusion events.
A typical application of MEMS for *in vitro* extracellular recordings can be represented by the use of multielectrode arrays (MEA), cell culture dishes with embedded surface microelectrodes [1]. MEAs are distinguished for their ability to collect a medium-high throughput of parameters and high performances through less expensive and miniaturized setups [2]. Despite these advantages, it is fundamental to consider that MEAs can not collect small extracellular signals without an external multi-channel preamplification stage.
For this purpose, this work describes the proper steps for designing a preamplification read-out device to be interfaced with one single electrode of a MEA.
Specifically, the single-channel read-out device is interfaced with a 4×4 Micro-Graphitic Single Crystal Diamond Multi-Electrode Array (μG-SCD MEA) realized by the University of Torino. Consequently, the designed device represents only the first crucial step to implement a complete future device extended to all the available electrodes.
The μG-SCD MEA can be implemented for various types of cells and tissue cultures

such as central and peripheral neurons, muscle cells, retinas, in slices, or dissociated cell cultures. However, this study focuses on primary dopaminergic neuronal cell cultures. Specifically, the μG-SCD MEA possesses high-time resolution and sensitivity for the detection of the quantal exocytosis of neuronal synaptic vesicles as well as spontaneous neuronal firing activity [3]. For this purpose, the realized printed circuit board contains two customized circuits on the same preamplifier. The first can be used for amperometric measurements (exocytosis activity), the other for potentiometric ones (spontaneous activity).
For these kinds of measurements, a LabVIEW interface is implemented to set the specific electroanalytical configuration on the electrode (amperometry or potentiometry), record the signals, and send proper monophasic or biphasic stimulation patterns to the cell culture. In contrast to most commercial devices, which implement just a single electroanalytical method, the designed device aims to interchange the electrode configuration quite simultaneously in the same experimental setup.
Therefore, this work tried to fulfill these requests and give the main tools for the future design of a complete preamplification stage extended to all the available electrodes of the μG-SCD MEA. Through this future perspective, it will be possible to obtain various information from different sites of the cell culture.
The following work starts from the chapter "Background". This first chapter reports the basic notions concerning the electroanalytical methods and the electrophysiology of neuronal signals. The "Commercial MEA system" chapter describes the main functionalities of the standard device used by the University of Torino. This description leads to the main functionalities that the designed device and the software interface have to perform. The following chapter, "μG-SCD MEA system", shows the workstation setup and the steps for developing the single-channel read-out device. While the resulting performances are reported in the chapter "Results". In particular, this chapter describes a noise analysis of the device interfaced with a physiological solution and an amperometric application on PC12 cell lines. Furthermore, it presents LTspice® simulations and a study on the noise effect of the feedback resistor of the primary preamplifier circuit. Finally, it introduces two different active filtering stages that can be used to improve the general performances. The last chapter, "Conclusion", summarizes the general results and gives some tools for the future perspectives of this work.

Chapter 2

Background

2.1 Electrochemistry fundamentals

In the long-gone 1793 year, Alessandro Volta communicated to the Royal Society that electricity could be produced *"[..] by the simple mutual contact of metals of different sort [...]"* on the opposite edges of a moisturized paper, thus discovering the intimate relation between chemistry and electricity [4].
Since then and the following studies, electrochemistry is now applied in different fields from the study of corrosion, power and energy to biosensing and electrolysis analysis. Its research focuses the attention on the relationship between electrical energy and an identifiable chemical or biological change through matter. The effect of electricity involves transferring electrons from one chemical species to another, thanks to redox reactions. These reactions typically cross an interface between an electrical signal transducer (electrode), generally a metallic phase and a conductive solution (electrolyte); thus, allowing an external detection.
The simplest electrochemical model consists of two different electrodes: the working electrode or the indicator electrode and the reference electrode, shown in the figure 2.1.
In particular, when dissimilar metals (electrodes) are connected in the same electrolyte, they produce a cell potential, which involves redox reactions in a region called: electrical double layer (EDL). Thus, the electrodes' surfaces ionize and interact with the ions in the solution, giving rise to an electrostatic behavior. This electrolytic system can be split into two reactions: the oxidation half-reaction and the reduction half-reaction. Both of them are individually balanced, concerning the electroneutrality principle [4].
The reference electrode is employed because a complete cell usually involves two-electrode equations. Hence, to simplify the system, it is a standard-issue to consider just one of the two reactions involved, placing an electrode at a fixed potential

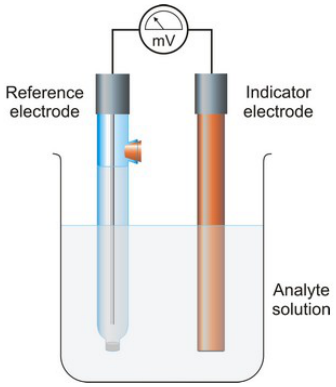

Figure 2.1: Electroanalytical cell setup with two electrodes. The potential of the working electrode against a reference electrode is the measure of the concentration of a species in the solution [5].

on the other half of the cell. In this way, the concentration of any ionic species involved on its surface is held at a fixed value, becoming a reference point for the measurements.
A common practice is to introduce as the reference electrode an Ag/AgCl electrode, distinguished by its stable half-cell potential (E^0= +0.222 V) over time and with the change of temperature [6]. The related half-cell reaction is shown below:

$$AgCl(s) + e^- \iff Ag(s) + Cl^-(g) \tag{2.1}$$

To sum up, the electrochemical measurements want to quantify the charge transfer due to the half-cell reactions within the interface at the electrode surface.
In the next section are described the fundamental relations through which these electrical phenomenons take place.

2.1.1 Fundamental relations in electrochemestry

An electrochemical cell respects important relations:

1. Gibbs free energy:
$$\Delta G = \Delta(U + pV) + \Delta(TS) \tag{2.2}$$
The previous equation can be simplified under the conditions of constant pressure and temperature as following:
$$\Delta G = -nEF \tag{2.3}$$
where ΔG is the free energy charge, n is the stoichiometric number of electrons in the process involved (mol), E is the potential difference between the

electrodes of a cell (V) and F is the Faraday constant (C/mol). This equation explains the spontaneity of the cell reaction. The more positive the cell potential difference is the more spontaneous the tendency of the reaction proceeds [4].

2. Nernst equation:
$$E = E^0 - \frac{RT}{nF}\ln(Q) \tag{2.4}$$
The Nernst equation is essential to understand the relation between the cell potential with the standard potential and the electroactive species. In particular, the equation (2.4) is obtained relating the Gibbs relation (2.3) to the standard potential E^0 and the reaction quotient Q, which is the ratio between the concentration of the species of the half-cell reduction and the species of the half-cell oxidation.
Thus, it is possible to understand that the cell potential variations can be predicted in different chemical and thermodynamic conditions.

3. Faraday laws:
$$m = \frac{MQ}{zF} \tag{2.5}$$
where m is the mass of the free species at an electrode, M is the molar mass of the species and z is the valency number of ions of the species. This equation summarized the Faraday laws. The first Faraday law highlights the correlation between the mass of a substance released at the electrodes and the total electricity produced. On the other hand, the second Faraday law says that the same quantity of charge passed through different electrolytes produces an equal number of chemical equivalents. Hence through the equation above, it is possible to calculate the mass of the substance produced at the electrode's surface.

These relations are fundamental to understand the basic principles of the electroanalytical methods implemented in the designed read-out system. When internal or external processes occur in the sample containing the cell culture, the electrochemical equilibrium change, and the transfer of ions from the cell culture to the electrode surface gives rise to electrical phenomena.
The next subsection explains in detail the two electroanalytical methods used to detect these kinds of signals.

2.1.2 Electroanalytical methods

The electroanalytical methods are used to investigate the information of the analyte in an electrochemical cell, from different points of view [7]. The major categories can be divided in:

1. Potentiometry: the study of the difference of potential between two electrodes.

2. Voltammetry: the study of the electrochemical reactions of an analyte species, subdivided into controlled potential (i.e., constant potential, or shifted potential) and controlled current techniques.

3. Coulometry: the study of the current of the electrochemical cell over time.

This work focuses the attention on potentiometry and a sub-class of voltammetry, amperometry. The following electroanalytical methods are studied in a two electrodes system, which is the one implemented by the MEA chip.

Potentiometry

Potentiometry passively measures the potential of a solution between two electrodes in an almost negligible current state. It mainly measures the spontaneous electrical activities between the working electrode (WE) and the reference electrode (RE), which is set at a known and constant overtime potential (typically ground referenced). The potential difference on the two electrodes depends on the surface redox reactions which happen into the solution [8]. In particular, when the potential of the working electrode varies in respect to the constant potential of the reference electrode, a measure can be detected. The sensitivity of the system to the ions of interest depends on the working electrode's characteristics that are electrical-active to the specific analyte. The potentiometric schematic is shown below.

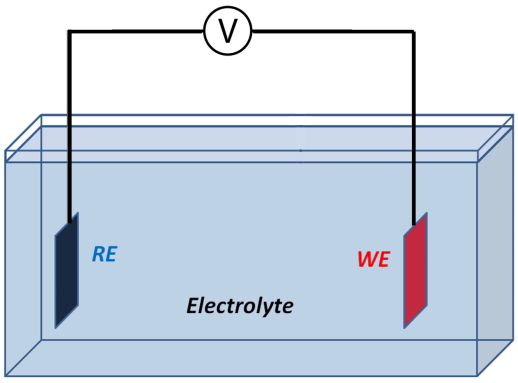

Figure 2.2: Two electrodes potentiometric system [9].

In general, the potentiometric biosensors provide the means to research into the excitable cells the parameters related to the spontaneous electrical activities of the cells. According to the equation (2.4), this electroanalytical method measures a

potential difference, which depends on the observed analyte concentration.
In the section 2.2, its specific application is treated in detail.

Amperometry

This technique measures the current which flows in an electrochemical cell by holding an appropriate fixed potential between the electrodes. In particular, in a two electrodes system, the constant potential, later called bias voltage (V_{bias}), is set between the reference electrode (RE) and the working electrode (WE). In this way, a current can diffuse to the working electrode and can be detected [10], see the schematic in the figure 2.3. According to the equation (2.5), the quantity of charge transferred at the interface between the working electrode and the electrolyte is proportional to the concentration of the analyte involved, which is the variable researched.

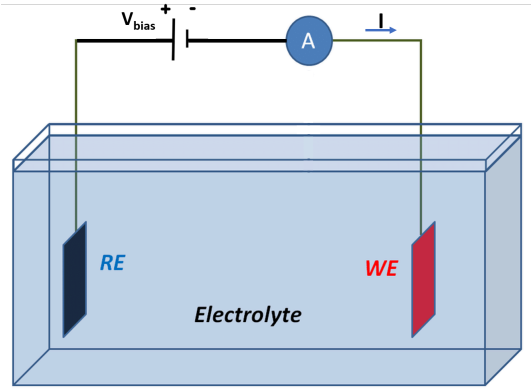

Figure 2.3: Two electrodes amperometric configuration [9].

In this electroanalytical configuration, few considerations have to be made.
At first, the potential applied has to be appropriately chosen regarding the occurred chemical reactions and the materials of the electrodes. Consequently, the current diffusion on the working electrode happens just if the cell potential is high enough to overcome the electrode potentials, the ohmic resistance of the solution, and the anodic and cathodic overvoltage [11].
In addition to this, it is important to specify the character of this current. Electrochemists are interested in detecting just the Faraday current due to diffusion effects, thus the only information related to the analyte concentration. Nevertheless, in the sample analyzed, there is an unwanted side effect that can twist the value of the Faraday current [12]: the presence of a capacitive current. The capacitive current is due to the storage of charges of the electrical double layer (EDL) created between the electrodes' surface and the electrolyte [13]. This effect has only a physical

meaning and not a chemical one. In fact, the interface creates a capacitor that accumulates charges and produces a current described by the equation below:

$$I_c = -\frac{dQ}{dt} = -AC_{dl}\frac{dE}{dt} \tag{2.6}$$

Where A is the electrode's surface area, C_{dl} is the differential double layer capacity, and E the electrode potential.
If E is not kept constant, the capacitive current flows through the electrode's surface and is summed to the Faraday current. Consequently, since the capacitive currents are usually larger than the faradaic ones, the sensitivity of the amperometric measurements is extremely limited [14]. In a quiescent solution, the capacitive current can be distinguished by a faster decay than the Faraday one [13], as shown in the figure 2.4.

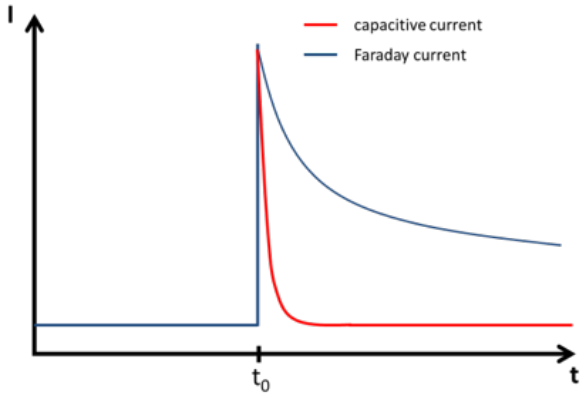

Figure 2.4: Comparison between the capacitive and Faraday current through time [12].

Moreover, since the capacitive current is unaffected by the analyte's concentration, the ratio between the Faraday current and the capacitive current can be improved, increasing the analyte [14].
All these expedients have to be integrated into the applied system to obtain a coherent amperometric configuration.
Generally, amperometry is applied to study the excitable cells in different experimental conditions. Above all, in an extracellular recording, this method provides the means to analyze the concentration of oxidable substances released by the cells. It mainly focuses on the detection of exocytosis phenomena that reveal the main biochemical parameters of specific pathologies.

The next section details how the excitable cells' signals are generated and their main applications.

2.2 Electrophysiology: the study of excitable cells

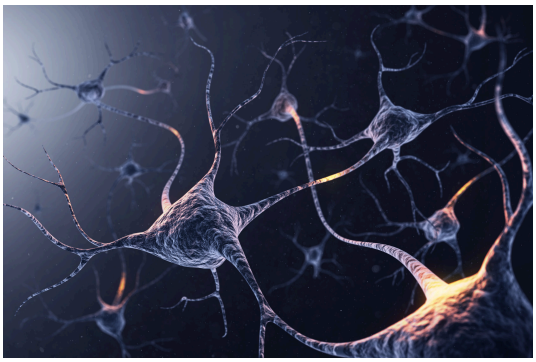

Figure 2.5: Example of excitable cell: colored model of a neuronal net [15].

The previous section mentioned that the electric signals from excitable cells are usually detected by introducing specific electrodes in the observed cell culture.
The particular branch of physiology which deals with the electrical and chemical phenomena associated with the excitable cells is electrophysiology. Electrophysiology became a useful means to study the nervous and muscular system, with a significant influence on neuroscience. In particular, it helped to understand the electrical and chemical behavior of neuronal cells. The application of electrophysiology in *in vitro* cultures allows the evaluation of minute changes in the ion channel activity from the level of a single neuronal cell membrane to a complex neuronal network [16].
The recording of the electrical activity, in terms of potentials and currents involved, allows the diagnosis of different pathologies and the improvement of the level of consciousness of the biological functionalities.
These specific electric signals are generated by the selective change of the cell membrane permeabilities to inorganic ions (e.g., H^+, Na^+, Ca^{2+} and K^+). These ions are released by the voltage-gated ion channels on the neuronal cells' membranes and cause the triggering of action potentials (APs), whose properties are explained in the subsection 2.2.1. The ion channels play a fundamental role in the evaluation of the cell functions such as cell growth, metabolism, morphological change, adhesion, and proliferation [1]. Specifically, they mediate the electrical signals' conduction of the APs across the synapses, modifying the cellular activity.

Moreover, through the ion channels, it is possible to study the cell activity modulation in the presence of specific chemical substances. Drugs, organic and inorganic molecules can promote the opening, therefore, the membrane's depolarization, or block the conductance through the channels. Consequently, the neuronal electrical activity can also be a means to research the side effects of specific substances.
The external detection of these electric signals is possible because, when the charged particles diffuse between the cytoplasm (intracellular fluid) and the extracellular fluid, they reach the electrode, changing the electrochemical equilibrium at the interface. Consequently, the resulting redox reactions allow the intra- or extracellular recordings. As a result, the signals obtained can trace the membrane potential; thus, the APs containing the researched information.

2.2.1 Neurons and action potentials

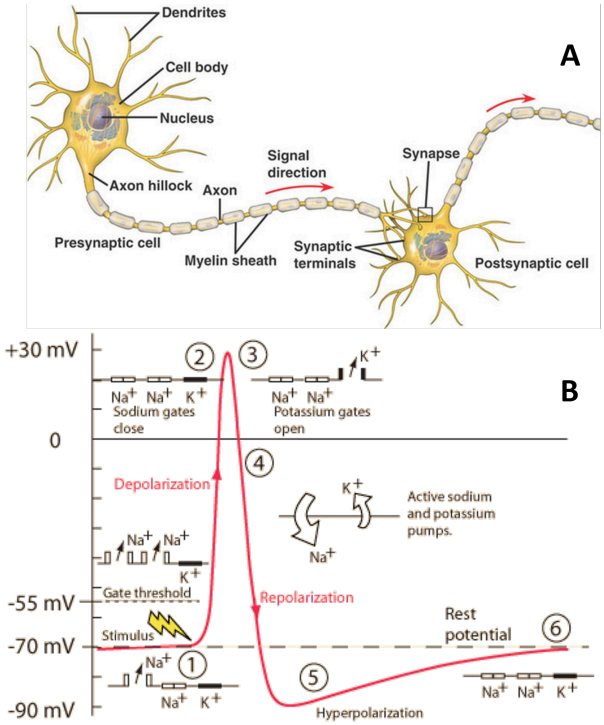

Figure 2.6: (A) Anatomy of a neuron. (B) Plot of an action potential [17].

The primary information about the electrical and chemical properties of excitable cells is hidden in the APs, whose shape is typically described by the trace in the figure 2.6.
The APs are the electrical signals relative to the cell membrane permeability change

due to the aperture or closure of sodium- (Na^+) and potassium- (K^+) gated ion channels. In fact, the flow of the charged particles causes the depolarization and repolarization of the cell membrane.
In a neuronal cell (see figure A 2.6), the APs are passed to other cells through the synapses. The synapse can be of two different kinds: electrical or chemical. The electrical one consists of the AP passage through direct gap junctions, the chemical one (the most prevalent) of the release of neurotransmitters into the synaptic cleft. These neurotransmitters (i.e., glutamate dopamine, GABA, etc.) bind to the postsynaptic neuron's receptors, opening or closing the gated ion channels, thus changing the membrane potential.
The AP takes place when the membrane potential overcomes a specific threshold potential or gate threshold (see figure B 2.6). Every electrically polarized cell reaches the electrochemical equilibrium from outside and inside the cell in a resting condition, achieving a membrane equilibrium potential (rest potential) at approximately -70 mV at time zero. When the cell potential changes and perturbs the resting equilibrium, the AP passes through the axons to the synapses, mostly at the dendrites' level, and propagates in only one direction to the next neuron [18]. Moreover, the neurons receive on dendrites and soma numerous synaptic contacts which can excite and inhibit. Thus, to generate APs in the initial part of the axon, proper synaptic summation phenomena are necessary. This summation involves two surrounding potential fields created by the neurotransmitter-receptor interaction, which are:

- Excitatory postsynaptic potential (EPSP)
- Inhibitory postsynaptic potential (IPSP).

In particular, EPSPs are mediated by channel receptors permeable to Na^+ and K^+ by the main excitatory neurotransmitter glutamate; IPSPs are typically mediated by channel receptors permeable to Cl^- or from receptors through the means of GABA and Glycine (to a lesser extent) [19].The effective combination of these electric signals causes the rising of spikes that can be recorded and studied externally, explaining important physiological information about the brain activity.

Dopaminergic neurons

This study focuses on midbrain dopaminergic neurons (in the substantia nigra pars compacta and ventral tegmental area), thus, the cells that produce dopamine. Dopamine is a neurotransmitter that belongs to the class of catecholamines. It is synthesized from the amino acid tyrosine (Tyr) through a biosynthetic pathway that includes the enzymes tyrosine-hydroxylase (which transforms the Tyr in L-DOPA) and decarboxylase of the aromatic amino acids (which transforms L-DOPA in

dopamine) [20]. The dopaminergic neurons participate in critical biological processes that regulate movement, motivation, and cognitive functions such as reward associations and habit learning. Dysfunctions in dopaminergic neuron circuitry implicate several neuropsychiatric disorders such as addiction and schizophrenia. The selective degeneration of dopamine also leads to the pathological condition that characterizes Parkinson's disease.
According to the impact on the physiological functions of dopamine, the research usually conducts the study on its associated biochemical processes. Specifically, it focuses on the electroanalytical signals, which derive from the oxidation reactions (see figure 2.7) consequent to the release of dopamine in the cell culture. These electroanalytical signals can be recorded externally through techniques that span over multiple temporal and spatial scales.

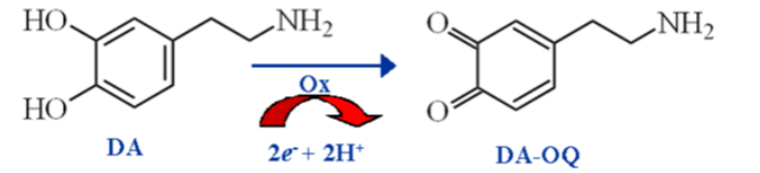

Figure 2.7: Oxidation reaction of dopamine. The dopamine (DA) is oxidized to orthquinone dopamine (DA-OQ) [21].

To sum up, the neurophysiological characteristics of dopaminergic neurons are peculiar and identifiable with electrophysiological techniques.
The following subsection illustrates the main *in vitro* electrophysiological techniques, which help the research reach a better level of consciousness of the brain functions [22]. For this purpose, it focuses the attention on the analysis of the single-cell activity recordings (intracellular recordings) and the cell network recordings (extracellular recordings).

2.2.2 Principle of *in vitro* electrophysiological methods

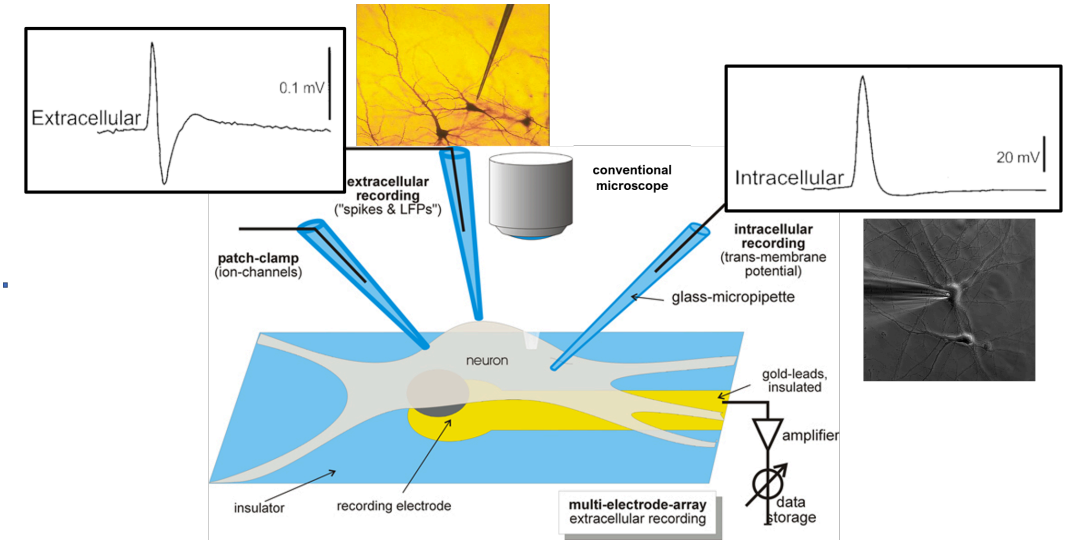

Figure 2.8: Example of intracellular recording (patch-clamp technique) and extracellular recording (MEA technique). The MEA's recording electrode collects the data through an external read-out system through gold-leads insulated, an amplifier system and a data storage [23].

As a neuron fires, an AP propagates through the cell and generates a flow of electric current near the ion channels due to the resulting redox reaction. This current brings to a potential signal difference that can be detected externally by using proper recording microelectrodes. From this, two kinds of information can be obtained:

- single-unit recordings (intracellular recordings): the potential detection of individual neurons.
- cell networks recordings (extracellular recordings): the information related to the electrical spikes of many neurons.

The tools used in these recording techniques are entirely different, as shown in figure 2.8.
The single-unit recording is applied for studying a single or multiple ion channels' activity of individual neurons. In particular, it requires a microelectrode insertion within the cell membrane, typically a patch-clamp glass-micropipette or sharp electrode. Since this membrane area is tiny due to the small tip of the microelectrode, there is a good chance that just one or a few ion channels are located in the patched

membrane. Individual ion-channel currents can thus be recorded. This kind of recording is characterized by monophasic depolarizations and higher and lower noise signals. However, in this case, it is needed an invasive setup that mostly causes damages to the cell membrane. For this reason, the recording duration is short and it lasts in few minutes.
Conversely, the extracellular recording measures the voltage change outside the cell, implementing one or arrays of microelectrodes (MEAs) closed to the cell surface [24]. MEAs are less suited for single-cell recordings due to their low spatial and temporal resolution compared to patch-clamp systems. As a result, the microelectrodes do not measure the membrane potential directly. On the opposite, they detect monophasic depolarizations related to the membrane potential variations. The amplitude of these recordings is smaller and depends on the distance between the signal source and the electrode. The signals obtained by this kind of recording are consequently more complex and contain the information of all the trans-membrane currents that occur near each electrode. Contrarily to the previous case, the higher throughput allows studying a cell network's behavior and long duration recordings, typically from days to weeks.
The characteristics of these two recordings are compared in the table 2.1.

Table 2.1: Electrophysiological recordings: comparing between the intracellular and extracellular characteristics

Technique	Intracellular recording	Extracellular recording
Throughput	Single-cell recording (max 2-3 cells at the same time)	Multiple cell recording (hundreds cells/ cell networks)
Signal characteristic	Monophasic depolarization ($\sim mV$)	Biphasic depolarization ($\sim \mu V$)
Electrical characteristic	Low noise (electric signals not distorted, "isolated" spikes)	High noise (electric signals attenuated, multiple spikes)
Type of electrodes	Patch-clamp or sharp electrodes	MEAs or neural probes
Recording duration	Few minutes (due to the cell damage caused by the invasive electrodes)	Days to weeks (depending on the cell culture growth)

The applicability of each technique is dependent upon numerous factors, including the cell/tissue preparation, the desired manipulation to apply, the type of information researched (single-cell level or network level), etc.
To sum up, the most used electrophysiological methods applied for the analysis of the signals from *in vitro* neuronal cell cultures usually use:

- The manual (or automated) patch-clamp technique for the intracellular recordings.

- Multielectrode arrays (MEAs) for the extracellular recordings.

The following section is focused on the extracellular recording of cultured neuronal cells through MEAs. In fact, the work of this thesis has to deal with a proper MEA chip, whose basic principles are thus essential to the design steps of the read-out device.

2.3 Principles of MEA for extracellular recording in cultured neuronal cells

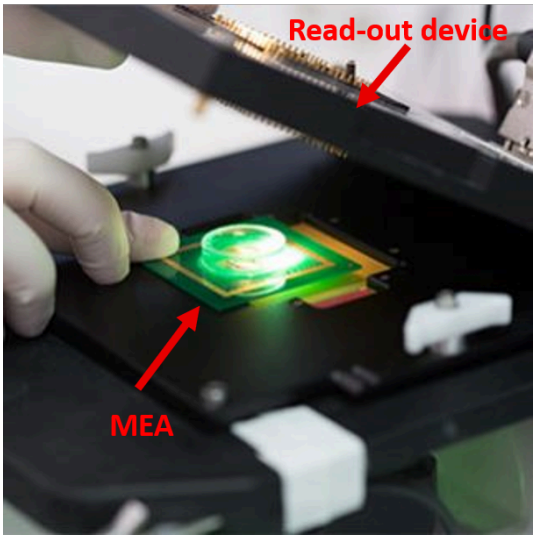

Figure 2.9: Example of a recent MEA technology [25].

As explained in the chapter 1, multielectrode arrays (MEA) play an essential role in detecting appropriate extracellular recordings. Most of these cell-based biosensors evaluate the cell functions by detecting electrochemical signals such as current, potential, conductivity or impedance. The electrochemical measurements through a MEA are usually performed through the electroanalytical methods of potentiometry and amperometry, already described in the section 2.1.
According to the schematics reported in the figures 2.2 and 2.3, the working electrode is now represented by every single electrode of the MEA submerged in the cell culture. In contrast, the reference electrode is typically characterized by a larger surface electrode (usually in Ag/AgCl) fixed at a constant potential.
The extracellular signals are collected thanks to the spreading of electroactive

chemical species from the microelectrode surface to the linked conductive collectors. In addition to this, passivation layers on the MEA are essential to separate the exposed specific areas from the substrate of the chip.
As a result, the MEA works essentially as a cell culture-interface that connect the independent electrical signals from each electrode to the external electronic circuitry (see figure 2.10).

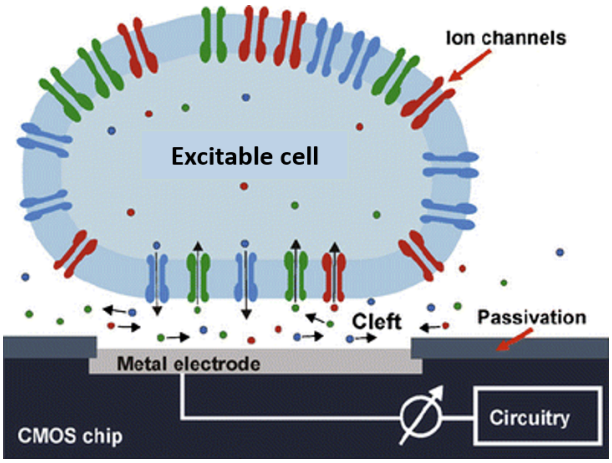

Figure 2.10: MEA technology coupled with an external read-out device enables the extracellular recording of an excitable cell [26].

The processed signals collected and stored externally then reveal the information related to the analyte's concentration in question. As said previously, the change of concentration of inorganic ions (H^+, Na^+, Ca^{2+}, K^+, etc.), released by the voltage-gated ion channels on the excitable cells' membranes, is related to an indirect measure of the membrane potential. Consequently, the extracellular signals obtained are fundamental for evaluating the cell functions because they contain information about the cell growth, metabolism, morphological change, adhesion, and proliferation [1].
To reach the advantages of this technology, a read-out system must be introduced to properly amplify the detected extracellular signals. Moreover, the extracellular signals are characterized by different electrical characteristics, depending on the electroanalytical method used. For this purpose, the next section explains the main signal features which distinguish an amperometric recording from a potentiometric one.

2.3.1 Typical electroanalytical signals from dopaminergic neuronal cells

The electric model behind the interface between the MEA and the cell culture can explain the particular shape of the extracellular signals.
During the observation of the cultured cells, each electrode of the MEA becomes part of the extracellular environment in which the cells can grow up and communicate (see figure 2.11). The extracellular field potentials are generated when the cultured cells adhere to the substrate and can be detected if the neuron is closed enough to the electrodes. In an ideal configuration, the neurons spread their bodies and axons on the electrode surface through the electrolyte, exposing the cleft to the electrode site (see figure 2.10). As a consequence, a small volume of electrolyte stays between the cells and the microelectrodes, creating a solid-liquid interface.

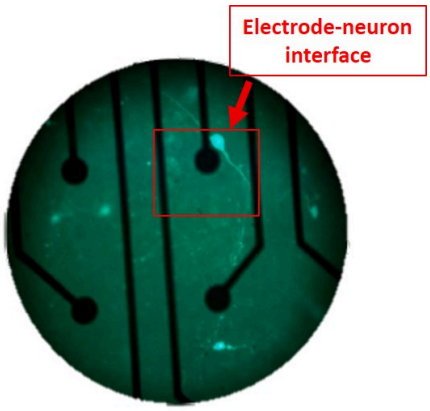

Figure 2.11: Figure of a dopaminergic cultured neuron closed to the active region of a MEA's electrode [27].

The simplified electrical model of an electrode in an electrolyte can be represented with a capacitor (capacitive phenomena) in parallel with a resistor (conductive phenomena) [1]. However, the complete equivalent model of a MEA's microelectrode facing a neuron is more complex, and it can be simplified by the schematic in figure 2.12. When a cell produces a trans-membrane current (I_M), it passes it through the "junctional membrane" and the simplified electrode impedance. The "junctional membrane" is the interface between the neuronal membrane and the electrode site, while the "non-junctional membrane" is the opposite interface. Both of them are represented by the simplified parallel between the resistance (R_{nj} and R_j), which depends on the protein structure capable of carrying ions, and the capacitance (C_{nj} and C_j), which depends on the properties of the phospholipid bilayer that allows the charges separation.

The resulting voltage at node A, the signal relative to the trans-membrane potential, thus the source of interest, is amplified by a proper external amplification circuitry. As it is possible to see from the schematic, this voltage is also proportional to the sealing resistance R_{seal}, which depends on the chemical composition of the solution, the temperature, and the geometry of the electrolytic cell [1]. The larger R_{seal} is, the better the signal corresponds to the trans-membrane potential (if R_{seal} is infinite, the voltage corresponds to a whole-cell patch configuration) [28].

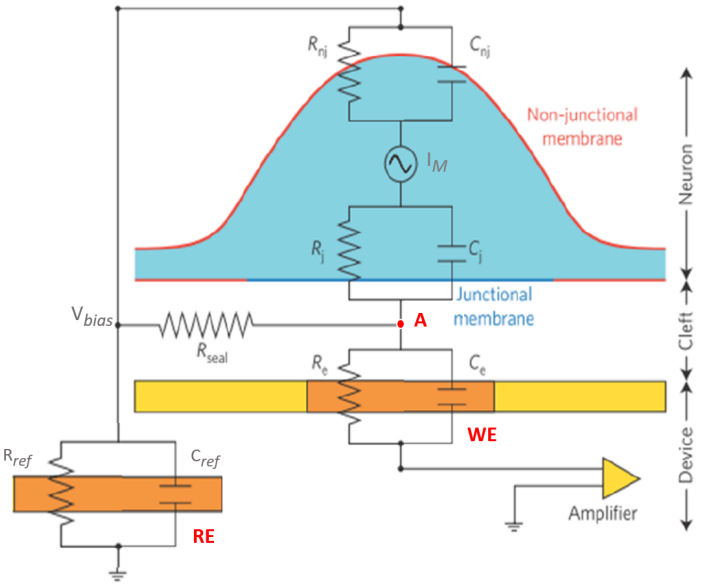

Figure 2.12: Equivalent circuit model of a MEA's electrode-neuron interface. The schematic shows a neuron (blue) on a microelectrode's surface (yellow). The recorded voltage at node A (red) originates from the trans-membrane currents, which flows through the cleft at the working electrode site (WE).

Thus, a MEA can record a change of potential as a function of time due to the capacitive coupling of the device with the neuronal culture environment.
Clearly, this model takes into account only the interface between a single neuron and an electrode. In truth, an electrode usually sums all the trans-membrane currents in closed proximity. This complicated the analysis. However, nowadays, spike sorting analysis programs are developed to subtract a single-cell activity from the recorded signals [28].
To sum up, the linear electric model of the figure 2.12 can explain why the signal recorded by the electrodes has a different shape from the expected AP trace.

In particular, thrashed out studies model it on a second-order high-pass filter with a half-maximal cut off frequency, given by the resembling of the junction membrane resistance (R_j), and the capacitance of the MEA's electrode (C_e) [29]. Consequently, the extracellular recorded signal can be simplified as the first derivative of the AP that occurs in the observed neuronal cell, changed in sign.

As shown in the figure 2.13, a typical extracellular signal is characterized by a high background noise band and, in most cases, it looks like a negative peak of tens µV followed by a smaller positive peak.

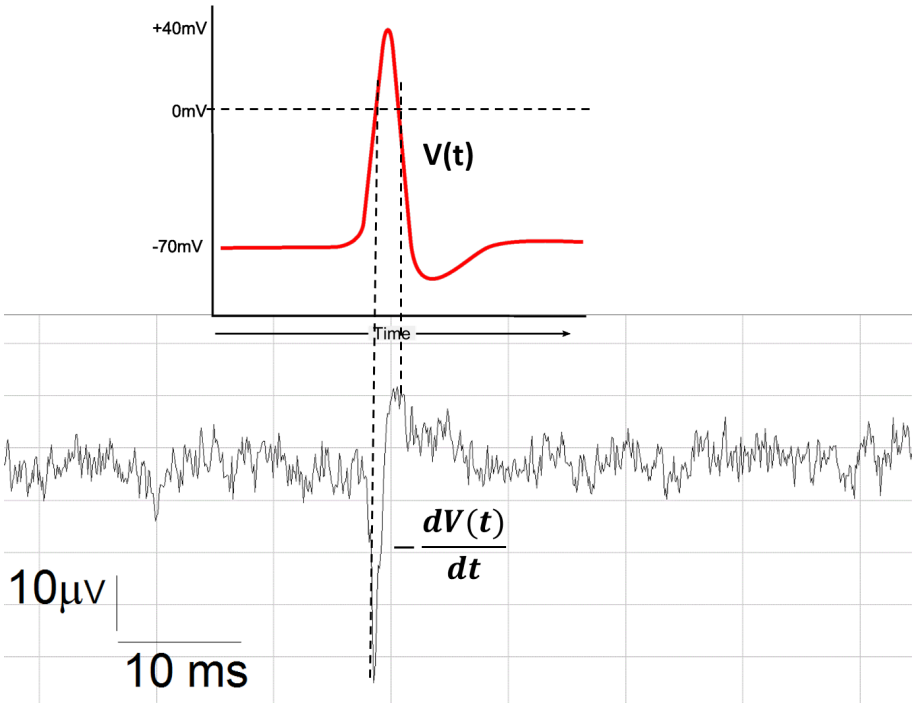

Figure 2.13: Comparison between the neuronal action potential (red trace) and the extracellular signal recorded by an electrode of the MEA (black trace). As it is possible to see by the dashed lines, the extracellular signal is the first derivative of the AP signal changed in sign.

As introduced in the section 2.3, the extracellular recordings from dopaminergic neuronal cells are usually detected by two specific measurements:

1. Amperometric recordings: the current measure due to the change of concentration of inorganic ions, by applying a bias voltage (V_{bias}) between the working and the reference electrode.

2. Potentiometric recordings: the spontaneous potential recording of the neuronal

cells in a negligible current state.

These extracellular recordings have to deal with unstable parameters. Both of them are characterized by an amplitude and frequency that can vary in each different experiment according to [30]:

- the type of the primary cell culture (slice/explant/dissociated cell culture)
- the neuronal sub-population selected
- the number of active electric neurons involved inside the culture
- how long the cell culture is kept suspended (in vitro days DIV)
- the nature of the medium in which the cells are located

While they depend on the recording system in terms of [31]:

- the overlap between the neurons and the MEA's electrodes (e.g., area of contact and tightness)
- the MEA's electrodes (e.g., geometry and internal impedance)
- the analog signal processing integrated into the readout system (e.g., the system's gain, bandwidth, and behavior outside of cutoff frequencies)
- the digital signal processing through the data acquisition board (e.g., sampling rate and digital filtering)

Hence, to design a proper read-out device, it is crucial to identify the main electrical characteristics which distinguished each electroanalytical recording. For this purpose, the extracellular signals from dopaminergic neuronal cells are addressed in detail now below.

Amperometric recording

Amperometry is an electroanalytical technique that allows the detection of single exocytosis phenomena. In particular, this technique is applied for studying the kinetics involved in the fusion and opening of single secretory vesicles in the presynaptic membrane. The spikes amplitude of the signal recorded detect the concentration of the neurotransmitters released by these fusion events (see the equation (2.5)).
In general, the amperometric spikes from neuronal cells can be recognized by positive peaks with:

- An amplitude of 10-100 pA.

- A firing frequency that can vary from 0.6 to 15-30 Hz.
- A noise background of around 10 pA peak-to-peak.

An example of amperometric signal from mice's pheochromocytoma adrenal medulla cells (PC12) is shown in the figure 2.14.

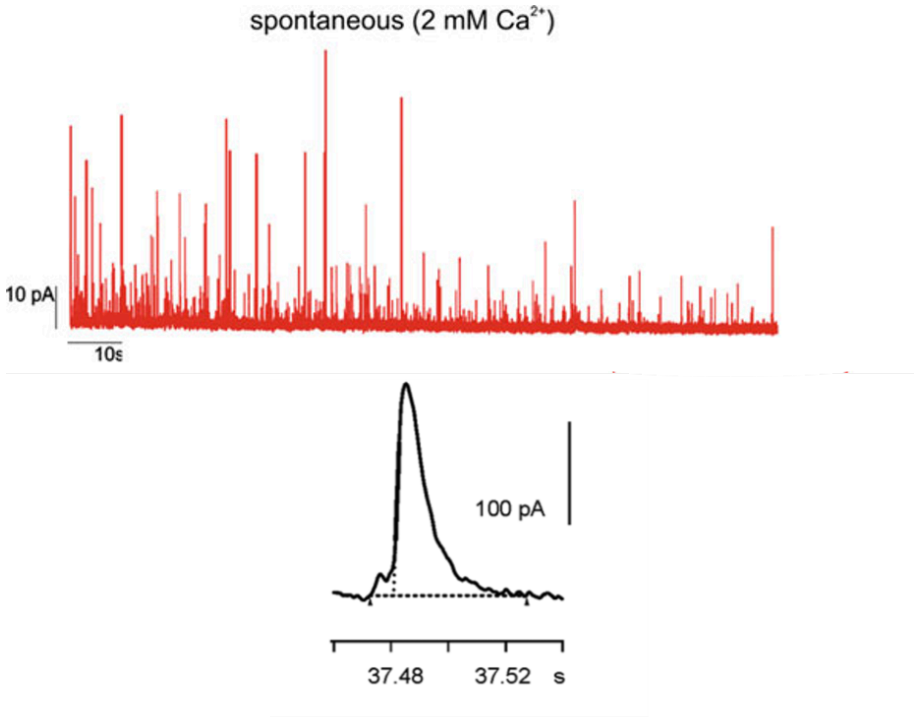

Figure 2.14: Example of amperometric recording from pheochromocytoma of the adrenal medulla cell's rat (PC12 cells), through a MEA's electrode. Above: the spontaneous amperometric activity at 9 DIV. Below: two enlargements of the main trace. The peaks detect the dopamine oxidation [32].

Each spike represents the current associated with the dopamine content of PC12 cells cultured on a MEA [32].
To perform this kind of recording, it is fundamental to choose the bias voltage (V_{bias}) between the working and the external reference electrode.
As seen in the subsection dedicated (subsection 2.1.2), the working electrodes measure the current just if the bias voltage is high enough for making possible the current diffusion. A good compromise is to set the V_{bias} at 800 mV, in general, less than 1 V to avoid cell damage. Usually, this value is selected evaluating the peak of oxidation of the oxidable observed analyte (e.g., adrenaline in a Tyrode solution) throughout steady-state voltammograms sweeping the voltage within a

certain range. The optimal V_{bias} is then related to the maximum value of the ratio between the analyte oxidation current and the water-based solution one [33].
The advantage of this electroanalytical method is that the measurements can be performed in few days. Amperometric signals can be recorded from mice cell lines derived by pheochromocytoma adrenal medulla (PC12). The PC12 cell line cultures are usually preferred because they can synthesize and release dopamine (with a Ca^{2+} dependent mechanism) after just 3/4 days from their plating in the culture dish for typically 15-30 minutes [34].
On the other hand, the low peaks of current which characterize these electroanalytical signals make the system very sensitive to external source noise. The chapter 4 describes how the single-channel read-out device has to be designed for minimizing as much as possible the current leakage and the noise contribution.

Potentiometric recording

Potentiometry is an electroanalytical method that measures the potential of a solution between two electrodes in almost a negligible current state. As described in the section 2.1.2, the variation of the potential on the working electrode depends on the variation of the analyte concentration in the sample.
In the extracellular recording of neurons, this method is used to detect the spontaneous action potentials (APs) in the cell culture. The typical potentiometric spikes from this kind of culture are represented by negative peaks with:

- An amplitude of 10-800 μV
- A firing frequency that can vary from 0.7 to 15-30 Hz.
- A noise background of around 20 μV peak-to-peak.

A typical example of extracecellular signal in potentiometry, can be seen in the figure 2.15 [27]. In this case, primary cultures of mesencephalic dopamine neurons from embryonic (E15) C57BL6 TH-GFP mice are usually analyzed [35]. In contrast to the cell lines used in amperometry, which are just plated on the Petri dish for few days, these cultures are more difficult to handle. During the culturing, the cells need to grow and adhere to the substrate adequately coated (e.g., poly-L-Lysine). Usually, the potentiometric measurements can be performed at 14 DIV, when the neurons generally start their spontaneous electrical activity. Consequently, this kind of measurement needs more time and technical skills before being fulfilled.

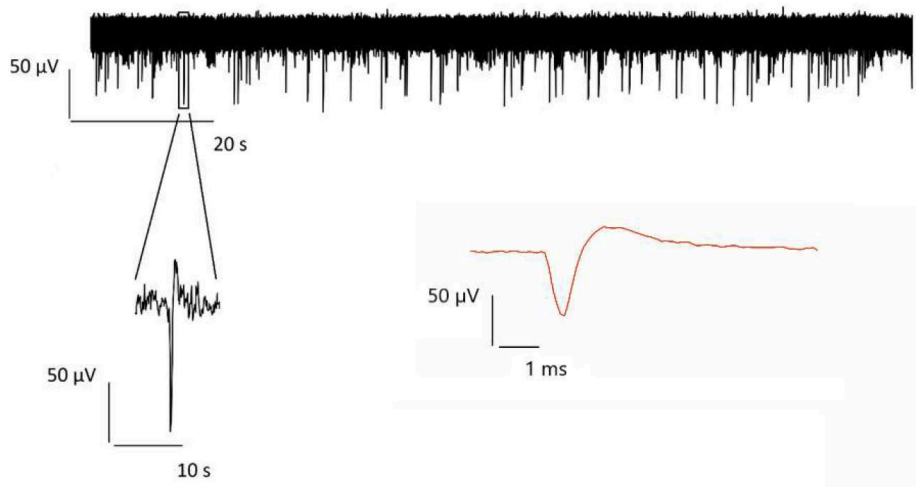

Figure 2.15: Example of potentiometric neuronal signals from one electrode belonging to a conventional MEA. Above: the potentiometric trace of the spontaneous activity at 9 DIV; lower left: enlargement of a single extracellular spike. Bottom right, the potential mediated over a period of 40 s (in red) [35].

In this application, the range of frequency and amplitude is more variable than in the previous case. In fact, the frequency of the spontaneous potentials and the signal amplitude depend on the cell culture maturation [35]. Thus, it is essential to consider how many days are passed from the beginning of the measurements. An example of how the electrical activity trend varies as the in vitro days (DIVs) pass is shown in the analysis below. From the figure 2.16, it is possible to notice two significant aspects:

1. The firing frequency increases as a function of the DIV.

2. The amplitude of the signals varies according to the DIV, typically increasing when the cell culture is maturated (above 14 DIV).

These considerations give an idea of how much time has to be dedicated before performing a potentiometric measurement.

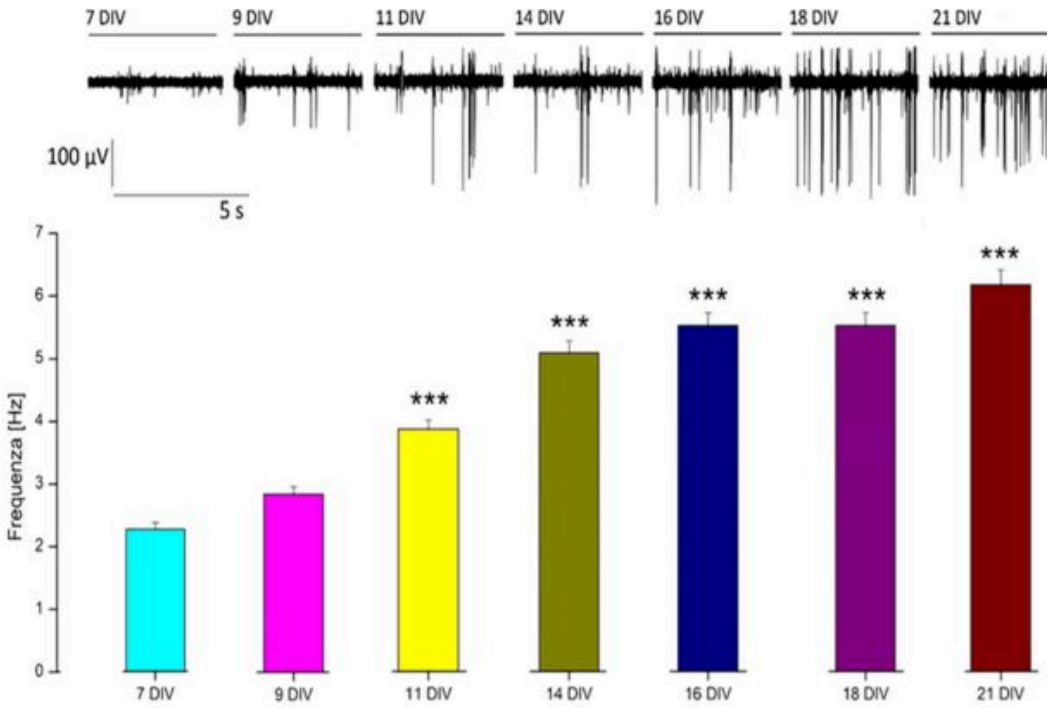

Figure 2.16: Traces of the neuronal electrical activity recorded by the same channel at different DIVs (above). Below: the related average frequency graph at 7, 9, 11, 14, 16, 18, 21 DIV. The significance (indicated with an asterisk) is referred to the cell culture at 7 DIV [27].

To sum up, this section was useful to understand the electrical characteristics of the two different recording traces and give an idea of their main applications.
In addition to this, it was possible to observe that the potentiometric signals have larger amplitudes compared to the amperometric ones. Thus, to read the signals correctly, an external circuitry should consider a different gain for each recording configuration. In contrast, the noise constraints on the amperometric recordings should also fit the potentiometric ones. Therefore, a read-out device can customize with the same amplifier a particular circuit for each electroanalytical method (read chapter 4).
However, before proceeding with the realization of the read-out device, it is fundamental to know what kind of functions and options a commercial device usually implements. For this purpose, the next chapter presents the main characteristics of a conventional MEA system.

Chapter 3

Commercial MEA system

3.1 Workstation for extracellular recording with a conventional MEA

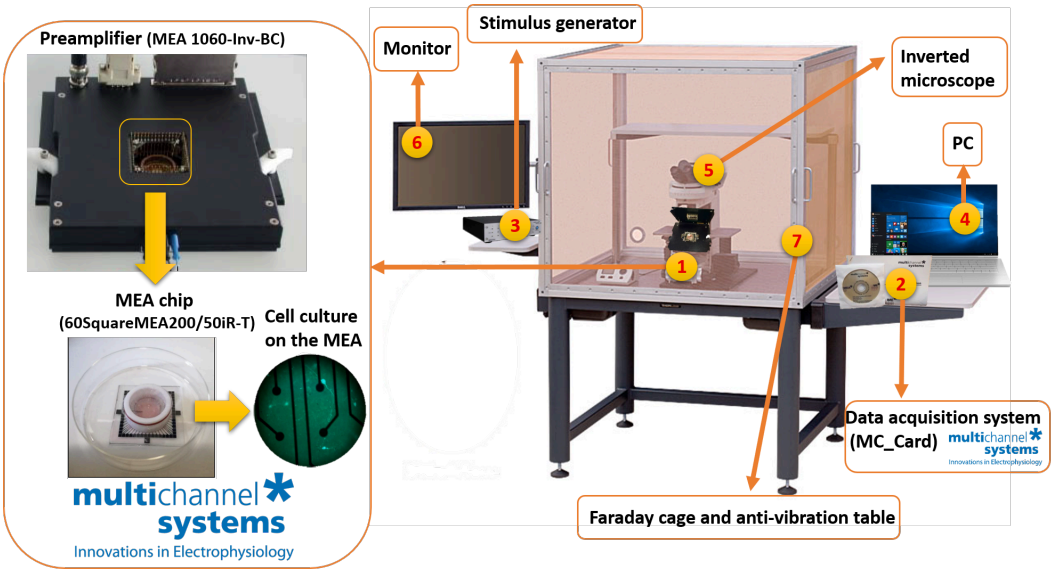

Figure 3.1: Sketch of the ideal workstation for a MEA system.

This chapter aims to show a standard MEA system equipped with a proper preamplification stage and a software interface. Particularly, it studies the main options and applications that had to be integrated into the designed custom system (read chapter 4); thus, allowing the fulfillment of the fundamental requisites. The observation on the preamplifier gave a general idea of what the circuit had to include.

At the same time, the software highlighted what the researchers need to control and set from outside. For this purpose, it is presented a system supplied by Multi Channel Systems MCS GmbH that the University of Torino used in their previous researches. However, as later explained, the following system allows just a single electroanalytical method, potentiometry. On the opposite, the custom device had to integrate also another configuration mode, amperometry.

An ideal sketch of the extracellular recording system through a conventional MEA is shown in the figure 3.1.
It typically consists of a MEA chip coupled with a suitable read-out device (preamplifier) with a proper amplification stage. Through this preamplifier, the extracellular signals from multiple sites of the MEA can be simultaneously recorded. The whole system is further protected into a Faraday cage to shield the low-frequency interferences, and it is arranged over an anti-vibration table to limit environmental vibrations. In this particular setup, a general-purpose stimulus generator can send voltage pulses to the culture cell. Stimulations can be used in these applications to lead to excitation or inhibition of the cultured cells' electrical activity. The recorded data are then sent to a PC equipped with an A/D conversion board to collect and analyze the extracellular signals. At last, an inverse microscope with an external monitor is used to observe the cell culture.

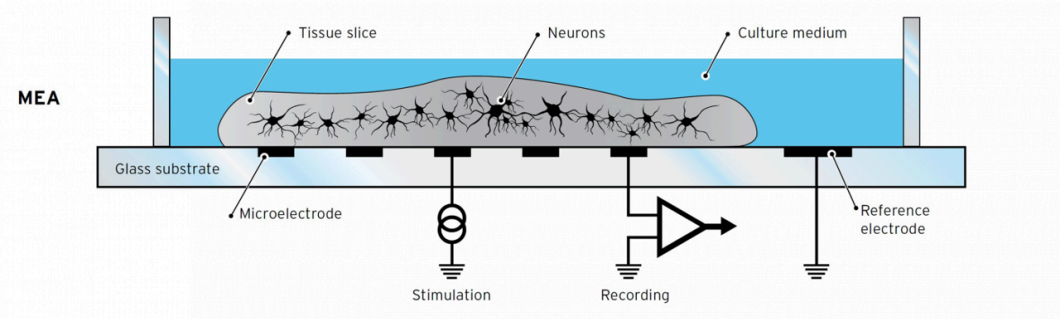

Figure 3.2: Example of the main functionalities of a MEA system: extracellular recording and stimulation option on cultured neuronal cells [23].

The schematic in the figure 3.2 resumes the main possible approaches applied to the observed neuronal cell culture. Two options are possible:

1. Extracellular recording

2. Stimulation option

For applying these options, a MEA system has to include specific components. The following model, chosen as an example, is a 60-electrodes MEA system (MEA60-System) designed by the company Multi Channel Systems MCS GmbH. The MEA60-System equipment includes:

- MEA chip: "60SquareMEA200/50iR-T".
- Read-out device: "MEA 1060-Inv-BC".
- External stimulus generator.
- Data acquisition system: "MC_Card".

The main components of the MEA60-System can be illustrated by the schematic in the figure 3.3.

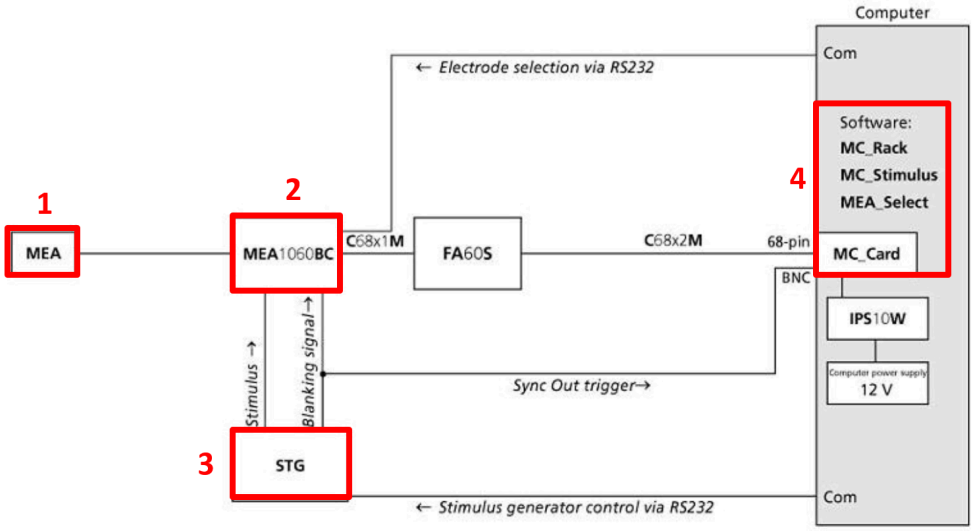

Figure 3.3: MEA60-System schematic. Squared in red the main components: the MEA chip ("60SquareMEA200/50iR-T"), the read-out device ("MEA 1060-Inv-BC"), the external stimulus generator and the data acquisition board ("MC_Card") [36].

This particular MEA system allows neuronal signal recording at many sites. Moreover, it simultaneously stimulates the cell culture within the array, even using the same electrodes set for the recording. However, for the stimulation, it is needed an external stimulus generator which sends the pulses.
To complete and perform these measurements, the MEA60-System data acquisition

board includes three specific software. One ("MEA_ Rack") is used to set the recording or the stimulation option on each electrode. The second ("MC_ Stimulus") is to select the stimulation pulse generated by the external generator, and the last ("MEA_ Select") to visualize and post-process the recorded signals.
Each component and its main functionalities are analyzed in the sections below.

3.2 MEA chip "60SquareMEA200/50iR-T"

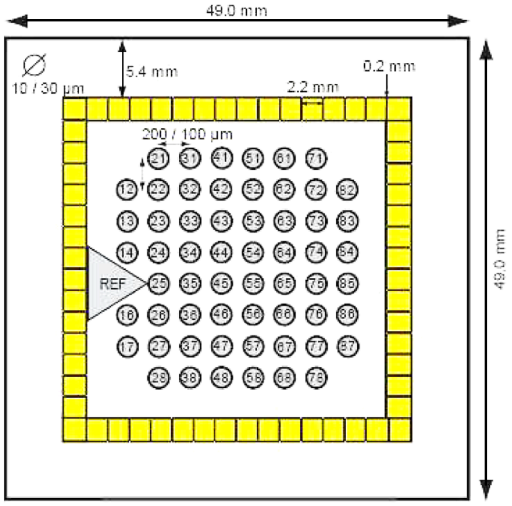

Figure 3.4: "60SquareMEA200/50iR-T" electrode layout. The number on each electrode represents the relative preamplifier pin to be interfaced [37].

The Multichannel Systems MEA chip is the model "60SquareMEA200/50iR-Ti". This MEA chip consists of a glass square recording area of 49 mm length and 1 mm thick. In this area, 60 electrodes (59 working electrodes and 1 internal reference electrode) with a diameter of 30 µm are aligned in an asymmetrical 8 × 8 grid with interelectrode distances of around 100- 200 µm.
The electrodes are made of TiN (Titanium nitride), robust and heat-stabilized biocompatible material with good electrical conductivity properties and a small electrode impedance (< 100 kΩ).
Multichannel Systems suggests this kind of planar MEA for long-time experiments, which fits in the extracellular recording's requisites. In fact, thanks to the presence of the material TiN, these electrodes can be reused and sterilized for several times (up to several weeks and even months).
As it is possible to see from the figure 3.4, the multi-electrodes are connected to

the the edges by means of Ti conductor tracks and a series of gold pins. Each unit collects the extracellular signals produced from the neurons from the culture chamber (a glass cylinder) to the external preamplifier [37].

3.3 Read-out device "MEA 1060-Inv-BC"

The preamplifier "MEA 1060-Inv-BC" is a read-out device that collects and properly amplify the signals from the culture chamber before sending them to the data acquisition system. The MEA chip is placed directly into the MEA preamplifier, and its gold contact pads are pressed onto the lid of the MEA preamplifier (see figure 3.5) [36]. The particular geometry allows to place the preamplifier on the plate of an inverted microscope. In this manner, it is possible to couple the microscopic investigations of the cultures to the electrophysiological recordings.

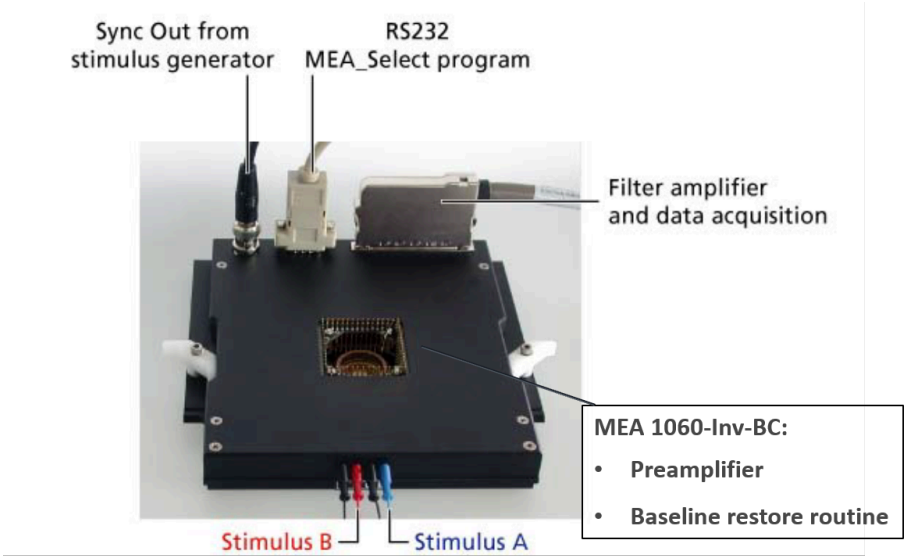

Figure 3.5: Read-out device "MEA 1060-Inv-BC" [36].

The read-out device "MEA 1060-Inv-BC" contains a specific 60-channel preamplifier with a fixed hardware gain of 55, chosen by the customer, and a bandwidth with a cut-off frequency of 8500 Hz (see figure 3.7). The preamplifier is also equipped with a blanking circuit to prevent saturation of the amplifiers in the case of electrical stimulation or higher DC offsets. For this reason, the "MEA 1060-Inv-BC" preamplifier circuit integrates a baseline restore routine. This circuit acts like a high-pass filter with a very low cut-off frequency of roughly 0.02 Hz. As a result, a slow process (1-2 minutes) due to the small cut-off frequency is integrated.

This process can be faster if all the electrodes are grounded before starting the baseline routine. For this purpose, the system implements also a grounding option of the electrodes.

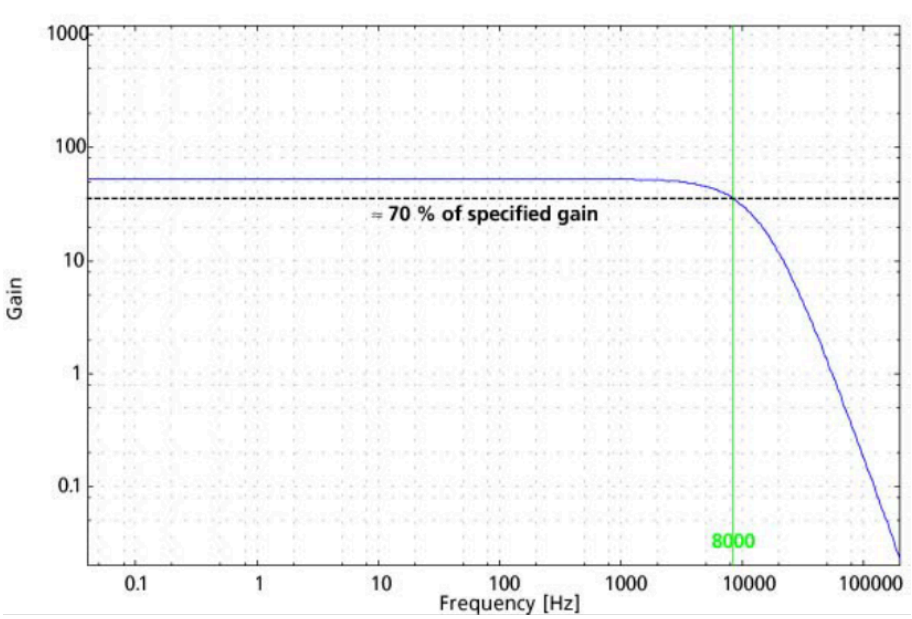

Figure 3.6: Bode plot of the single-stage "MEA 1060-Inv-BC" preamplifier.

In addition to this, the "MEA 1060-Inv-BC" can also integrate a second stage 60-channel amplifier filter. In this case, a band-pass filter between 10 Hz and 3 kHz and a further amplification of 20 is obtained. Consequently, the total hardware gain is fixed at 1100 (see the blue trace in the figure 3.7).
However, Multichannel Systems usually advises to acquire the raw data with the single-stage preamplifier and change the frequency band applying a digital pass-band filter through the "MC _ Rack" program (read section 3.5). As a result, the band-pass filter obtained with the single-stage preamplifier and the "MC _ Rack" program are just slightly different (see the black trace in the 3.7).

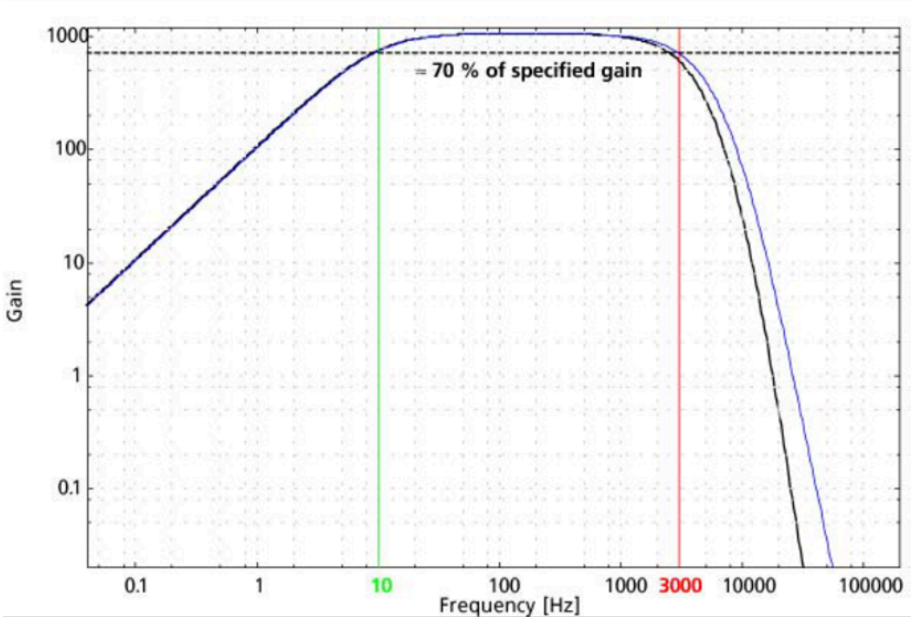

Figure 3.7: Bode plots. In blue, the Bode plot related to the second-stage "MEA 1060-Inv-BC" filter amplifier. In black, the one related to the single-stage "MEA 1060-Inv-BC" preamplifier after a digital filter.

To sum up, the MEA 1060-Inv-BC preamplifier reads the signals and sends them to the data acquisition board. In addition to this, it can receive commands from outside. Specifically, the "MEA_Select" software allows the selection of the electrode mode configuration (recording mode or stimulation mode). Consequently, the electrode can be set to record or receive the chosen pulse stimuli from the external stimulus generator. Finally, it is possible to select the baseline restore routine for compensating the DC offsets.

3.4 Stimulus generator

The stimulation option is useful in these applications because it allows the study of neuronal cell reactions. A signal pulse generates a transient voltage gradient that polarises the cell membrane and leads the electrical activity to excitation or inhibition. For this purpose, the typical stimuli used are monophasic or biphasic patterns.
In the MEA60-System, it is possible to send the external pulses to the selected electrodes of the MEA chip by setting up an external stimulus generator. Expressly, the stimulus generator is set through the "MC_ Stimulus" program (read section 3.5). This software interface allows the selection of the specific pattern (biphasic or

monophasic) and its main parameters (e.g., duration of the stimulus, period). The Multichannel Systems recommends using only monophasic voltage pulses to ensure that the voltage on the electrode reaches zero at the end of the pulse. Moreover, according to some articles, it is advised to select voltage pulses lower than 1 V (generally between 100 mV to 900 mV) to avoid damage to the cells or the electrodes [38]. As a consequence, the electrodes should offer a high charge-injection capacity. Without this feature, the system can be lead to an irreversible electrochemical reaction at the interface between the electrode and the cell culture [23].
Two typical monophasic and biphasic pulses with a duration of 100 µs for each phase and with an amplitude of ± 1 V are reported in the figure 3.8.

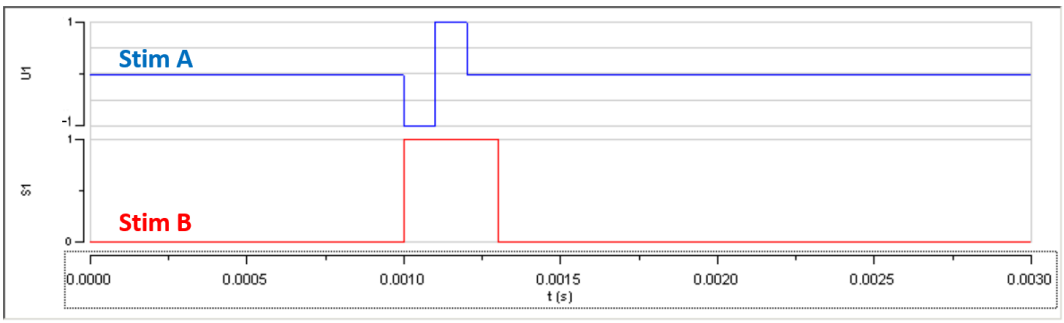

Figure 3.8: Example of two stimulation patterns. In blue: the plot of the biphasic pulse, Stimulus A. In red: the plot of the monophasic pulse, Stimulus B.

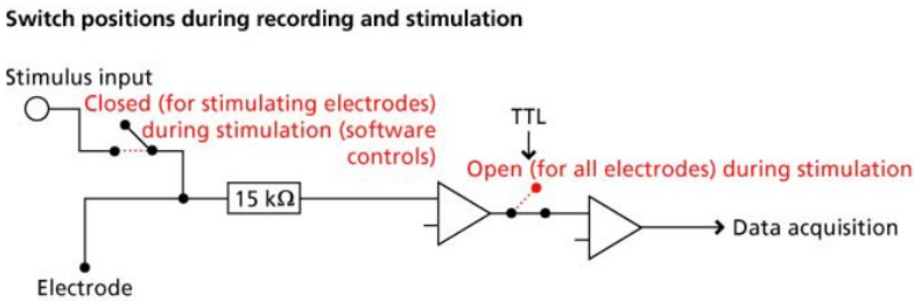

Figure 3.9: Schematic circuit of the blanking circuit.

Simultaneously to the stimulus option, the MEA60-System can apply a blanking circuit, typically a TTL pulse (Sync Out signal) that drives a switch. During the blanking signal, the stimulus input is connected only to the selected electrodes for the stimulation. Simultaneously, all the electrodes (in both the configuration modes) are disconnected from the preamplifier. In this way, the preamplifier's

voltage outputs are held constant (usually grounded) when the stimulus is applied. Thus, the preamplifier saturation is effectively prevented, and the stimulus artifact on the recording electrodes is reduced (see figure 3.9).

3.5 DAQ "MC_Card"

The Multichannel Systems equipment is provided of an acquisition board, the "MC_Card". This board contains three software: the "MC_Stimulus", the "MEA _Select" and the "MC_Rack".
The "MC_Stimulus" allows to customize the pattern of the stimulus A or B (figure 3.8) that can be selected through the "MEA_Select" program and to communicate with the external stimulus generator.

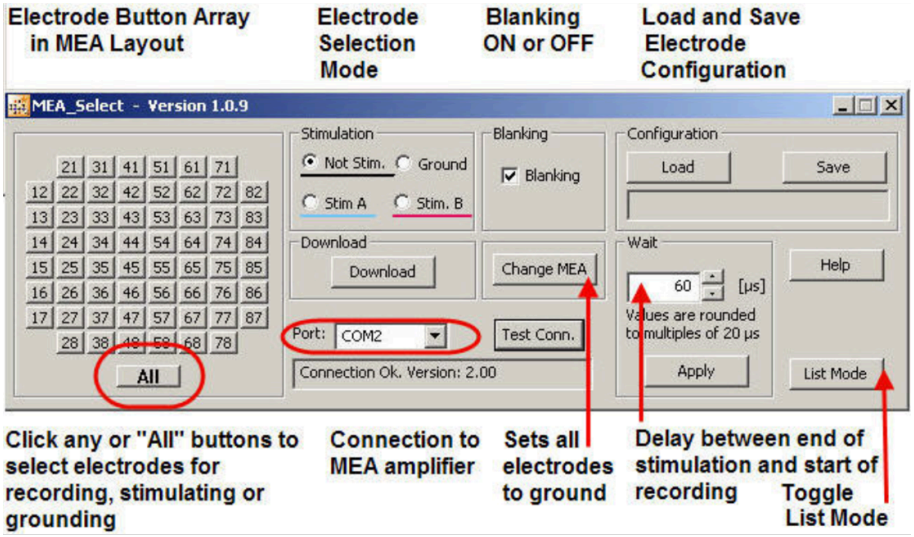

Figure 3.10: "MEA_Select" program software interface.

Secondary, the "MEA_Select" shown in the figure 3.10, represents the main configuration interface. In fact, through this interface is possible to:

- set the electrode configuration mode: recording mode ("Not Stim.") or stimulation mode or ground mode ("Ground").
- select the stimulation mode: biphasic stimulation ("Stim A") or monophasic stimulation ("Stim B") (figure 3.8).
- select the delay between each stimulation and recording ("Wait").
- switch the blanking circuit ("Blanking")

- select ("Load") or save ("Save") a customized electrode configuration.
- set the baseline restore routine ("Change MEA").

Finally, the recorded data on each channel can be observed through the "MC _ Rack" software. Through this interface, it is possible to have a wide range of applications that allow signal processing and peak detection. The interface of all the 59 observed working electrodes can be seen in the figure 3.11.

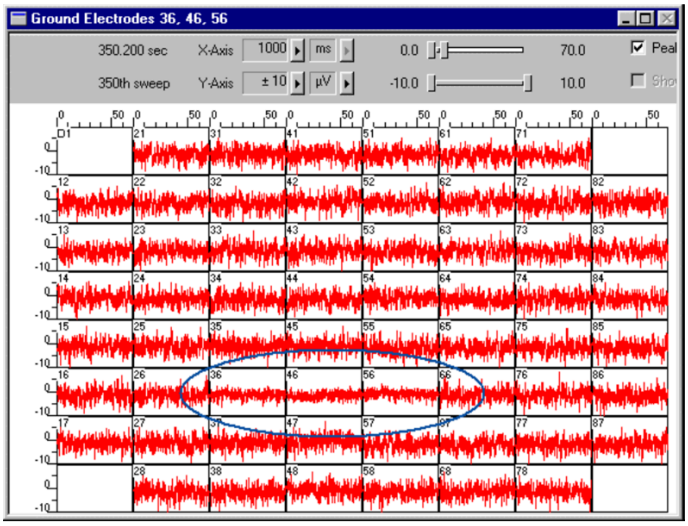

Figure 3.11: "MC_Rack" display. In this example the electrodes 36,46,56 are grounded. As a result, the noise level of these electrodes is reduced.

To sum up, this chapter gave the idea of the main functionalities that a MEA system has to integrate. In this way, it is possible to customize the new one for the desired applications.
The next chapter describes the customized MEA system aimed to study the amperometric or potentiometric recordings from dopaminergic neuronal cells.

Chapter 4

μG-SCD MEA system

4.1 Workstation for the extracellular recording with the μG-SCD MEA

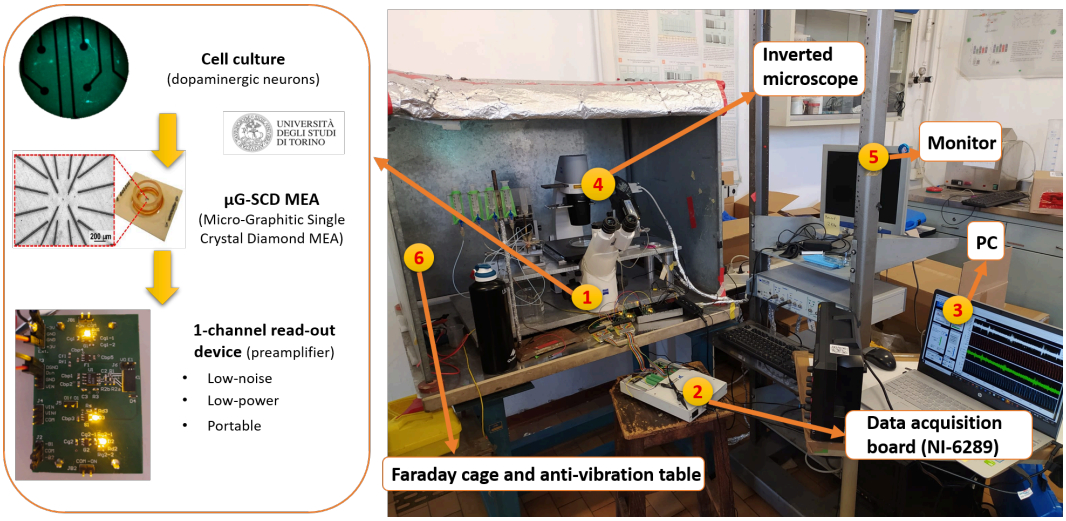

Figure 4.1: Sketch of the workstation for the μG-SCD MEA system.

In this chapter, a customized MEA system is presented. This system implements a 4×4 Micro-Graphitic Single Crystal Diamond Multi Electrode Array (μG-SCD MEA) chip realized by the University of Torino, a designed single-channel read-out device and a LabVIEW software interface.

The sketch of the extracellular recording system through the μG-SCD MEA is

shown in the figure 4.1.
The μG-SCD MEA is interfaced with a single-channel read-out device (preamplifier). This read-out device can be applied to just one selected working electrode and represents the starting point for realizing a complete preamplifier extended to all the 16 available channels. Contrarily to the commercial MEA read-out device, this system is customized to analyze the extracellular recordings from cultured neuronal cells. Specifically, it can interchange two different electroanalytical configurations, which can be almost simultaneously performed on the same chip. It is possible to select the electrode mode configuration for amperometric or potentiometric measurements.
In a similar way to the commercial MEA read-out device, the designed one also allows the simultaneous stimulation option. In particular, monophasic or biphasic patterns can be sent to the whole culture through an external AgCl reference electrode. Conversely to the commercial system, both the acquisitions and the specific stimuli are given by the National Instrument data acquisition board (NI-DAQ): the NI-6289. Consequently, a LabVIEW interface allows the visualization, recording, and post-processing of the extracellular signals. Overall, the whole system is protected within a Faraday cage to avoid electromagnetic interference and arranged over an anti-vibration table to limit every other kind of environmental noise. Finally, an inverse microscope with an external monitor is used to observe the cell culture during the experiments. To sum up, the two read-out devices are compared in the table 4.1.

Table 4.1: Comparison between the commercial device "MEA 1060-Inv-BC" and the μG-SCD MEA read-out device.

Commercial MEA read-out device	**μG-SCD MEA read-out device**
60-channels read-out device	Single-channel read-out device
Potentiometric electrode mode configuration	Potentiometric/ Amperometric electrode mode configuration
Recording on 59 WEs	Recording on 1 WE
Stimulation (optional) on 59 WEs	Stimulation (optional) on the RE
General-purpose stimulus generator + DAQ	NI-DAQ
Three software interfaces	LabVIEW interface

In the next paragraphs, every single component used for the following application is described. Overall, the text focuses on the main steps for designing the read-out device. Thus, its working principle for the amperometric and potentiometric measurements.

4.2 μG-SCD MEA

In this project, a 4 × 4 Micro-Graphitic Single Crystal Diamond Multi Electrode Array (μG-SCD MEA) realized by the University of Torino was used (figure 4.2). This model has a 4×4 matrix of 16 independent graphitic electrodes embedded into a single-crystal diamond substrate. The electrodes, characterized by a $\sim$ 20 × 3.5 μm^2 surface area, are aligned in a substrate of 5 × 5 × 0.4 mm^3 in size. As reported in the article [33], the electrodes were characterized through cyclic voltammogram analysis. In particular, they report a resistance of 5.3 ± 7.7 kΩ, depending on the length of the microelectrodes until the edges of the chip, and a normalized surface capacitance, given by the double-layer evaluation, of 2.24 ± 0.09 mF cm^{-2}.
The materials and the shape designed allow the analysis of the culture sample through inverted microscopy. The conductive properties of the graphite (active region) and the high biocompatibility, chemical inertness, insulation property, and optical transparency of the diamond are essential elements for good performances.

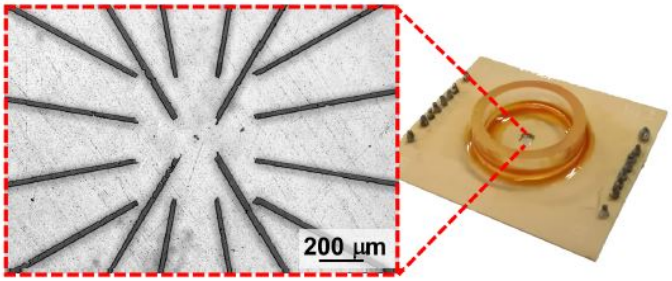

Figure 4.2: Micro-Graphitic Single Crystal Diamond Multi Electrode Array (μG-SCD MEA) [33].

To combine both materials, the MEA was processed using a MeV-ion-beam-implantation-based method by inducing the formation of vacancies throughout the diamond surface and then a temperature thermal annealing. This process allows the space-selective phase transition from the diamond to graphite to promote the conduction [35]. The end-points of the electrodes emerge in the center of the 1 mL culture dish chamber (Petri dish) to detect the biological signals and onto the surface's edges, allowing the interfacing with the designed read-out device and the LabVIEW input/output environment. In this work, the μG-SCD MEA chip was fixed on a signal collector chip for connecting the electrodes to the electronic read-out device (see figure 4.3). In this way, it was possible to interface the electronic device to the cell culture by choosing the desired electrode.
The MEA chip was used many times during previous experiments. Consequently,

before performing any measurement, it was necessary to confirm the working principle of the electrodes.
For this purpose, stimulation signals were injected through the NI-DAQ with an external reference electrode submerged in a physiological solution (pH 7.4 Tyrode's solution of (mM): 130 NaCl, 4 KCl, 2 CaCl_2, 2 MgCl_2, 10 glucose and 10 HEPES [35]). The signals resulted from the electrodes merged in the sample solution and collected on the green collector chip were then observed through the oscilloscope (Rigol MSO5104). It was necessary to check that the electrode response was the same in all the 16 electrodes.
From this check, it was possible to see that the electrodes 1, 2 and 8 did not work properly, thus they were excluded from the planned experiments.

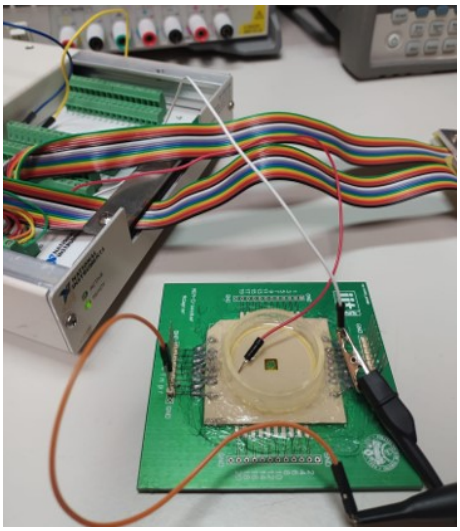

Figure 4.3: μG-SCD MEA on the signal collector chip (in green).

A working electrode with good performances in the presence of a monophasic and a biphasic stimulus has to show the behaviors illustrated in the figure 4.4.

In a real application, the μG-SCD MEA fixed on the green board collects the signals generated from the cell culture through external connectors to the read-out amplifier system. The LabVIEW interface communicates with the read-out system, selecting the electroanalytical configuration on the observed electrode and the stimulation by changing the V_{bias} potential on the external reference electrode (usually an Ag/AgCl). As said previously, these kinds of simulations are usually applied to observe the electroanalytical behavior of the cultured cells. In this case, the stimuli were applied to the solution just to test the response of the electrodes.

Figure 4.4: Working electrode response in a Tyrode solution. On the left: a monophasic stimulation of 1 V and a period of 100 ms (blue) and the electrode response (yellow). On the right: a biphasic stimulation of ± 1 V and 50 ms for each phase (blue) and the electrode response (yellow).

4.3 Single-channel read-out circuit

The first step in designing the external circuit was to consider the preamplification circuit for one single-channel (or electrode) of the μG-SCD MEA chip. In this way, it was possible to optimize the performances, study all the linked complications and give the main tools to the future device applied to all 16 electrodes. As said previously, the cultured cell's signals have very small magnitudes: 10-100 picoamperes for the currents and 10-800 microvolts for the spontaneous potentials. The main idea was to properly amplify those signals in the 0.3 - 1 kHz bandwidth, choosing an operational amplifier with low-noise specifications.
In the following subsections is explained how the circuit is implemented for each electroanalytical method.

4.3.1 Amperometric circuit

For converting a very small faradaic current into a readable value, a low-noise electronic interface is required. One of the standard read-out circuits used in this application is based on a trans-impedance amplifier (TIA) with a large gain and low noise. As shown in figure 4.5, this scheme is composed by an operational amplifier with a feedback resistance (R_{TIA}) which converts the current in an output voltage $V_{out,TR}$ [2]. The gain of the TIA (R_{TIA}) has to be large enough for amplifying the small inputs from the cells. In this work, a R_{TIA} of 10 MΩ was considered.

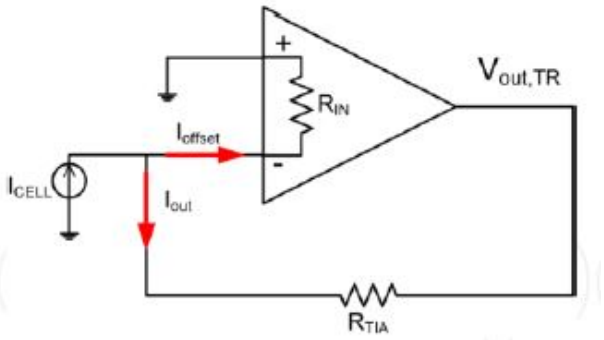

Figure 4.5: TIA circuit scheme [2].

The output signal is given by:

$$V_{out,TR} = -I_{CELL}R_{TIA} \tag{4.1}$$

where I_{CELL} is the input current and R_{TIA} the feedback resistance.
Consequently, the amperometric configuration mode in a two-electrodes system combined with an electronic interface of this kind can be simplified in the figure below. The V_{bias} on the RE is set at 800 mV to make possible the current diffusion through the WE, as advised in the article [33].

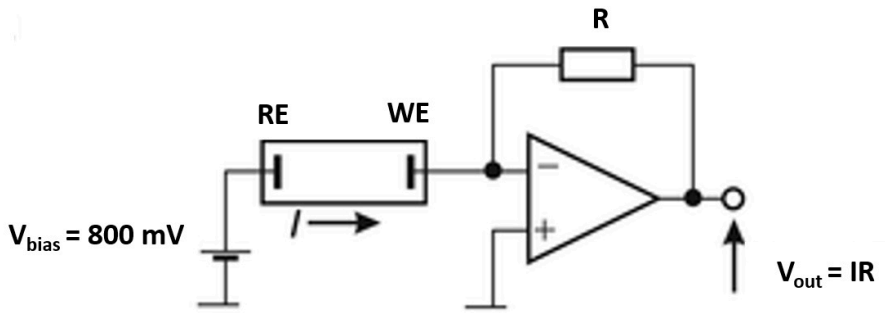

Figure 4.6: Amperometric electrode mode configuration interfaced with a TIA circuit.

The equation 4.1 is an ideal model. In a real situation (figure 4.7), an active element such as an operational amplifier, the thermal effects due to the circuit components and the total equivalent impedance of the electrodes and electrolyte interfaced with the external circuit (R_D and C_D) always introduce some limitations. Considering all the input noise sources statistically independent, the total power spectrum density (PSD) of the noise is summed by the following contributes:

1. the input-referred current noise of the operational amplifier ($\overline{i^2_{n-op}}$)
2. input-referred voltage noise of the operational amplifier ($\overline{e^2_{n-op}}$)
3. the thermal noise of the feedback resistor ($\overline{i^2_R}$)
4. the thermal noise of the electrode-electrolyte interface ($\overline{i^2_D}$)

In particular, due to the capacitive behaviour of the electrode-electrolyte interface, the thermal effect due to the resistor R_D is strongly frequency dependent. Its PSD is given by:

$$\overline{i^2_D} = \frac{4kT}{R_D(\omega)} \qquad \left[\frac{A^2}{Hz}\right] \tag{4.2}$$

Where k is the Boltzman constant and T the absolute temperature. The highest the frequency is, the lowest impedance (R_D and C_D) is given. Thus, this noise source can be minimized at low frequencies.

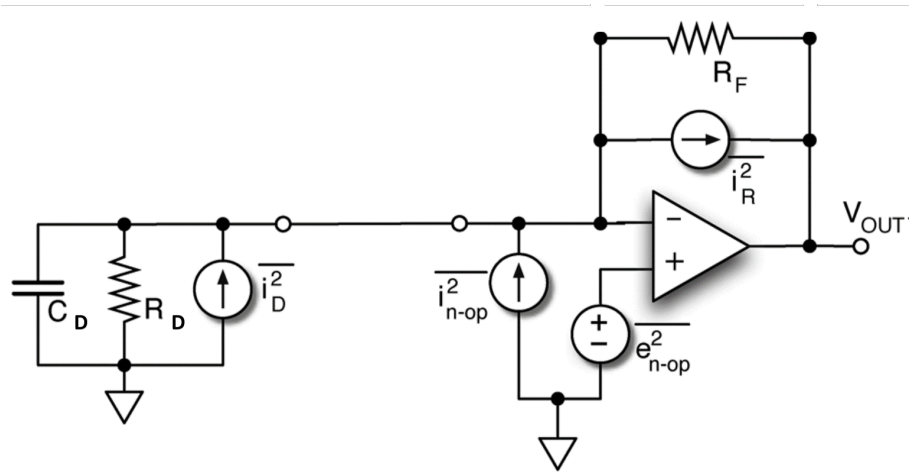

Figure 4.7: TIA coupled with noise sources [39].

These noise sources can limit the read-out of the small input current, decreasing the signal-to-noise ratio. In this application, it was essential to choose a R_F with a high value to properly amplify the small input of current from the cell culture. As a consequence, since the thermal noise contribution is flat with the frequency, the thermal noise due to the feedback resistor is the dominant noise contribution [39]. However, if a feedback capacitor C_F is added to the circuit (see figure 4.8), the thermal noise in a RC circuit does not depend directly on the value of the resistance. In fact, larger resistance creates more noise, but the designed low-pass filter also filters it more [40].

Moreover, the combination of the input capacitance to the electronic interface (later called C_{IN}) and the e_{n-op} without a feedback capacitor (C_F), can create an input current noise given by:

$$i_n = 2\pi e_{n-op} C_{IN} f \tag{4.3}$$

This noise increases linearly with the frequency, and in the worst case, can even become dominant to the thermal noise. Thus, it is important to add to the circuit a feedback capacitor C_F with a proper value. In this manner, the noise current can be flatted off and the stability of the TIA can be checked (read the subsection 4.3.4) [39].
To sum up, a simple solution to prevent this effect and improve the signal-to-noise ratio is to submit a capacitor C_F in parallel to R_F. Consequently, the circuit interfaced with the MEA chip can be schematized through the equivalent circuit of the figure 4.8.

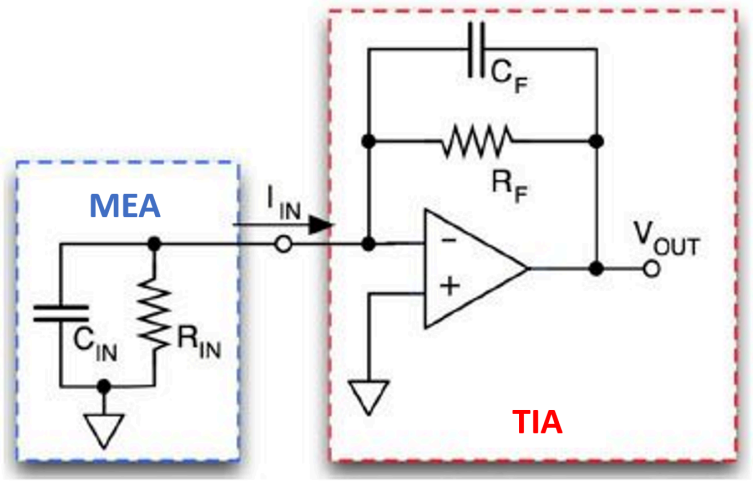

Figure 4.8: TIA circuit interfaced with an approximate equivalent model of a biosensor [39].

Thus, the transfer function of the TIA becomes:

$$V_{OUT} = \frac{R_F}{1 + j2\pi f R_F C_F} i_{IN} \tag{4.4}$$

The section 4.3.4 shows how the component values were specifically designed. In addition to these restraints, it is fundamental to limit the other sources of noise by choosing an operational amplifier that has [41]:

1. a very small input bias current (usually less than 2 pA) to read correctly the input current

2. a low voltage offset (usually less than $\pm$ 300μ V at low frequencies), which is less than a possible offset given by the electrodes (order of few tens mV)

3. a small current ($pA/\sqrt{Hz}$) and voltage noise ($nV/\sqrt{Hz}$)

4. a small input capacitance, to limit the signal distortion, but not too low for limiting the current leakages.

4.3.2 Potentiometric circuit

For reading the small potentiometric signals, it was chosen an Inverting Operational Amplifier (IOA) configuration (fig. 4.9).

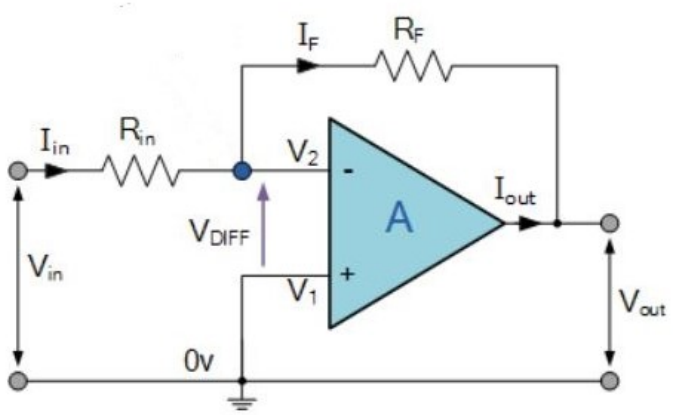

Figure 4.9: IOA circuit scheme [42].

The transfer function of this circuit is given by:

$$V_{out} = -V_{in}\frac{R_F}{R_{in}} \tag{4.5}$$

As a result, the potentiometric configuration mode in a two-electrodes system combined with the circuit of figure 4.9 can be simplified as shown below. The V_{bias} on the RE is set at 0 V to detect the spontaneous potentials between the two electrodes.

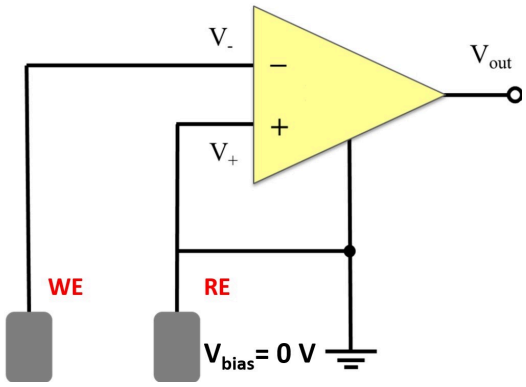

Figure 4.10: Potentiometric electrode mode configuration interfaced with an external IOA.

For this kind of configuration is important to choose an operational amplifier with [43]:

1. low-input offset voltage (low than $\pm$ 300 μV)
2. a small voltage noise ($nV/\sqrt{Hz}$)
3. an appropriate gain-bandwidth product (GBP)
4. a good slew rate to minimize the slew-induced distortion.

The main idea for designing the single-channel read-out device was to choose a single operational amplifier for both circuits. In this way, in a future project that implements all the available electrodes of the MEA chips, the number of components is minimal. Moreover, the noise restraints in the potentiometric circuit are similar to those in the amperometric one. Thus, a particular circuit for each electroanalytical method with the same operational amplifier can be implemented. Since the potentiometric signals are characterized by an amplitude of 10-800 μV, the gain for this electroanalytical method was fixed at 1000. A R_{in} of 10 kΩ was then chosen. In addition to this, when R_F assumes large values, such as in this application, it is usually advised to introduce components that reduce the thermal noise, which affects the measurements. For this purpose, the capacitor C_F in parallel to R_F added previously improves also the filtering efficiency and the circuit stability in this case.

The next section describes how the operational amplifier was selected for accomplishing both the electroanalytical methods.

4.3.3 Low-noise operational amplifier

As said previously, the main component of the read-out device is the operational amplifier. Moreover, the operational amplifier properties have to fit with both amperometric and potentiometric configurations properly. According to this purpose, different datasheets had to be compared. The following list shows the ones that could mainly satisfy the specifications mentioned above:

1. AD8034
2. AD8646 and AD8067
3. ADA4530-1
4. LTC6268 or LTC6268-10

The choice was carried on by observing each characteristic reported and throughout the simulation software LTspice®.
In particular, each operational amplifier was simulated in the amperometric configuration and the potentiometric one. As reported in the section 2.2, 10 - 100 pA signals for the amperometry and 10 - 800 μV for the potentiometry are expected. According to these input ranges, some DC simulations in LTspice® were performed to study if the input bias currents and the voltage offsets of each operational amplifier could affect the measurements.
The resulting circuit schematics are represented in the figure 4.11. Each circuit reported a gain of 10^7 for the TIA (equation (4.1)) and 1000 for the IOA (equation (4.5)).

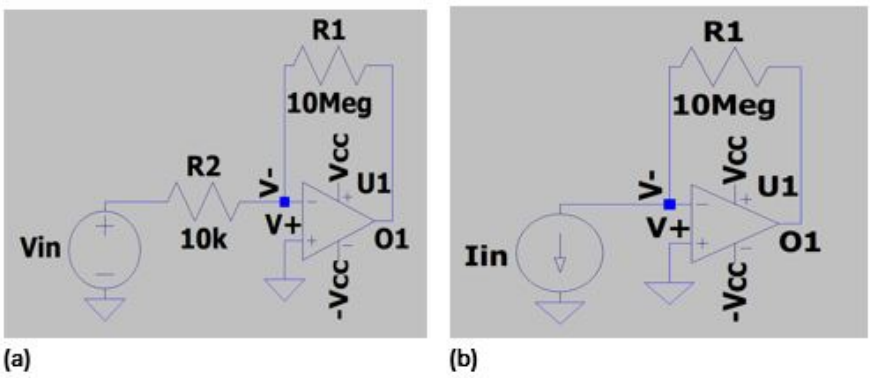

Figure 4.11: LTspice® simulations scheme (a) amperometric circuit (b) potentiometric circuit.

Each operational amplifier characteristics and performances were compared as follows:

1. AD8034. The specifications of this operational amplifier can be compared in the table 4.2.

Table 4.2: AD8034 FET operational amplifier specifications.

Specifications	**Typ. value**
Input bias current (pA)	2
Input voltage offset (mV)	1
Input current noise (fA/ $\sqrt{Hz}$)	f= 100 kHz 0.7
Input voltage noise (nV/ $\sqrt{Hz}$)	f=100 kHz 11
Input source capacitance (pF)	1.7
Supply voltage (V)	± 12
GBP (MHz)	80

As it is possible to see from the table 4.2, the AD8034 needs a high dual power supply, which can be a problem in terms of consumption for this kind of application. Moreover, from the LTspice® simulations, it was possible to observe that the operational amplifier had:

(a) high input bias currents (around 2 pA). In fact, with 10 pA of input, the read-out current was 7.89 pA, while with an input current of 100 pA, the read-out current resulted in 9.79 pA.

(b) high input voltage offset (typ. 1 mV), which is not suitable for the potentiometric configuration.

2. AD8067 and AD8646. These operational amplifiers have similar characteristics, thus they were studied simultaneously. Their useful specifications are shown in the table 4.3 . From the specifications below, it is possible to observe that both the operational amplifiers work with a lower supply voltage and are characterized by a low input bias current.

Table 4.3: AD8067 and AD8646 FET operational amplifiers specifications.

Specifications	**AD8067 (typ.)**	**AD8646 (typ.)**
Input bias current (pA)	0.6	2
Input voltage offset (mV)	0.2	0.3
Input current noise (fA/$\sqrt{Hz}$)	f= 10 kHz 0.6	f= 10 kHz 0.6
Input voltage noise (nV/$\sqrt{Hz}$)	f=10 kHz 6.6	f=1 kHz 8
Input source capacitance (pF)	2.5	2.5
Supply voltage (V)	± 5	± 5
GBP (MHz)	54	24

Moreover, the simulations showed a good response for each input current, above all for the AD8067 operational amplifier. An output current of 9.59 pA (9.50 pA for the AD8646) resulted from an input of 10 pA and 99.5 pA (97.9 pA for the AD8646) from 100 pA.
However, despite these good performances, the LTspice® simulations highlighted high input voltage offsets for this application. In the simulated circuit, an offset compensation was required for both components. In addition to this, the input source capacitance had a relatively large value for both cases.

3. ADA4530-1. This operational amplifier has very good performances due to its femtoampere input bias current. The main specifications are shown below.

Table 4.4: ADA4530-1 operational amplifier specifications.

Specifications	**Typ. value**
Input bias current (fA)	± 20
Input voltage offset (μV)	8
Input current noise (fA/$\sqrt{Hz}$)	f= 0.1 Hz 0.07
Input voltage noise (nV/$\sqrt{Hz}$)	f=10 kHz 14
Input source capacitance (pF)	8
Supply voltage (V)	± 5
GBP (MHz)	2

It reports advantages in terms of:

- very low input bias currents
- low input voltage offset
- very low input current noise
- a low dual voltage supply.

The LTspice® simulations showed good performances in both circuits. The ADA4530-1 was not the operational amplifier chosen because there was no version with more than two operational amplifiers in the same package. In fact, the read-out device has to integrate few components in a future perspective, guaranteeing the device portability. Moreover, it showed a relatively high input voltage noise, limited gain-bandwidth product, and high input source capacitance in both configurations (differential and common mode). However, it could be a good candidate for working electrode measurements.

4. LTC6268 and LTC6268-10. These operational amplifiers fit properly to this application. The two operational amplifiers are characterized by the following specifications.

Table 4.5: LTC6268 and LTC6268-10 FET operational amplifiers specifications.

Specifications	**LTC6268 (typ.)**	**LTC6268-10 (typ.)**
Input bias current (fA)	± 3	± 3
Input voltage offset (mV)	0.2	0.2
Input current noise (fA/$\sqrt{Hz}$)	f= 100 kHz 5.3	f= 100 kHz 7
Input voltage noise (nV/$\sqrt{Hz}$)	f=1 MHz 4.3	f=1 MHz 4.0
Input source capacitance (fF)	100	100
Supply voltage (V)	± 3	± 3
GBP (MHz)	420	4000

Remarkably, they represented a good compromise compared to the ADA4530-1. In addition to the extremely low input bias current, the LTC6268 and LTC6268-10 are also characterized by a higher gain-bandwidth product, a low input source capacitance, and low voltage noise. Similarly, they require a low dual supply voltage.
Moreover, it is possible to buy two operational amplifiers in the same package, an advantage for designing a more complex system integrating all the available working electrodes. Finally, they also implement a SOIC package with two unconnected pins that can be used, in a PCB design, to create an input guard ring to protect the circuit against leakage of currents (as explained later in the section 4.5.3).
LTspice® simulations with these two components did not show significant differences: they performed a good read-out of the input ranges in both configurations. Thus, it was chosen the one with the best specifications. In conclusion, the LTC6268 was selected because it has a lower input current noise.

To sum up, LTspice® simulations helped to compare different kinds of operational amplifiers and choose the main one whose characteristics fit better into the design of the project. The results reported that LTC6268 was selected to correctly read the low bio-electroanalytical signals and follow its sub-millisecond time variations. However, this software simulator is not enough to predict the circuit stability and the noise in an application with cell cultures, so further tests had to be performed. The following section describes the additional components added for filtering, improving the stability of the circuit and their values assigned.

4.3.4 Filtering and component values design

As seen from the previous subsection, LTC6268 is a very low input capacitance, input-referred current noise, and voltage noise operational amplifier. Despite this, the source noise list in the subsection 4.3.1 contributes to affect the measurements, above all in the amperometric configuration, which is the most critical.
It was explained that the performance of the circuit could be improved by adding passive filtering elements (read subsection 4.3.1 and 4.3.2). Specifically, in both the electroanalytical configurations, a feedback capacitor C_F had to be added in parallel with the feedback resistor R_F to improve the signal-to-noise ratio and avoid problems linked to the coupling of the total input capacitance (C_{IN}) with the operational amplifier. Thus, the first step was to optimize the value of the feedback capacitor to fulfill the requirements for both circuits. In addition to this, similarly to the commercial system, the potentiometric circuit implemented a specific band-pass filter. While, in both configurations, a passive low-pass filter was added at the output of the operational amplifier. The choice of each electrical circuit component is addressed in detail as follows.

Design of the feedback capacitor (C_F)

The technical documentation of the LTC6268 by *Linear Technology Corporation* explains how to design the feedback value properly. The operational amplifier contributes to the noise in terms of:

1. the input-referred voltage noise (called e_{n-op} in the section 4.3.1).
2. the input-referred current noise (called i_{n-op} in the section 4.3.1).

These noises also depend on the input capacitance C_{IN} (see figure 4.13). If C_{IN} is low, the input-referred current noise is reduced, while a higher noise gain amplifies the input-referred voltage noise [44].
Particularly, the last, as said in the 4.3.1 section, linearly increases with the frequency when coupled with the C_{IN}. Consequently, the input-referred voltage noise is usually dominant to the one related to the current.

When the operational amplifier configuration is just resistive, or characterized only by the feedback resistor R_F, C_{IN} and R_F create a pole at a specific noise gain which is calculated by the feedback factor $\beta(j\omega)$ [45]:

$$\beta(j\omega) = \frac{1}{1 + j\omega R_F C_{IN}} \tag{4.6}$$

Thus, the feedback factor can indirectly give information about the noise gain because its reciprocal represents the backward attenuation factor from the output to the input. Consequently, the pole created by C_{IN} can give rise to some oscillations and phase shift [44], that had to be checked. These oscillations are described by the natural frequency ω:

$$\omega = \sqrt{\frac{2\pi GBW}{R_F C_{IN}}} \tag{4.7}$$

The operational amplifier in a just resistive configuration was so studied in MATLAB. The parameters were set in the following code.

```
GBW=1.5*10^8;          % Gain-Bandwidth Product (Hz)
f=0:100:2.8*10^8;      % Range of frequencies (Hz)
A_vol= 200*10^3;       % DC open-loop gain (V/V)
Rf= 10*10^6;           % Feedback resistance (Ohm)
Ci=100*10^-15;         % Input differential op amp
                       capacitance (F)
C_MEA=20*10^-12;       % Approximated input
                       MEA-eletronic capacitance (F)
CIN=Ci+C_MEA;          % Total input capacitance (F)
```

From the code, the input capacitance C_{IN} was calculated with the parallel of the internal input capacitance of the operational amplifier and the approximated input capacitance of the MEA-electronic interface [46]. As a result, the single-pole response is given by:

$$A_{VOL}(j\omega) = \frac{A_{VOL}}{1 + j\omega R_F C_{IN}} \tag{4.8}$$

The open-loop gain and the reciprocal feedback factor versus frequency were plotted to explain why the circuit can oscillate.
In the figure 4.12, it is possible to see that these two trends intercept each other at a specific frequency, called intercept frequency (f_i). This frequency was an important parameter that indicates if the circuit had enough phase margin and few oscillations. According to the Barkhausen stability criterion, the circuit stability of the TIA could be checked by observing the rate of closure (dB/dec) of the two curves nearby f_i: if $A_{VOL} \geqslant 1/\beta$ the circuit would be stable. Moreover, if the phase shift is close to 360 degrees nearby f_i, heavy self-sustaining oscillations would be

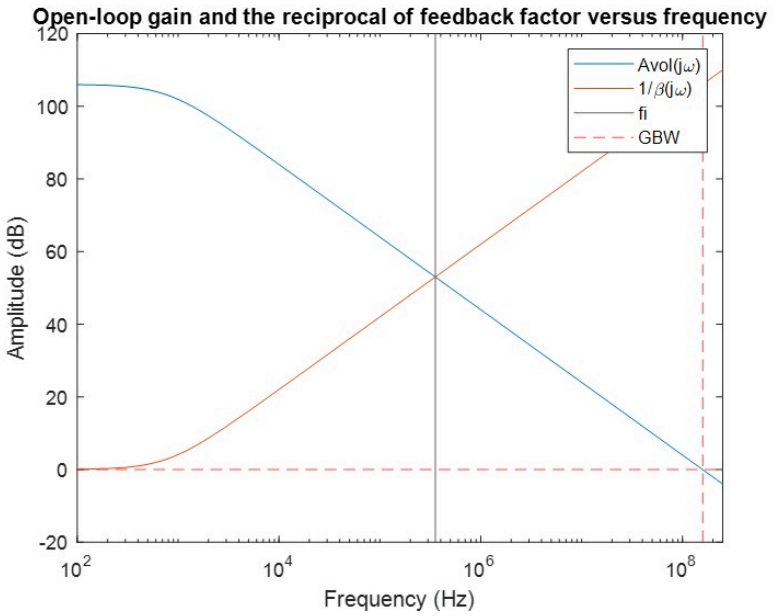

Figure 4.12: $A_{VOL}(j\omega)$ (blue) and $1/\beta(j\omega)$ (red) vs. frequency. The plot denotes the rate of closure between f_i (black) and observes the instability of the circuit. Moreover, the red dashed line indicates the GBW value as the frequency that intercepts the Avol at 0 dB.

present [46].
As expected from the previous observation, this configuration showed a rate of closure of about 40 dB/dec, which meant that $1/\beta \geqslant A_{VOL}$, thus there could be a phase shift and so oscillations. For this reason, a feedback capacitor was added, as shown in the complete circuit scheme of figure 4.13.

To minimize the oscillation and so shift the pole it was important to find the minimum value of the feedback capacitor C_F that guaranteed the stability. A small C_F made sure that the noise gain $(1/\beta)$ flatten out.
The feedback factor and the open-loop gain formulas with the adding of C_F became:

$$\beta(j\omega) = \frac{1 + j\omega R_F C_F}{1 + j\omega R_F (C_{IN} + C_F)}; \quad A_{VOL}(j\omega) = \frac{A_{VOL}}{1 + j\omega R_F (C_{IN} + C_F)} \tag{4.9}$$

As it is possible to see from the equations 4.9, the feedback factor in this case has a zero that balances the pole that originates the oscillations.
The optimal C_F was solved through a graphical approach, by finding the value of the intercept frequency f_i. In fact, the f_i is the vertex of the formed triangle

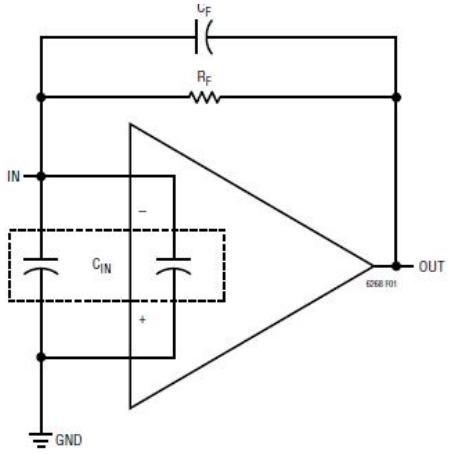

Figure 4.13: LTC6268: addition of the feedback capacitor [39].

between the two curves and the x axis. Thus, f_i was calculated as:

$$f_i = \sqrt{\frac{GBW}{2\pi R_F(C_F + C_{IN})}} \tag{4.10}$$

And it could also be found f_i with the following formula:

$$f_i = \frac{1}{2\pi R_F C_F} \tag{4.11}$$

From the combination of the equations 4.10 and 4.12, the ideal C_F was given by:

$$C_F = \frac{1}{2\pi R_F GBW}(1 + \sqrt{1 + 8\pi R_F C_{IN} GBW}) \tag{4.12}$$

Compiling the MATLAB code, the resulted ideal C_F was equal to its first nearest commercial value, that was 0.07 pF. This value represented the minimum required to ensure the stability of the circuit (see the yellow trend in the figure 4.15). Moreover, it is recommended an overcompensation take into account possible further limitations of the circuit. Therefore a C_F of 10 pF was chosen to ensure that the circuit would be very stable. At the same time, this value guaranteed that the noise gain curve is not completely flat, thus avoiding a very slow response (see the purple trend in the figure 4.15).
The low-pass filter pole resulted by the addition of the C_F in parallel to R_F could so be calculated as $1/(2\pi C_F R_F)$, obtaining a cut-off frequency 1.59 kHz.

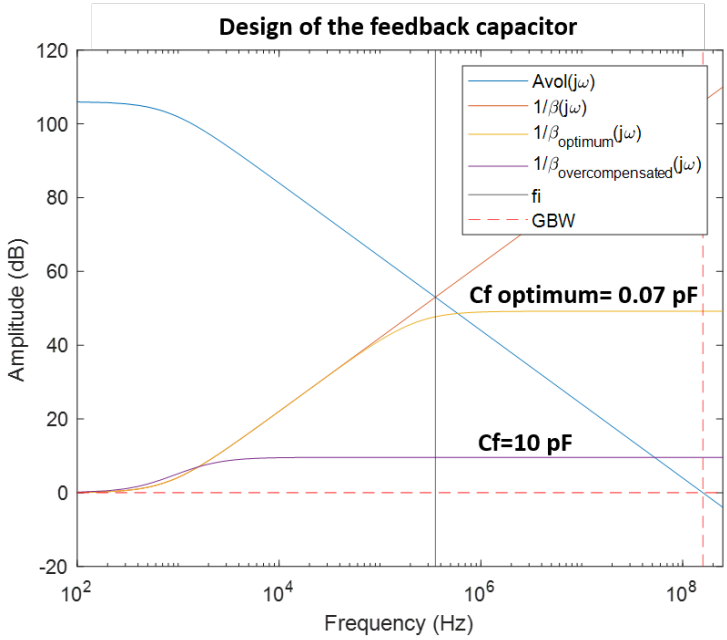

Figure 4.14: $A_{VOL}(j\omega)$ and $1/\beta(j\omega)$ vs. frequency. Each feedback gain plot represents a specific value of the feedback capacitor C_F. In particular, the optimal value (yellow trace), 0.07 pF, and the overcompensated one (purple trace), 10 pF (chosen value).

To sum up, this first step helped design the value of C_F and guarantee the stability of the circuit.
The following section describes the other filters added to the two circuits for further improving the performances.

Band-pass filter in the potentiometric circuit

As shown in the chapter 3, a read-out device typically uses an offset compensation, introducing a low-frequency zero in the circuit transfer function.
For this reason, a band-pass filter with a zero at 1.59 Hz, to not cut the slow extracellular signals, was added to the IOA circuit. Consequently, a capacitor of 10 μF was selected (see figure 4.15).
According to it, if a DC offset is present at the input of the preamplifier, the small capacitance restores the baseline to zero with the introduction of a certain delay of around 1 minute (this delay was taken into account in the LabVIEW interface 4.5.4).

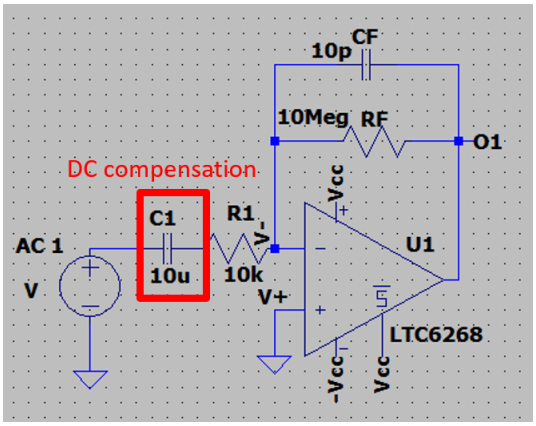

Figure 4.15: Potentiometric circuit scheme in LTspice®. Band-pass filter implementation.

Additional filtering and final circuit schemes

The two schematics were further improved by adding a passive low-pass filter ($R2$ and $C2$) with a cut-off frequency of 1.59 kHz to the outputs and an input capacitor ($C1$). The single-pole of the passive low-pass filter was useful to reduce the noise beyond the pass-band gain of the signal. Consequently, the output RC filter behaves as an anti-aliasing filter, reducing the amplification of the signal coupled with the noise at higher frequencies. Instead, the input capacitance was added to limit even more the effect of the input bias current.
Finally, the amperometric final circuit is shown in the figure 4.16. While the potentiometric one is represented in the figure 4.17.

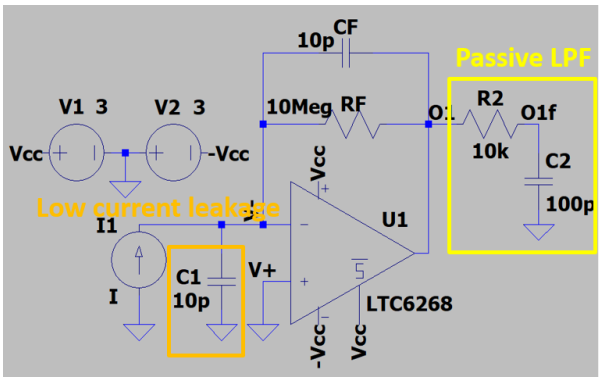

Figure 4.16: Final amperometric circuit.

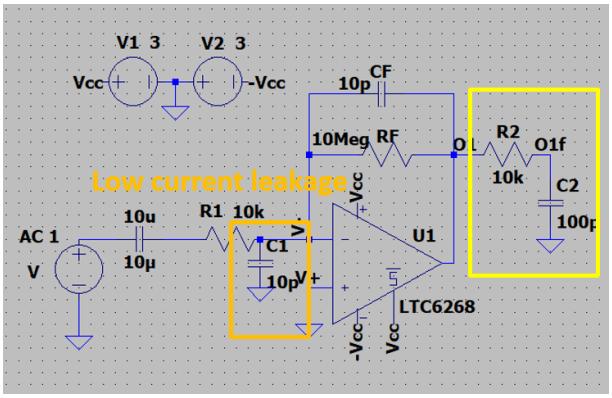

Figure 4.17: Final potentiometric circuit.

To sum up the characteristics of the final circuits, the Bode plots related to the two electroanalytical measurements were simulated through LTspice®, as shown in the figures 4.18 and 4.19.

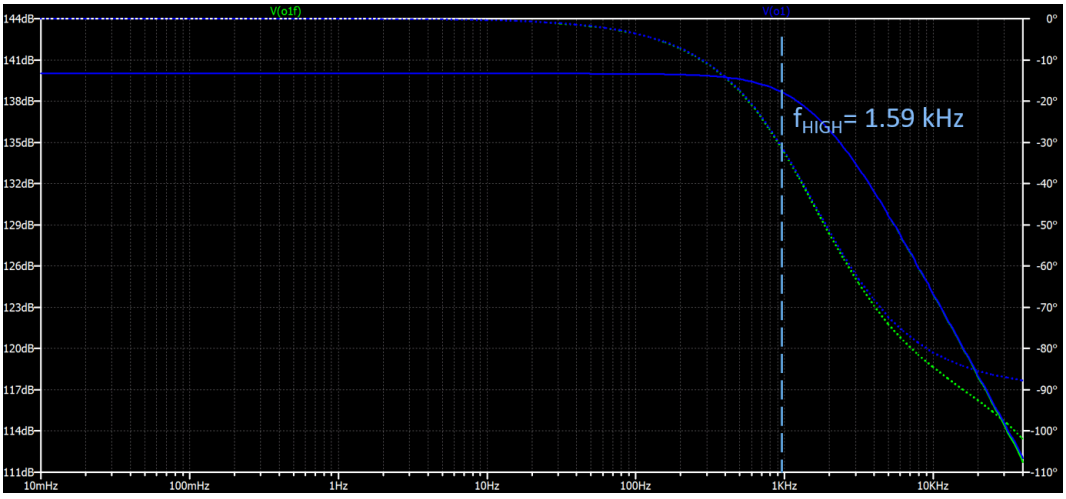

Figure 4.18: Amperometric Bode plot. Bode magnitude plots (in blue) and Bode phase plots (blue and green dashed traces). In the blue dashed trace, the phase plot of the direct output (O1). In the green dashed trace, the phase plot of the filtered output (O1f).

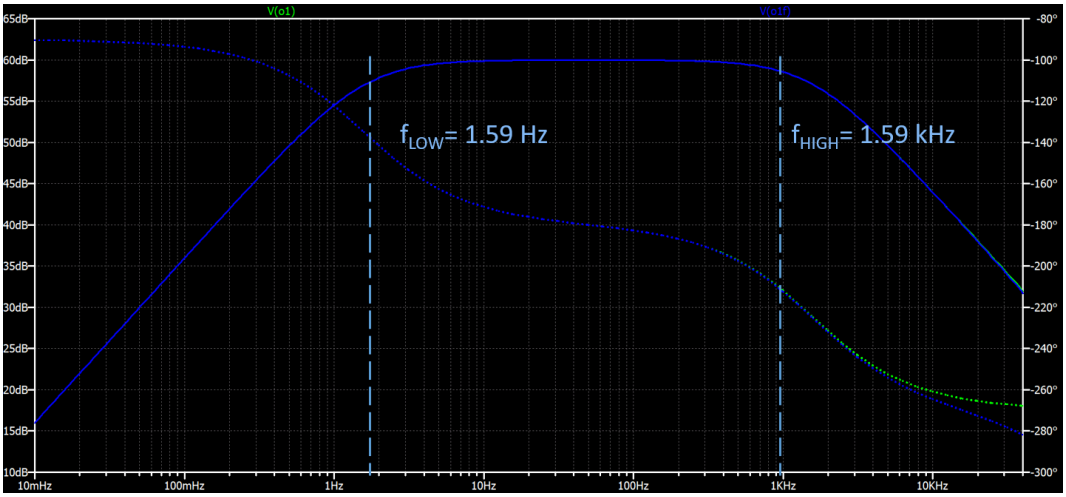

Figure 4.19: Potentiometric Bode plot. Bode magnitude plots (in blue) and Bode phase plots (blue and green dashed traces). In the blue dashed trace, the phase plot of the direct output (O1). In the green dashed trace, the phase plot of the filtered output (O1f).

In the next section, the designed circuits were tested on the breadboard to check their general working principle.

4.4 Test of the circuits

Before proceeding with the design of the printed circuit board of the single-channel read-out device, the circuits had to be evaluated. Thus, some tests were performed. Despite this, it was easy to observe all the difficulties of simulating very small bio-signals through tabletop instrumentation. The following tests were not enough to predict the performances of the circuit interfaced with extracellular signals.

4.4.1 Test of the TIA circuit

Generating very small currents of few tens of picoamperes (10-100 pA) is challenging. However, the small input current source of a trans-impedance operational amplifier, which is amplified by the high gain of the TIA, could be simulated by a photodiode whose equivalent model is made by a current source (I) in parallel with a junction capacitance (C) 4.20.
A photodiode operates correctly if inversely polarized, that is, if the voltage at its terminals is higher in the cathode (n zone) than in the anode (p zone). Typically, the photo-current output changes linearly with the incident light power, from a

few picoamperes up to a few milliamperes. Moreover, the photodiode should be set in a photovoltaic mode to contain the noise and make possible the detection of small measurements [47].

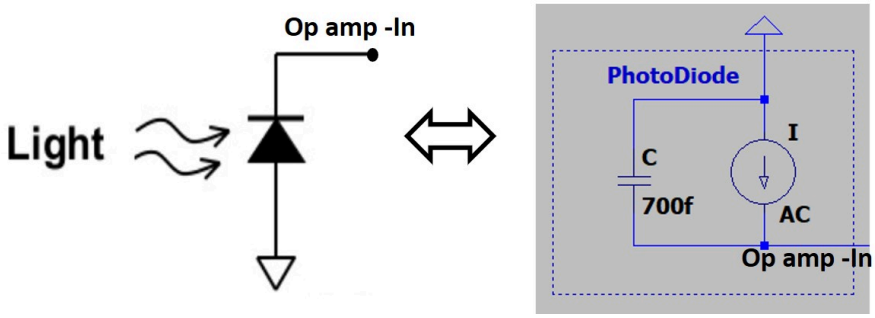

Figure 4.20: Photodiode in a photovoltaic configuration (on the left) and the equivalent circuit model in LTspice® (on the right).

However, all the features of a photodiode were not necessary to this application. Thus, a cheap component sensitive to visible light was used to test the behaviour of the TIA circuit in the presence of low currents. For this purpose, this simulation were performed by using a LED as a photodiode in a photovoltaic configuration (see figure 4.21).

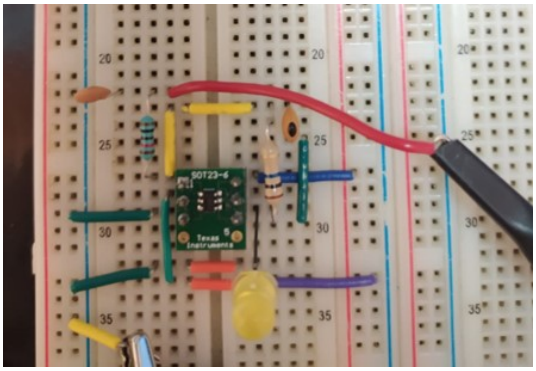

Figure 4.21: Yellow LED as the low current input source of the LTC6268 TIA's circuit.

All LEDs, in addition to emitting light, are also sensitive to light. As a result, they are not as sensitive as photodiodes which are explicitly designed for this purpose.
Despite this, LED allows reading an electrical signal proportional to the light

intensity. Generally, they are more sensitive towards the wavelength for which they were built.
For this purpose, it was implemented a yellow LED mostly sensible to light sources of typically 589 nm (yellow light). After adding the LED in a reverse bias mode to the LTC6268 circuit (figure 4.21), it was observed that the system could detect even the environmental light by covering and uncovering the LED with a black box.
The main simulations were then performed using a mobile phone flashlight, and the outputs from the TIA were observed on the oscilloscope (Rigol MSO5104). Through a bench multimeter (34401A Digital Multimeter), it was possible to see that, with the minimum distance between the LED and the light source, the LED could detect a maximum current of about 1-3 μA. From this result, it was possible to hypothesize that the current injected from the environmental light or the flash source with a larger distance was even smaller. In fact, the values of the currents were impossible to be measured accurately because of the environmental light noise and the main variables linked to the setup of the measurement (e.g., incident lights, the distance between the light source and the breadboard). The working principle

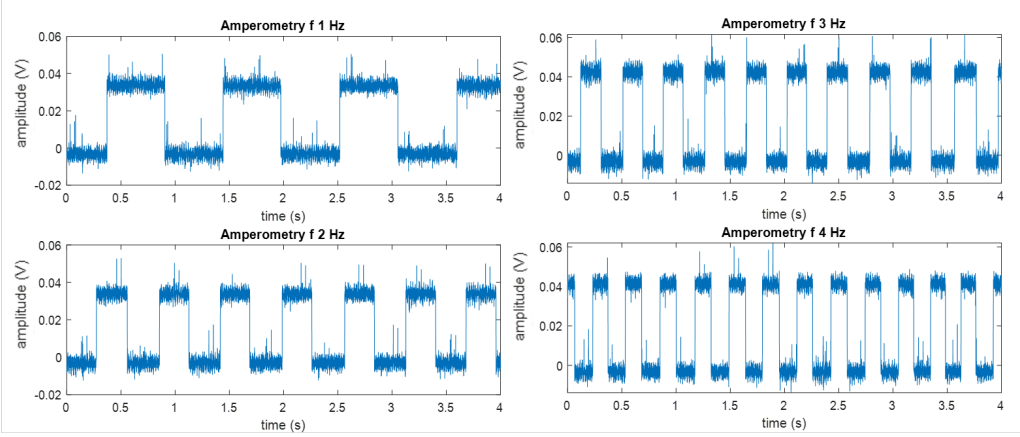

Figure 4.22: Test of the TIA circuit. Plots of the output voltages after applying a mobile phone flashlight with four available frequencies: 1 Hz, 2 Hz, 3 Hz and 4 Hz.

of the TIA circuit was tested not only by detecting small currents but also small currents at different frequencies. An Android app ("Flashlight") that controls the mobile phone flashlight in terms of frequency was chosen to fulfill this request. Through it, four kinds of frequencies were selected: from 1 to 4 Hz. The mobile phone was set at the same distance through a box 4×4 cm, and the four different frequencies were applied. The related output voltages from the TIA were then

collected through the NI-6289 DAQ, saved from a LabVIEW interface in a LVM file extension, and finally plotted on MATLAB. The results can be observed in the figure 4.22. The results showed that the system could detect the small current peaks and followed the change of frequencies. From the vertical sensitivity of the amplitude axis and the known gain of the TIA (10^7), the currents involved in this setup were approximate of few nano amperes. The values obtained were far from the tens picoamperes requested from a typical amperometric measurement with cell cultures. Thus, the performances of this configuration can be adequately proved just with the setup of interest.

4.4.2 Test of the IOA circuit

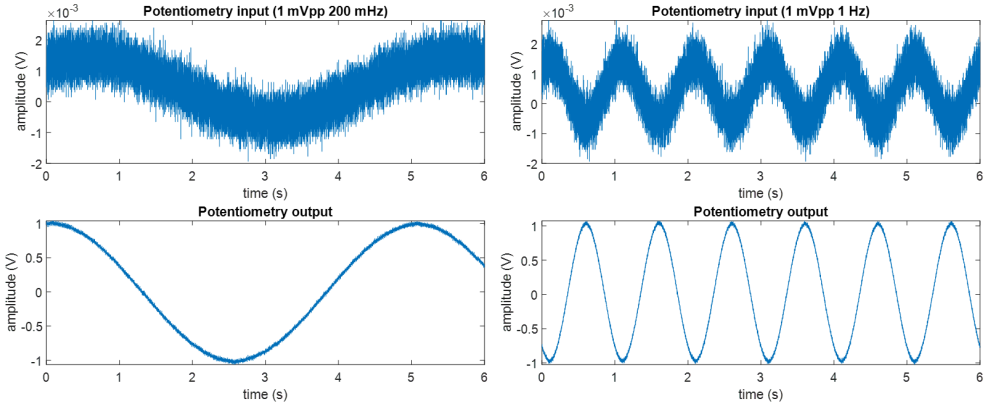

Figure 4.23: Test of the IOA circuit. On the top, the IOA inputs. On the bottom, the output voltages. On the left, the input and output voltages resulted from the injection of a sinusoid of 1 mV_{pp} and 200 mHz. On the right, the input and output voltages resulted from a sinusoid of 1 mV_{pp} and 1 Hz.

For simulating the detection of the spontaneous neuronal potentials (about 10-800 μV), the LTC6268 operational amplifier circuit in the IOA configuration was tested with the introduction of low-frequency sinusoidal waveforms.
The external function-arbitrary waveform generator, an Agilent 33250A of 80 MHz, was set to perform the minimal available parameters. This model could perform sinusoidal waves of the minimum amplitude of 1 millivolt peak-to-peak, which is almost near the extreme value of the range of the extracellular signals. After considering the amplitude limitations, there were then chosen two sinusoidal signals of the same amplitude (1 mV_{PP}) and two different low frequencies of, respectively, 200 mHz and 1 Hz. The input voltage signals were then sent to the IOA, and both the inputs and outputs were collected with the LabVIEW interface and plotted on

MATLAB. As a result, the input signals and the relative amplified output signals (IOA gain of 1000) are shown in the figure below.
The general working principle of the two circuits was demonstrated. Thus, the printed circuit board could be finally designed.

4.5 Printed circuit board of the single-channel read-out device

The single-channel read-out device was designed with Altium Designer (Altium Ltd.). The size of the board was set to 4.08 × 6.48 cm. The complete preamplifier schematic, which integrates the two circuits (TIA and IOA) to be applied to the two electroanalytical measurements, can be seen in the figure below. While, the 3D model can be seen in the figure 4.25.

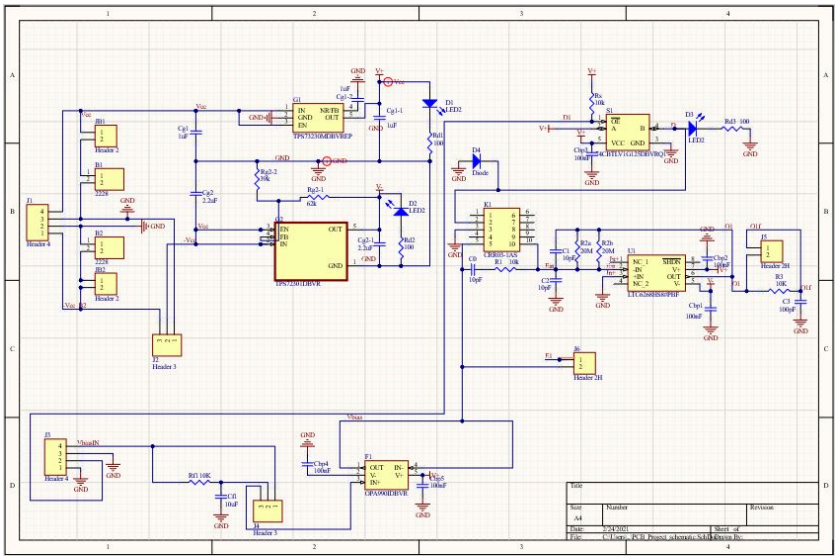

Figure 4.24: Single-channel preamplifier PCB schematic.

4.5.1 Mode of operation of the PCB

The mode of operation of the PCB can be explained dividing the schematic in three parts:

1. Power supply circuit schematic.
   As further analyzed, the preamplifier device needs a dual power supply of ± 3 V. The figure 4.26 shows the power supply schematic, which integrates

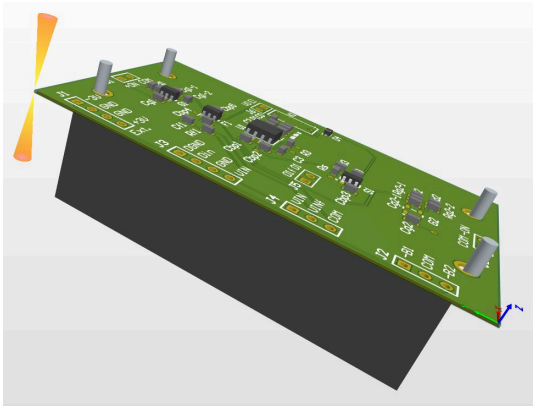

Figure 4.25: 3D model of the single-channel preamplifier PCB.

two external lithium batteries of 3.6 V on the bottom layer of the PCB (see the black elements in the 3D picture 4.25). Three external jumpers have to be connected to the connectors $JB1$ and $JB2$ to link the input voltages to the voltage regulators: one for the positive voltage supply, the other for the negative one. The two LEDs ($D1$ and $D2$) were integrated into the circuit to confirm if the power supply occurred. Finally, the additional header ($J1$)

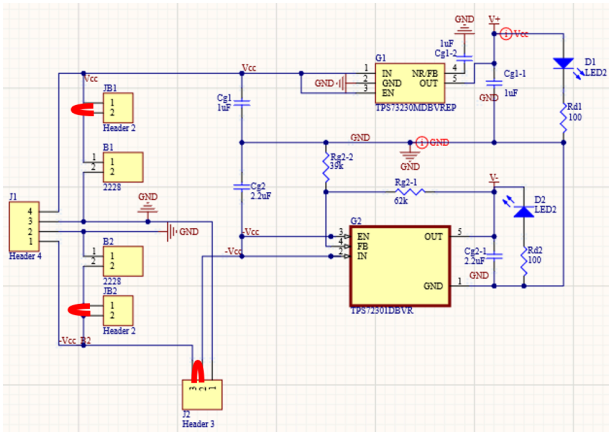

Figure 4.26: Power supply electric schematic. The external jumpers (red archs) have to be added to connect the lithium batteries.

was added for testing the PCB by giving an external power supply with a programmable DC power supply (Rigol DP832A with 3 Channels).

2. Electroanalytical configuration modes circuit schematic.

The two circuits for the amperometric and potentiometric measurements (figures 4.16 and 4.17) were implemented into the schematic below. The input from the electrode of the MEA is taken from the pin 1 of the header $J6$ ($E1$). The element that allows the switching of the configuration is the SPST (Single Pole Single Throw) reed relay (CRR03-1AS). This element is driven by the switch $S1$, which is consequently driven by a high/low logic output from the NI DAQ through the digital signal called $D1$. To check if the reed relay is switched, a LED ($D3$) was added to the output of the switch. The mechanism is explained as follows. When the reed relay switch is open (see pin 5 and 10 in the figure 4.27), the resistance R1 in series with C0 is not short-circuited, so the schematic is configured in potentiometry. In this case, the open resistance of the relay can be considered negligible (typically around 150 Ω). On the other hand, R1 and C0 are short-circuited. The low input current from the electrode $E1$ passes through pins 5 and 10 of the reed relay and arrives at the inverting input of the LTC6268 operational amplifier.

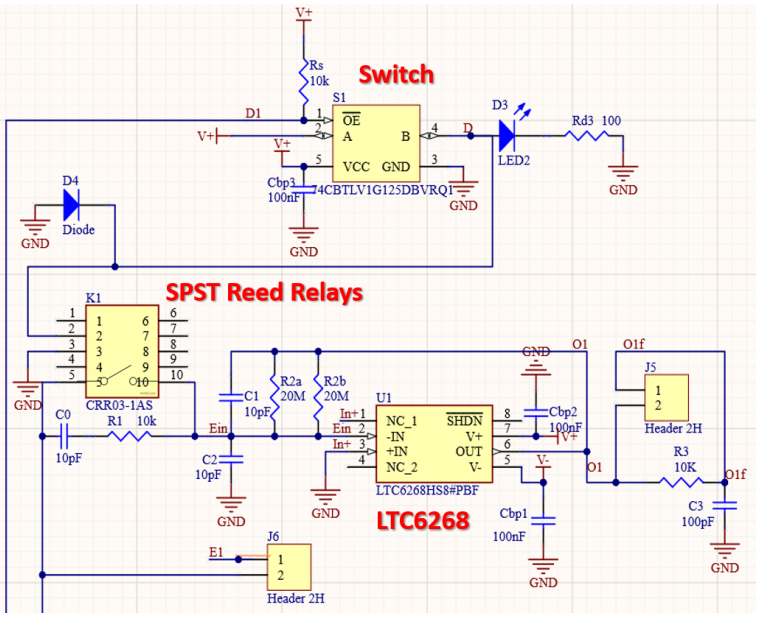

Figure 4.27: Electroanalytical configuration modes circuit schematic. The amperometry is possible when the reed relay is closed, while the potentiometry when the reed relay is opened. The logic signal driven by the LabVIEW interface ($D1$) arrives at the switch ($S1$) and consequently at the reed relay ($K1$).

Moreover, a diode ($D4$) is connected in parallel to the relay coil. Since an inductor (the relay coil) cannot instantly change its current, the diode provides

a path for the current when the coil is not supplied. Otherwise, a voltage spike would occur, causing arcing on the switching contacts or other damages. Finally, the amplified outputs (filtered and no-filtered) from the operational amplifier ($U1$) are then collected on the header $J5$, from which they are sent to the LabVIEW interface.

3. Bias voltage circuit schematic.
   The user can select the bias voltage provided by the NI DAQ on the header $J3$ (pin 4) through the LabVIEW interface.
   This voltage can be low-pass filtered, stabilized, throughout the operational amplifier ($F1$), and externally collected from the header $J6$ (pin 2). The output has to be placed into the analyte throughout the external reference electrode.
   It was important to hold this voltage at a constant value, as explained in the section 2.2. Therefore, an operational amplifier voltage buffer and LPF with a cut-off frequency of around 16 kHz were implemented.

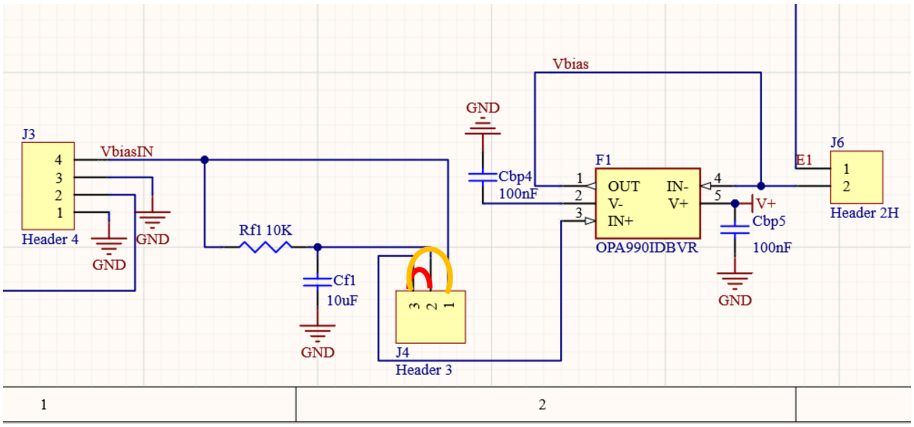

Figure 4.28: Bias voltage circuit schematic. The external jumper has to be added on the header $J4$ between the pin2-pin3 (red arch) for a filtered bias voltage or between the pin1-pin3 (orange arch) for a no-filtered one.

In the next subsection, each component of the single-channel read-out PCB is briefly described.

4.5.2 Components

PCB	Manufacturer code	Description	Power supply	I	I quiescent	Input	Output
G1	TPS73230-EP	P. Voltage regulator LDO	-	Dropout 250mA (typ.)	1 µA	1.7-5.5 V	3 V
G2	TPS72301DBVR	N. Voltage regulator LDO	-	Dropout 200mA (typ.)	1 µA	-10 - -2.7 V	-3 V
S1	74CBTLV1G125DBVRQ1	LV single FET bus switch	3 V	Max. channel current 128 mA	15 µA	$\overline{OE}$ LOW	Switch ON
K1	CRR03-1AS	SPST Reed Relays	3 V	Operating current 43 mA (typ.)	40 mA	-	-
F1	OPA990IDBVR	Operational amplifier	3 V	-	120 µA	-	-
U1	LTC6268HS6#TRMPBF	Operational amplifier	±3 V	-	16.5 mA	-	-
B1-B2	2228	Battery Holder AA	-	-	-	-	-

Table 4.6: Single-channel device PCB components

1. TPS73230-EP and TPS72301DBVR: as shown in the table above, the circuit needs a dual power supply of ± 3 V, which is dropped externally by two lithium-ion batteries of 3.6 V. The two low-dropout voltage regulators (LDO regulators) were chosen because of their ability to maintain the voltage supply at the load constant during most of the battery discharging. The positive voltage regulator (TPS73230-EP) is a fixed-voltage version, so it is internally regulated, while the negative voltage regulator (TPS72301DBVR) needs an external divider to scale the output voltage. The voltage divider was made of two resistors R_1 and R_2 in parallel. Their values were designed through the formula reported from the datasheet:

$$V_{OUT} = -1.186\left(1 + \frac{R_1}{R_2}\right), \qquad R_1 + R_2 \simeq 100k\Omega \tag{4.13}$$

   Since the sum of the two resistors has to be around 100 kΩ and V_{OUT} has to be 3 V, it was selected a R_1 of 67 kΩ and R_2 of 39 kΩ. Furthermore, recommended values of capacitors were added into the circuit in both LDO regulators schemes for guaranteeing stability, improving the noise rejection and the transient response, as suggested in their technical reports.

2. 74CBTLV1G125DBVRQ1: is a low-voltage single FET bus switch. The switch is enabled when the output-enable ($\overline{OE}$) is low. This switch has the aim of connecting and disconnecting the reed relay to the power supply. In this way, it is possible to choose the electroanalytical configuration for the single electrode.

For this purpose, a high/low logic signal from the LabVIEW interface is sent, depending on the configuration. A low input signal (of 0V) allows an amperometric mode, while a high input signal (of 3 V) a potentiometric one. The switch was added to the circuit for making the National Instrument (NI 6289) and the hardware communicate. The analog output of the NI 6289 can provide a maximum drive current of 5 mA, which could not be enough for the good operation of the relay (read the specifications of CRR03-1AS). The pin $\overline{OE}$ is tied to high through a pull-up resistor to limit the current consumption and avoid undesirable switching. The value of the pull-up resistor (R_S) was determined by the supply voltage (V_{CC}) and the current-sinking capability of the driver (I_S), see equation 4.14.

$$R_S = \frac{V_{CC}}{I_S} \tag{4.14}$$

When the input logic value is kept low, the I_S for a standard TTL is assumed to be around 40 μA and so the maximum value of R_S becomes:

$$R_S = \frac{V_{CC}}{I_S} = \frac{3V - 0V}{40\mu A} = 75k\Omega \tag{4.15}$$

while for a high input voltage value, the current is dropped by the NI 6269 and so the minimum value of R_S is:

$$R_S = \frac{V_{CC}}{I_S} = \frac{3V - 0V}{20mA} = 150\Omega \tag{4.16}$$

Thus, a R_S of 10 $k\Omega$ was in the range and could satisfy the circuit design.

3. CRR03-1AS: is an SPDT reed relay made of a coil protected by a small ceramic package for insulation and solder ball option (1AS). It was added to the circuit for the benefits of its electromagnetic principle. It results in a more energy-efficient alternative and it has a very high off-state contact resistance (Typ. 1 TΩ) than a semiconductor-based switch component. Moreover, it can switch at higher frequencies, it is characterized by a small static contact resistance (200 mΩ maximum) and a bounce-free behavior. The CRR03-1AS relay can switch when the nominal voltage of 3 V powers the coil and a specific electric current passes through it. This model guarantees an excellent operating principle if a current of about 43 mA passes through the coil (whose typical resistance is 70 Ω). Consequently, the previous switch was added to the circuit to prevent malfunction due to the low current provided by the NI DAQ.
   Thus, when the coil is adequately supplied, the switch is enabled, the pins 10 and 5 are connected, allowing the amperometric configuration. Conversely,

if the coil is not supplied, the pins 10 and 5 stay opened, allowing the potentiometric configuration (see figure 4.26).

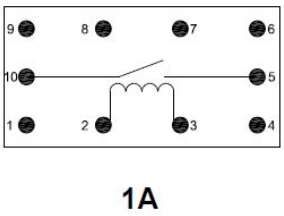

Figure 4.29: CRR03-1AS: pinout scheme

In this way, through the LabVIEW interface the user can choose the proper electroanalytical configuration.

4. OPA990IDBVR: is an operational amplifier in a voltage follower configuration. It is characterized by a low offset voltage (typically $\pm$ 300 μV) and a low noise (typically 30 $nV/\sqrt{Hz}$ at 1 kHz) for avoiding loss of the bias voltage transfer. It is powered by a single power supply of 3 V. As said previously, the stabilized voltage (V_{bias}) is given as output through the connector $J6$, which represents the external reference electrode used to polarize the cell culture for the electroanalytical measurements.

5. LTC6268HS6TRMPBF: is the main amplifier used for the amperometric and potentiometric measurements. In this case, the choice of the package was fundamental for the application. The technical manual of this component suggests using the SOIC package, which is appropriately designed for low input bias current devices, as explained in the section 4.3.3. In particular, this package has extensive lead spacing, which insulates the two input pins (-IN and +IN) from other signals. The better insulation is due to the larger impedance created between the package plastic and the pinout. Moreover, the SOIC package has gull-wing leads which reduce the contamination-induced leakage [44].

6. 2228: is the AA lithium-ion battery holder.
   Two battery holders were implemented on the bottom layer of the PCB, allowing the dual power supply. The related two pins were soldered on the top layer letting a small space between the stainless steel of each battery holder and the bottom layer of the PCB with some hot glue.

4.5.3 Guard ring technique

In this circuit, it was fundamental to minimize as much as possible the leakage of current. For this purpose, the guard ring technique was applied. The concept of a guard ring consists of a filled copper polygonal shape that surrounds the high impedance node of the operational amplifier and is driven to the non-inverting input voltage (see the figure 4.32). The guard ring lowers the risk of current leakage. It does so by driving the guard trace to the same voltage potential of the high impedance conductor. If there is no potential difference between the high impedance conductor and the guard ring, there cannot be any current flowing through it [48]. However, since they are copper traces, like the other signal tracks on the board, they are not intended to block radiation, but they work like conductors. Thus, they are often connected to the ground so that the currents carried them on, accumulated from external surface currents, are unloaded on the ground [48]. In this way, the additional currents should not flow in the operational amplifier inverting input, avoiding modifying the measured desired current detected from the cell culture.

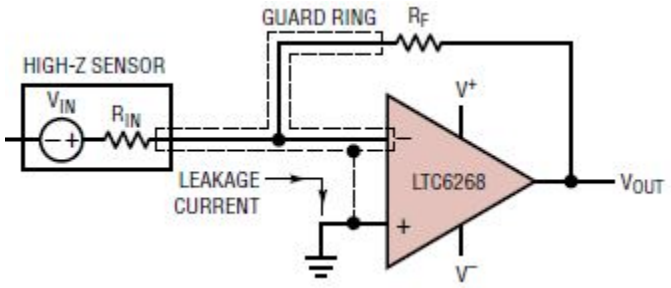

Figure 4.30: LTC6268 guard ring technique.

The high impedance node in this circuit starts from the MEA input (E1 on the header J6), and it ends on the operational amplifier's inverting input circuit (pin 2 of U1), including the feedback resistor (R2b-R2a) and the feedback capacitor (C1). The unconnected pin 1 of the operational amplifier was used to create the guard ring and driven it to the non-inverting input voltage, thus to the ground. In this way, the entire high impedance node is protected by the guard and, if there is any leakage of current, this is absorbed by the ground (the low impedance node), limiting measurement errors [44]. The yellow track in the figure 4.31 traces the guard ring input. Between the high impedance track and the guard ring, a gap of 0.2 mm was set. It was essential to contain this gap because the exposed guard ring tends to accumulate surface charges from outside and spread them rapidly over the operational amplifier inverting input [48].

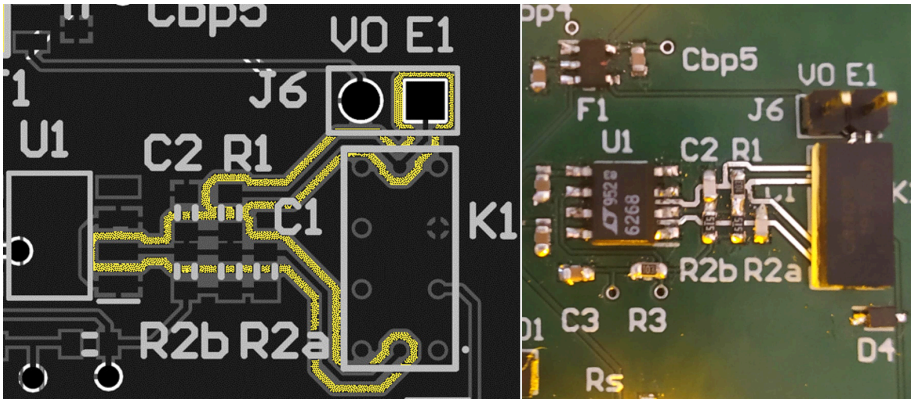

Figure 4.31: On the left: PCB zoomed footprints circuit with the yellow-highlighted guard ring path. On the right: zoomed PCB picture. It is possible to see the filled copper shape pathway.

4.5.4 LabVIEW interface

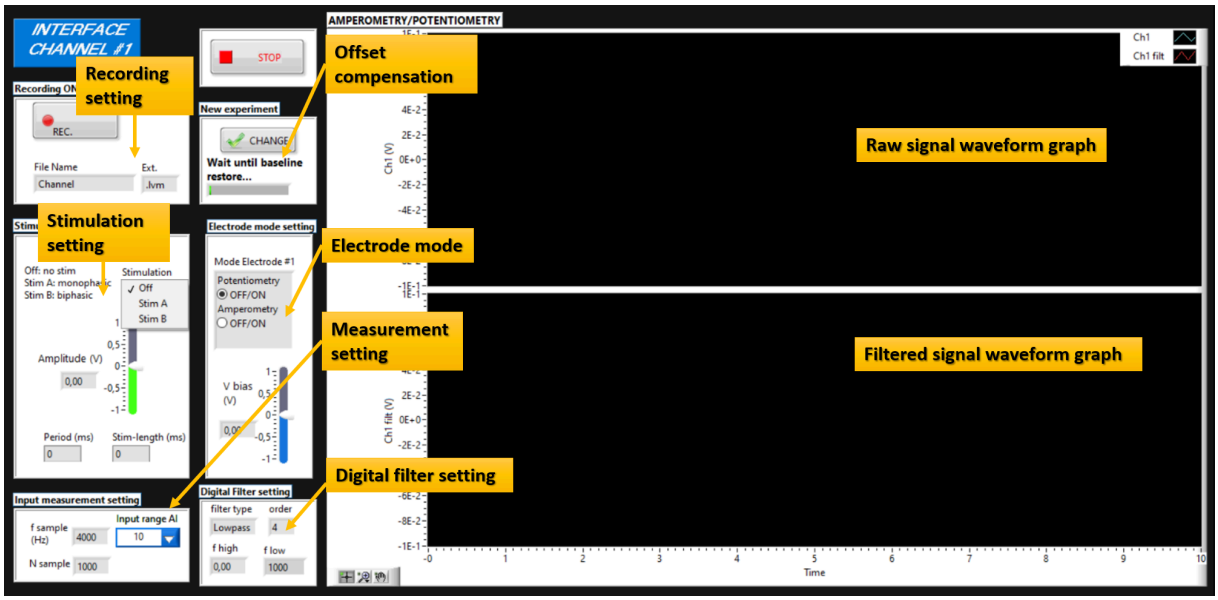

Figure 4.32: 1-channel read-out device's LabVIEW interface.

Above is shown the LabVIEW user interface. Throughout this application, it was possible to set the available configurations to perform the electroanalytical experiments, visualize the filtered and raw signals and save the data. In particular,

the red squares in the picture 4.32 represent the following setting options:

1. Electrode mode. Through this command, the electroanalytical configuration is selected: amperometry or potentiometry. If the amperometric mode is performed, the bias voltage ($Vbias$) is set automatically at the suggested value of 800 mV. Otherwise, values between -1 V to 1 V can be set. The output voltage, given by the analog output (AO1), is connected to the voltage follower and then to the reference electrode placed within the solution. In addition to the bias voltage, a constant output voltage of 3 V is given through the AO0 of the NI DAQ for driving the switch on the circuit. In this way, it was possible to change the circuit for the specific electroanalytical method mostly simultaneously.

2. Stimulation setting. Two stimulation patterns are possible: monophasic (Stim A) or biphasic one (Stim B). This command allows setting the amplitude, the stimulation length (ms), and the period between each stimulation (ms). By default, the control is set on "Off". Like the $Vbias$, it is also suggested not to overcome amplitudes of more than 1 V to avoid damage to the cell culture's neurons. The output stimulation is given through the same channel used for the $Vbias$, thus the analog output (AO1) of the NI DAQ.

3. Measurement setting. The user can decide the sampling frequency (4 kHz by default) and the number of samples for each channel. Moreover, depending on the experimental application, it is possible to change the analog input range of the NI DAQ. In this way, the extracellular signals can be measured with guaranteed accuracy from the input channel. In this application, one analog input is linked and visualized: AI0. In particular, "Ch1" is the output voltage from the preamplifier stage, "Ch1 filt" the output voltage digitally filtered on LabVIEW. Both signals are then visualized through the waveform graphs. Moreover, Chapter 5 introduces an active filtering stage. In that case, another analog input (AI1) related to the active filtered output was added to the application, and its raw and filtered signals were then visualized and could be saved in other columns of the LVM file.

4. Digital filter setting. Through this window, it was possible to change the kind of digital filter used. In particular, it allows changing low/high cut frequencies and the filter type (low-pass filter/ high-pass filter/ band-pass filter/ band-stop filter). The specific LabVIEW function internally estimates the order. By default, a Bessel digital low-pass filter is selected with a cutoff frequency of 1 kHz. Often for an accurate analysis, the raw data were studied and processed on MATLAB. For details, read the following subsection dedicated.

5. Recording setting. This command allows setting the file name and the file extension for saving the data. By default, the data are exported to a LVM file

extension. The data are stored in different columns: the first one represents the raw output signal from the preamplifier stage (Ch1), the second one the filtered signal (Ch1 filt). Successively, two other columns were added for the active amplifier stage. Automatically, if the "REC." button is pressed once, the application can save in different files the data if the electrode mode is changed. Moreover, if stimulation is set, it reports on the comments the kind of stimulation used (Off/ Stim A/ Stim B). The information related to the sampling rate, the number of samples used for each channel are also saved on the header page.

6. Offset compensation. This option scans the time needed for an internal circuit offset compensation. Before a new experiment is performed, it is usually advised to press the button "Change" and wait until the green progress bar stops running. During this time, through the waveform graph, it is possible to see the baseline restore, thus the signal going to zero. Before that time, it is suggested not to start the recording. Usually, it takes more or less 1 minute.

Digital filtering and introduction to peak detection

The choice of the digital filtering on LabVIEW was taken by the suggestions of many articles [49], [50] and [41]. It was demonstrated that IIR digital filters, which show a nonlinear phase response, can affect and comprise the distinctions of the neuronal spikes and the presence of the signal artifacts. For this reason, the raw signals were filtered through a linear phase (i.e., constant delay) response filter: the Bessel filter. Particularly, a 4th-order low-pass filter with a cut-off frequency of 1 kHz was selected. The maximally flat group delay on the whole pass-band of this filter guaranteed the minimum distortion over the entire extracellular signal band. Thus, the signals filtered on LabVIEW were exported in LVM file extension to MATLAB. In fact, through the MATLAB function "lvm_import.m", it was possible to import the LVM files into the MATLAB workspace. On MATLAB, the filtered signals were analyzed more in detail. A high-pass filter (i.e., 4th order Chebyshev type I filter) for deleting the medium value was implemented, and then a spike sorting method was introduced for detecting the extracellular spikes.
A study suggested finding the spikes from the background noise through an amplitude threshold based on the signal-to-noise ratio of the recording [50]. In particular, the threshold was estimated as a multiple of the noise's median absolute deviation, following the formula:

$$\hat{\sigma_n} = k\frac{median(|N|)}{0.6745} \tag{4.17}$$

Where N is the estimated noise calculated by filtering the signal with an elliptic band-pass filter of the 6th order [49] between 300 and 1000 Hz. Simultaneously, the denominator represents the inverse of the cumulative distribution function for

the standard normal distribution evaluated at 0.75, as suggested from the same study. Finally, k is the arbitrary constant that can be more or less restrictive. In this work, k was set in a range between 3 to 5. The formula 4.17 assumed that the noise is normally distributed (as demonstrated in the section 5.1).
In general, different algorithms could be applied (e.g. *Wave_clus* [50]) to isolate and classify the different peaks involved in an extracellular experiments. However, since this work is still premature for a concrete application in neuroscientific studies, this simple peak detection was just implemented to distinguish in general the peaks from the noise background.

The next chapter aims to analyze the performances reached from the designed read-out device by studying its strengths and weaknesses.

Chapter 5

Results

This chapter shows the main performances regarding the designed read-out device. At first, a noise analysis on the preamplifier's output signal related to the MEA submerged into a physiological solution was reported. An amperometric application on neuronal cell lines was then luckily performed with the collaboration of the University of Torino, despite the sanitary emergency. From these first two applications, it was possible to highlight the central performances and critical issues. Thus, two singular considerations were analyzed for improving the quality of the measurements. In particular, a noise analysis on the feedback resistor R_F helped understand the importance of introducing two-amplification stages. The system was then tested on a physiological solution, like the previous case.
Finally, the second observation emphasized the importance of adding an active filtering stage after the preamplification one. According to the last, two different filtering stages were then introduced and implemented on the breadboard to see how they could improve the performances of the designed device.

5.1 Noise amplitude analysis

The first useful analysis was to check if the amplitude of the preamplifier's output was comparable to the one required to read both amperometric and potentiometric signals. It was important to check if the noise amplitude was:

- around 10 pA_{pp} for the amperometric measurements.
- around 20 μV_{pp} for the potentiometric measurements.

Thus, to verify these restraints, an approximately isotonic solution with an interstitial fluid solution (Tyrode solution) was used as the electrolyte and placed inside the dish culture of the μG-D-MEA chip. One of the working electrodes submerged into the solution was then connected with a short cable from the signal collector to

the preamplifier. Simultaneously, the reference electrode was placed externally to the solution and fixed at the required bias voltage (V_{bias}).
For both measurements, the simulations were performed just looking at the output signals related to the MEA's electrode n° 11.
Once that all these expedients were adapted, the preamplifier's output signals were digitally filtered, as described in the section 4.5.4, stored through the LabVIEW interface in a LVM file extension, and exported on MATLAB. The analysis was therefore performed treating the recordings such as containing extracellular signals. The resulted noise was then analyzed as a white Gaussian process characterized by a flat power spectral density. This assumption was verified by plotting the power spectral density of one output signal and its normalized probability density function (see figure 5.1).

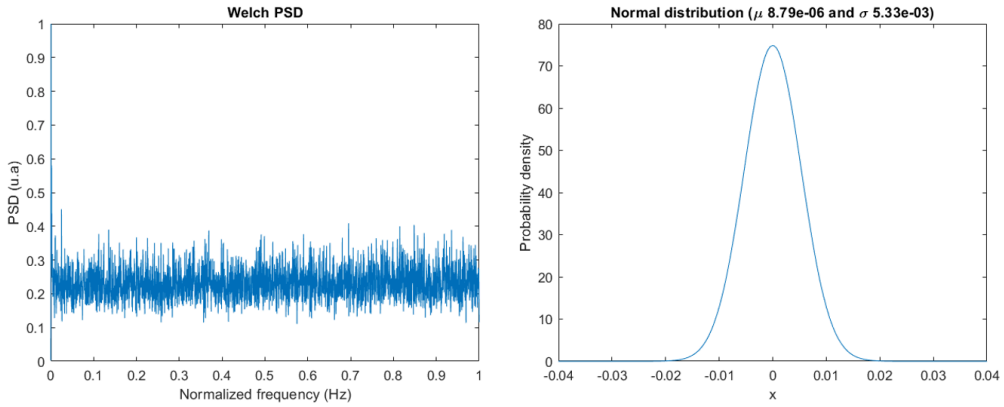

Figure 5.1: TIA's output noise: white Gaussian noise. On the left: The power spectral density over the normalized frequency. On the right: normal probability density function in the time domain.

Consequently, the noise amplitudes were calculated on MATLAB through:

1. the sample standard deviation, that for the case of a signal digitally high-pass filtered with an average null value, can be expressed as the root mean square amplitude, calculated with the following formula:

$$A_{rms} = \sqrt{\frac{\sum_i (A_i)^2}{n}} \tag{5.1}$$

   where A is the ith sample and n the total number of samples.

2. the peak-to-peak amplitude, thus the maximum-to-minimum difference of the waveform analyzed.

The figure 5.4 shows how the measurements were performed for the subsequent analyses.

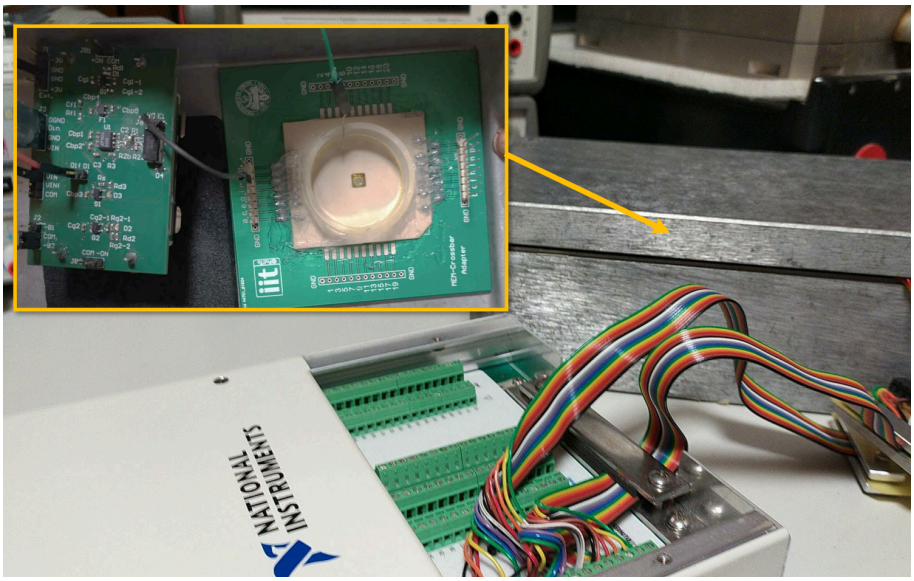

Figure 5.2: Noise simulation setup in a Faraday cage. The orange square shows the μG-SCD MEA on the signal collector. The electrode n° 11 is linked to the preamplifier's input.

The following subsections report the noise amplitudes and demonstrate the benefit of placing the system into a Faraday cage to protect the internal environment from any electrostatic field. However, it has to be considered that these tests highlighted the noise background that is just similar to the one present in a different experimental setup that involves neuronal cell cultures. These observations could not precisely predict the device's performance in the presence of the extracellular signals behind the background noise.

5.1.1 Amperometric measurement

An amperometric measurement has to evaluate extracellular signals characterized by peaks of 10-100 pA. For this reason, to recognize the peaks from the noise, it is requested that the noise amplitude of the preamplifier's output signal is almost $\pm$ 5 pA.
A first measurement of the noise was done by performing the electroanalytical experiment in two conditions: placing the preamplifier and the chip outside the Faraday cage and placing them inside.
The results can be compared from the MATLAB's plots of the figure 5.3. As it

is possible to see, the red output signal is almost half the output signal of the experiment performed without the Faraday cage. Thus, it is advised to use the Faraday cage to avoid the addition of external noise.

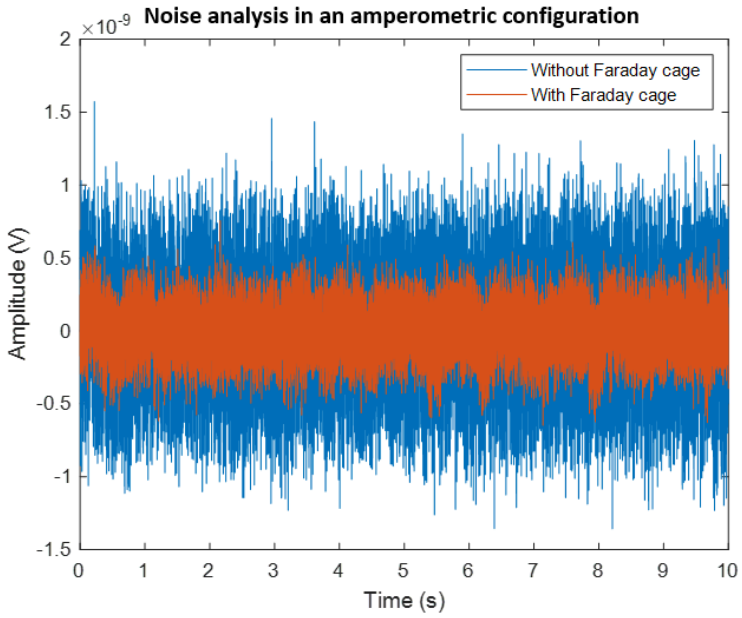

Figure 5.3: Noise analysis in an amperometric configuration. In blue, the output noise signal of the system outside the Faraday cage. In red, the output noise signal related to the system into a Faraday cage, normalized for the TIA's gain.

Consequently, the resulted noise intensities were:

- Case without the Faraday cage: 0.39 nA_{rms} and around 2.8 nA_{pp}.
- Case with the Faraday cage: 0.18 nA_{rms} and around 1.0 nA_{pp}.

In particular, to give an idea of the noise amplitude compared to the expected input currents, the voltage output signals were divided by the trans-impedance amplifier's nominal gain, which is given by the feedback resistor of 10 MΩ.
As a result, the amplitude of 1-2.8 nA_{pp} highlighted that the amperometric configuration did not satisfy the requirements. As said previously, the noise should be around 10 pA_{pp} for reading the small current peaks of the extracellular signals. However, the system had to be properly validated on a real application to discuss the concrete results (see section 5.2).

5.1.2 Potentiometric measurement

As said previously, a potentiometric measurement has to read extracellular signals, which are characterized by peaks of 10-800 μV of magnitude. Thus, for revealing the peaks, usually, it is acceptable to have a noise amplitude in a range between $\pm$ 10 μV.
Like the previous case, to verify these requirements, the experimental setting was performed in the potentiometric configuration setting the system outside the Faraday cage and then into it.
The output signals were divided by the nominal gain of the inverting operational amplifier in the preamplifier device, which is 10^3, and plotted on MATLAB. The figure 5.4 shows the resulted signals in the two cases. It is possible to notice that the system into a Faraday cage performed better performances. In fact, the noise is almost half of the configuration setting outside the Faraday cage.

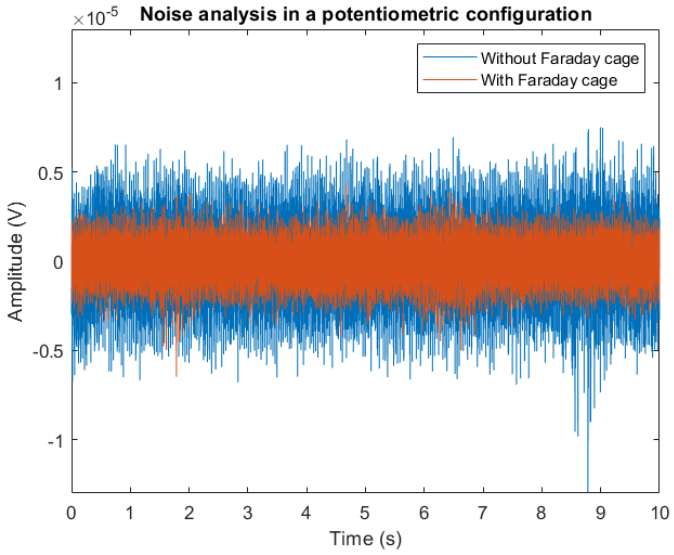

Figure 5.4: Noise analysis in a potentiometric configuration. In blue, the output noise signal of the system outside the Faraday cage. In red, the output noise signal related to the system into a Faraday cage, normalized for the IOA's gain.

Consequently, the resulted noise intensities calculated were:

- Case without the Faraday cage: 1.98 μV_{rms} and around 14 μV_{pp}.
- Case with the Faraday cage: 1.01 μV_{rms} and around 6 μV_{pp}.

From the noise resulted, it was possible to observe that the potentiometric configuration should fit the requirements for reading the small potential peaks of the

extracellular signals. An amplitude of 6-14 μV_{pp} is even less than the requirements. Despite this, to prove the performances, the setup has to be adequately tested with neuronal cell cultures. However, a potentiometric experiment requires more time and effort to be set; thus, it was unluckily impossible to be planned.

To sum up, the noise analysis in the two electroanalytical configurations gave an idea of the setup's possible critical issues. Hence, the observations done on the device's performances needed to be proved on a real application. The next section reports an amperometric experiment on PC12 cell lines.

5.2 Amperometric recording on PC12 cell lines

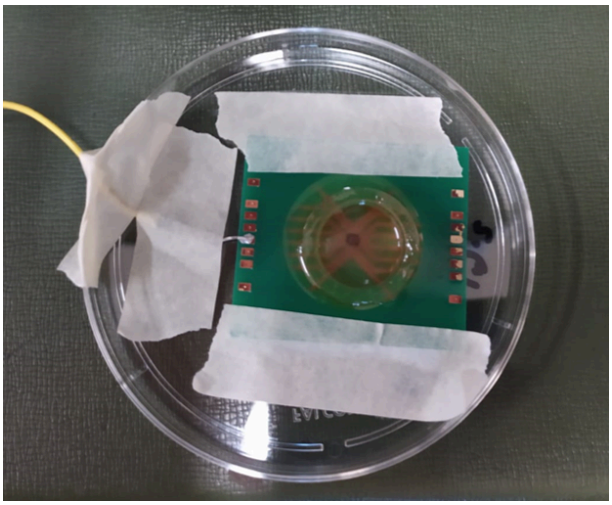

Figure 5.5: MEA's chip with the cell line used for the amperometric application.

A cell line of PC12 (read section 2.3.1) was prepared, placed in an incubator for 3/4 days before being tested and then dished on a μG-SCD MEA chip (see figure 5.5).
The experiment was performed with the designed read-out device in parallel with the standard device that the researchers usually use to perform amperometric experiments. This device played an essential role in finding the working electrode to which interface the designed preamplifier. However, it was not used to compare the performances with the designed read-out device directly but to give a general idea of the performances of the designed circuit. The two measurements implemented two different experimental conditions: the standard device recorded the signal from 16 electrodes throughout spring connectors that directly attach to the working

electrodes, the designed read-out device from just one electrode through an external cable connection. For this reason, the experiment was performed only to see if the customized circuit works.
The electrical activity of the cells was so observed through the standard device, and the electrode on which the electrical activity of the cells seemed to be more evident was selected.
Particularly, the electrode was connected to the preamplifier through a jumper fixed over it with a removable silver conductive paint provided by *RS Components*. This paint is used to make electrical connections on the non-weldable electrode surface, and it dried in about 10 minutes before being used. In this way, it was also easier to interchange both the devices for each test on the same MEA. Moreover, since the solder paste caused a weak or fragile connection, a paper tape was fixed on the jumper to avoid mechanical breaks (see the figure 5.5).
Finally, both systems were placed inside the Faraday cage, as shown in the workstation of the figure 4.1, and the extracellular recordings through the NI DAQ and the LabVIEW interface began. In particular, since the cellular activity lasts just a few over 30 minutes, only two tests were planned:

1. Dopamine injection test: the detection of the "leap" due to the addition of dopamine (L-DOPA) into the culture solution.

2. Single-electrode amperometric test: the amperometric measurement performed on one chosen electrode.

Each test is reported in detail as follows.

5.2.1 Dopamine injection test

The first test was performed to prove the working principle of the preamplifier device. In particular, this amperometric test aimed to detect the dopamine oxidation on the electrode surface. When the dopamine is released on the cell culture, depending on its concentration, it is possible to see a "leap", which is an index of the oxidation reactions (see section 2.2). Due to the high concentration of dopamine, the dopamine injection has not the shape of a peak. On the opposite, it is possible to observe a quick increase until a saturation level due to the dopamine diffusion in the whole solution. Moreover, PC12 cells incubated with the dopamine precursor (L-DOPA) usually increase the dopamine release, favoring the next amperometric experiment [34].
If this "leap" is appropriately detected and amplified, it would be possible to demonstrate the preamplifier working principle into this particular setup.
A sampling rate of 4 kHz was selected. The electrode 12 of the MEA's chip was chosen from the standard device and interfaced to the designed preamplifier. As a

result, the output signal is reported in the figure 5.6. From the graph below, it is possible to observe the dopamine "leap" and the following saturation level due to the oxidation. The current rose in few milliseconds and remained at a lower constant level, around 0.8 nA. The amplitude of the current reached depended on the concentration of dopamine oxidized on the electrode surface.
Despite the presence of the external jumper that connects the electrode to the input of the TIA circuit and the weak solder point on the MEA, in the complex, the preamplifier showed a suitable performance for this kind of test.
Thus, the system was ready to be tested on the detection of the extracellular peaks in the amperometric configuration.

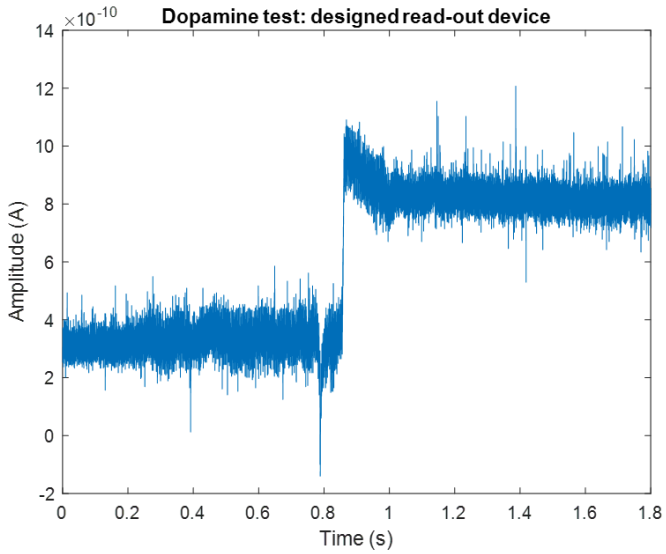

Figure 5.6: Dopamine injection amperometric test. In the blue trace the "leap" of current detected by the designed read-out device.

5.2.2 Single-electrode amperometric test

Initially, the amperometric signals were detected through the standard device used by the researchers. The bias voltage on the reference electrode was fixed at the suggested value of 800 mV, while the 16 channels of the MEA were visualized on another LabVIEW interface. By observing each channel, the extracellular signals were more evident on the 12th electrode. Consequently, it was the one analyzed and later interfaced with the designed device.
The extracellular signals were recorded with the fixed sampling rate of 25 kHz of the standard device [32] and digitally filtered (according to the section 4.5.4). The

output signal from the 12th electrode was then plotted on MATLAB, as shown in the figure 5.7.

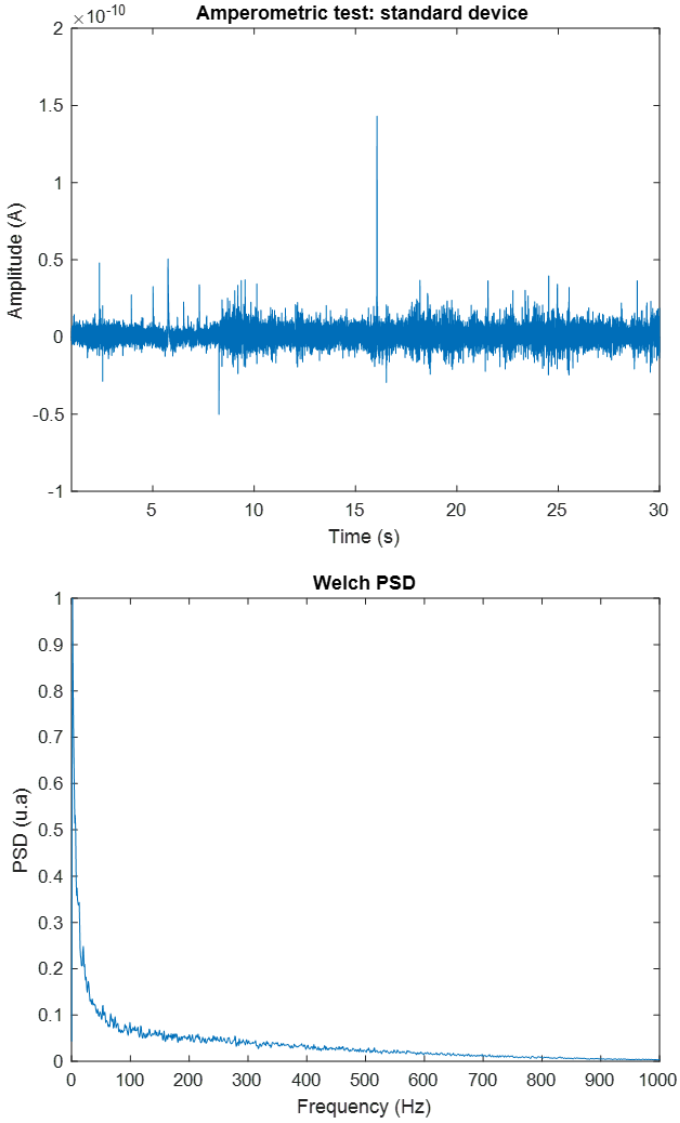

Figure 5.7: Single-electrode amperometric test through the standard device. On the top, the extracellular recording from the 12th electrode. The output current is plotted in function of time. On the bottom, the resulting power spectral density.

According to the theory, the amperometric peaks are characterized by a frequency range from 0.6 to 15-30 Hz. According to this, from the plotted power spectral density (figure 5.7), it was possible to observe an increase in the low-frequency

contributions. Simultaneously, the background white noise contribution, already introduced at the beginning of this chapter, was reduced for frequencies higher than 1 kHz through the digital low-pass filter.

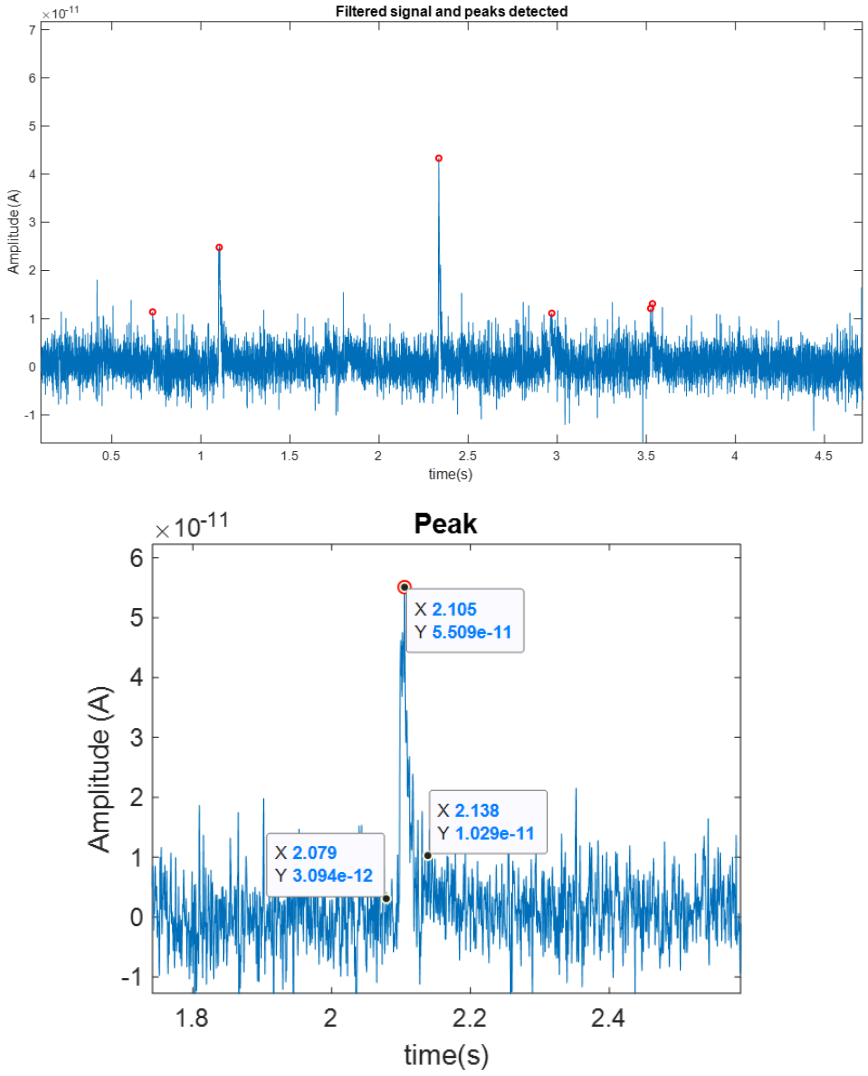

Figure 5.8: Amperometric recording through the standard device. On the top, in blue, the zoomed amperometric trace. In red circles, the detected peaks. On the bottom, a zoomed amperometric peak.

The whole extracellular signal seemed to be just corrupted by the noise by observing the trace in its complex. However, the amperometric peaks could be found on the trace by zooming on the extracellular signal and applying the peak

detection threshold, introduced in the section 4.5.4. As a result, the small current peaks detected can be seen from the zoomed traces shown in the figure 5.8. From this picture, it was possible to see that the noise amplitude reached from the standard device was around 10 pA_{pp}, as required from the measurement restraints [35]. The current peaks detected gave an idea of what is required by a front-end device interfaced with the MEA. As shown in the bottom zoomed trace of the figure 5.8, a typical amperometric peak has to show a quick raise of current (e.g., 55.09 pA) and slow time drift (e.g., around 59 ms).
Usually, the amperometric spikes recorded from 70 cells with the same MEA chip are characterized by peaks of a mean of 74 $\pm$ 5 pA [3]. From the whole trace recorded, the mean value of the peaks revealed was around 35.7 $\pm$ 20.8 pA, with a selected threshold of 18.40 pA. However, the variability of these values depends on many features, including biological variables and drug treatments (as explained in the section 2.3). These resulting performances are not expected from the designed read-out device. In fact, as said at the beginning of the section 5.2, the two analyses have two different experimental setups. Therefore, the analysis on the standard device represented just a general idea of what is expected from a preamplification stage but not a reason for comparison.
Finally, the single-electrode amperometric test of the designed preamplifier was conducted on the 12th electrode. In this case, the recordings were performed with a lower sampling rate of 4 kHz. The frequency of 25 kHz is used when the experiment aims to study the extracellular recording information; thus, the peaks and the amount of dopamine released. Hence, since this test aimed to verify only the working principle of the circuit and the peaks on the trace, a sampling rate of 4 kHz was enough for the purpose.
Like the standard device, the bias voltage was set at 800 mV on the external reference electrode, and the extracellular signal was collected through the preamplifier to the LabVIEW interface and plotted on MATLAB. The recorded signal and its power spectral density are represented in the figure 5.9.

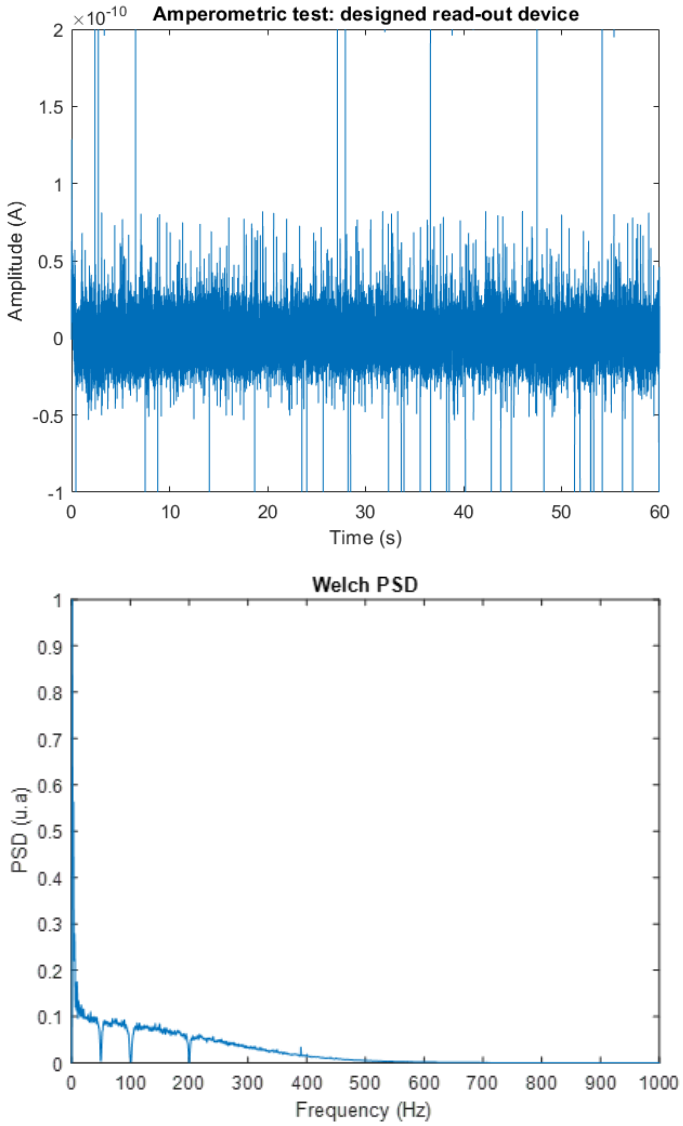

Figure 5.9: Single-electrode amperometric test through the designed read-out device. On the top, the extracellular recording from the 12th electrode. On the bottom, its power spectral density.

As it is possible to observe from the power spectral density, the trend is similar to the one analyzed from the standard device. Despite this, the signal was filtered with a low-pass filter at 400 Hz (instead of 1 kHz) to reduce the contribution of high-frequency noise and appeared corrupted by mains interference (50 Hz). For this reason, it was necessary to apply a recursive Notch filter at multiples of 50 Hz.

This resulting behavior was predicted before starting with the measurement. In fact, the cables that link the preamplifier first to the MEA and then to the NI DAQ impeded the complete closure of the device inside the Faraday cage, thus its total isolation from the external interference. Moreover, the conductive paint that links the electrode to the electronics probably introduced additional noise to the signal due to its mechanical instability.
Consequently, this test has to be observed considering the fact that the designed device is just a prototype of a future model.
The measurement was taken forward by examining the presence of the extracellular peaks. The zoomed trace can be seen in the figure 5.10.

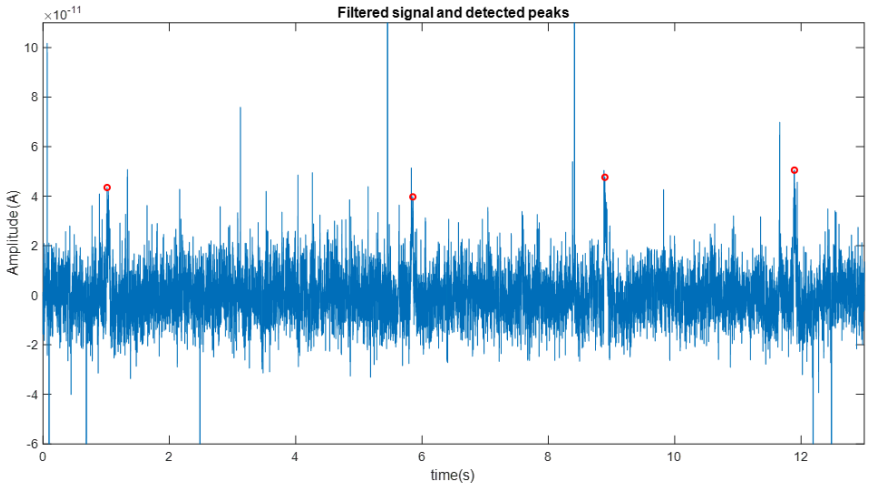

Figure 5.10: Amperometric recording through the designed read-out device. In blue, the zoomed picture of the amperometric trace. In red circles, the detected peaks.

As shown in the trace, some peaks were detected from the background noise. In particular, it was used a threshold of 36.70 pA (calculated as explained in 4.5.4), which was larger than the one used with the standard device. This was due to the lower signal-to-noise ratio. In fact, the output noise amplitude was around 20 pA_{pp}, almost double compared to the required restraint. Consequently, the shapes of the amperometric peaks were less well-distinguished from the background noise.
The figure 5.11 shows a zoomed peak of the recorded trace. Notably, it is characterized by an amplitude of around 47.64 pA and a time-width of few milliseconds ($\sim$ 72 ms), thus demonstrating the similarity with the theory.
To sum up, the critical issues which had influenced the quality of the extracellular signal on this setup were due to:

- The cables between the working electrode and the preamplifier, and the NI DAQ with the preamplifier.
- The solder point between the jumper and the working electrode.
- The lack of complete isolation of the device within the Faraday cage.
- The consequent additional digital filtering.

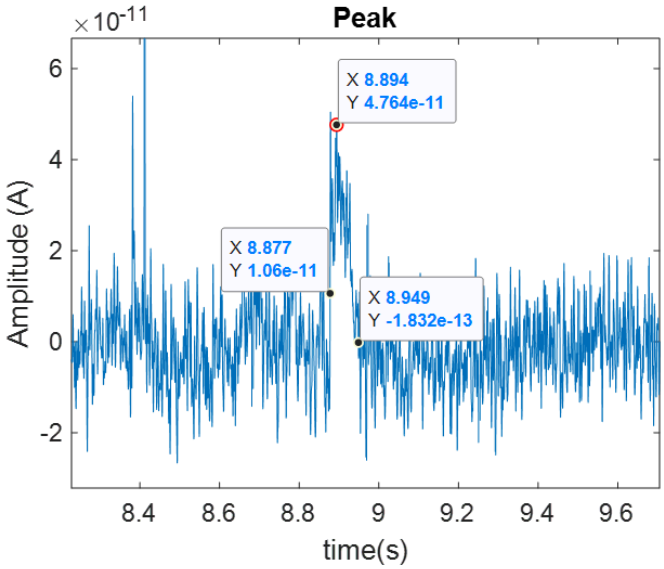

Figure 5.11: Amperometric peak detected through the read-out device.

Due to the short time of the cell activity for detecting the amperometric signals, which was a few more than 30 minutes, it was impossible to perform further tests. As a result, the two testes gave only a general idea that the circuit worked, but it has to be appropriately optimized and tested in both the electroanalytical measurements.
The next sections reported some useful tools that could improve the performances of the read-out device and give some ideas for a future perspective.

5.3 Analysis of the noise contribution of the feedback resistor R_F

The previous applications helped highlighted the main performances and critical issues of the system.

One of the main reasons the system is noisy could be due to the thermal noise or Johnson noise, as already introduced in the section 4.3.1. The Johnson noise is an electronic noise with a constant contribute in noise density due to the thermal agitations of electrons inside conductors and passive components, such as resistors. Its noise voltage density can be calculated as:

$$\bar{v_n} = \sqrt{4kTR_F} \qquad \left[V/\sqrt{Hz}\right] \tag{5.2}$$

where k is the Boltzmann constant and T the temperature. In the preamplifier circuit, the high-value feedback resistor R_F (10 MΩ) could so be the primary noise source that influenced the measurements.
For studying this critical issue, LTspice® noise simulations were performed. Particularly, the effect of the feedback resistor R_F was analyzed at the output of the most critical electrode mode configuration, the amperometry. Thus, the different values of R_F in the TIA circuit (see the figure 4.16) were swept from 10 kΩ to 10 MΩ with decade steps. This was possible thanks to the following SPICE directive:

```
.step dec param R 10k 10Meg 1
```

Where "R" is the variable to sweep (R_F), "10k" and "10Meg" is the desired range and "1" is the number of points per decade. Moreover, since the thermal noise also depends on the temperature (see the equation 5.2), the temperature was fixed at room temperature (25°C) through the command:

```
.param temp 25
```

The noise analysis in AC was then performed modeling to the inverting input of the TIA a current noise generator (see figure 5.12) and inserting the following SPICE directive:

```
.noise V(O1) IIN _noise dec 10k 1 30k
```

Where "V(O1)" is the output of the TIA, "IIN_noise" the current noise generator, "10k" the number of points per decade, and "1 and "30k" the noise bandwidth 1 Hz and 30 kHz.

The directive ".NOISE" allows a frequency domain analysis that computes the noise due to Johnson noise, but also the noises due to the active components such as shot and flicker noise [51]. The noise spectral density per unit square root bandwidth was then plotted in function of the frequency. The system was analyzed between 1 Hz (the lowest frequency of interest) and 30 kHz, considering an approximated span of one more decade from the low-pass filter's cutoff frequency at 1 kHz, which was integrated into the TIA circuit.
Finally, the resulting voltage noise density ($V/\sqrt{Hz}$) at the output of the preamplifier was plotted and compared to the different values of the feedback resistor, as shown in the figure 5.13.

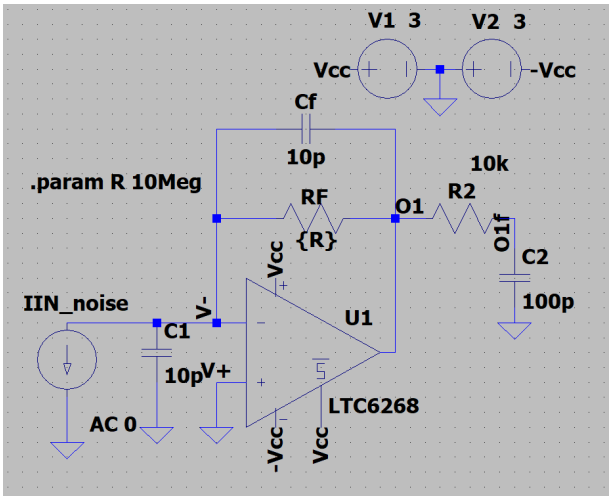

Figure 5.12: LTspice® noise simulation in the TIA circuit.

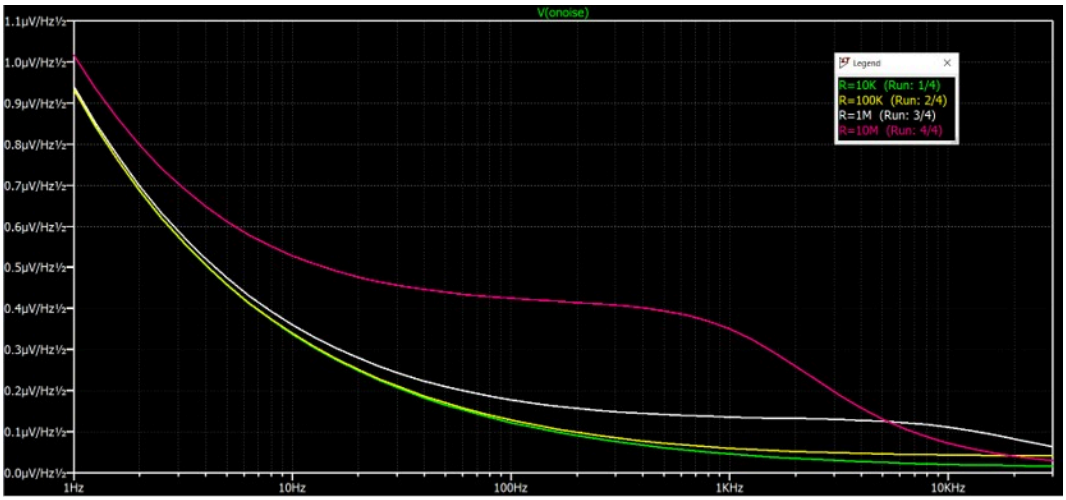

Figure 5.13: Total voltage noise densities in function of frequency for different values of R_F at the TIA's output. In green, the effect of R_F equal to 10 kΩ. In white, R_F equal to 100 kΩ. In red, R_F equal to 1 MΩ. In pink, R_F equal to 10 MΩ.

From the pink trace, it is evident that the highest value of R_F (10 MΩ) contributes more to the resulting noise density in the whole frequency range. To calculate the exact contributes values, the noise density curves were integrated for each value of R_F in the frequency range analyzed. This was possible through the

following two-measure statements:

```
.MEAS NOISE O1 INTEG V(onoise)

.MEAS NOISE RF INTEG V(rf)
```

Where "V(onoise)" is the total output referred noise at the output of the TIA "O1" and the "V(rf)" is the thermal noise due to the different values of R_F.
Finally, the integrated noise densities related to the output traces of the figure 5.13 and the R_F in the bandwidth between 1 to 30 kHz are reported in the table 5.1. From these values, it was possible to observe that the total voltage referred noise increases with higher R_F. In particular, the total voltage noise of 100 kΩ was almost twice compared to 10 kΩ, while the difference between 10 MΩ and 1 MΩ was less significant.
However, the largest gap resulted from the feedback resistor of 10 MΩ and the one related to 100 kΩ, whose ratio was around 2.57.
Similarly, the voltage noise referred just to the contribution of R_F increased decisively between the values of 10 kΩ and 1 M Ω and had similar values between 1 MΩ and 10 MΩ.

Table 5.1: Integrated output noise densities between 1-30 kHz for different values of R_F.

R_F (Ω)	**V(onoise) (μV)**	**V(rf) (μV)**
10 k	4.72	2.23
100 k	8.16	7.01
1 M	17.60	16.91
10 M	21.00	20.00

Another worthwhile command of LTspice® for this kind of analysis was to attribute to R_F the component option "noiseless". In this way, the software can ignore the contribution of the feedback resistor in the noise analysis. This feature was handy in this application because it also allowed considering the extra noise contributions.
The same simulation was so performed with the addition of this option. The resulting noise densities were plotted in the same frequency range, as shown in the figure 5.14. Mainly, each curve related to a specific value of R_F was almost overlapped, which confirmed the no-influence of the feedback resistor to the noise analysis performed.

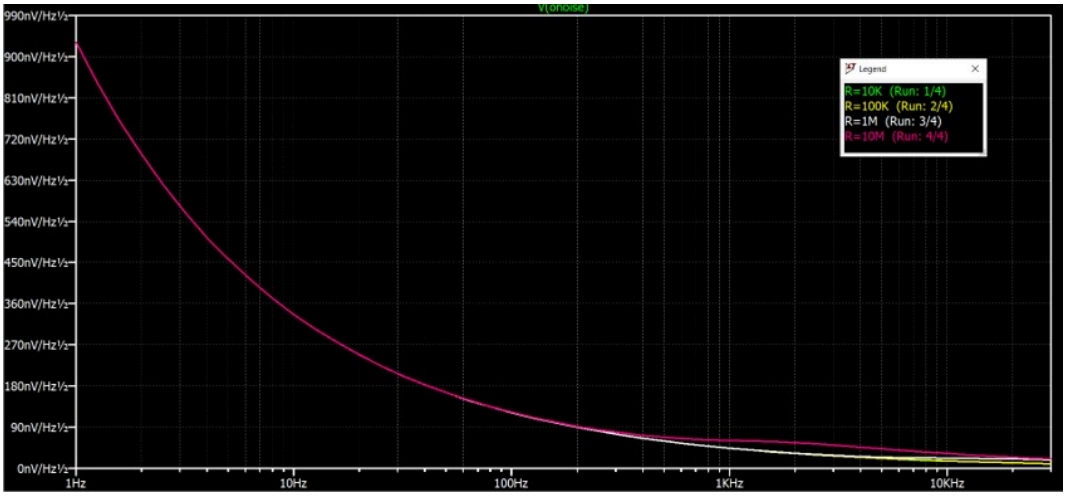

Figure 5.14: Total voltage noise densities in function of frequency at the TIA's output, without the thermal noise contribution. In green, the effect of R_F equal to 10 kΩ. In white, R_F equal to 100 kΩ. In red, R_F equal to 1 MΩ. In pink, R_F equal to 10 MΩ.

The total voltage noise was then calculated through the same measurement statements for the different values of R_F and reported in the table below.

Table 5.2: Integrated output noise densities between 1-30 kHz neglecting the thermal noise.

R_F (Ω)	**V(onoise)** (μ**V**)	**V(rf)** (μ**V**)
10 k	4.15	-
100 k	4.17	-
1 M	4.87	-
10 M	6.33	-

As it is possible to observe from the table 5.2, the voltage noise was almost the same for each value of the feedback resistor, and it increased slightly for the 10 MΩ resistance, around the frequencies 1 kHz and 10 kHz. While, the noise contribution of the feedback resistor was ideally null. Overall, it was proved that the prominent effect on the noise was due principally to the feedback resistor.
This observation brought to verify the effective influence of the feedback resistor values on the noise amplitude of the output signal of the preamplifier.
Once more, the TIA circuit's noise was studied by comparing the output signal with the designed feedback resistor of 10 MΩ and with a feedback resistor of 100 kΩ. The 100 kΩ resistor was selected because it showed a significant difference

from the 10 MΩ one, compared to the other resistors (10 kΩ and 1 MΩ). Thus, the 100 kΩ resistor was temporally soldered on the printed circuit board instead of the one designed and tested on the same setup used in the previous section 5.1. The Petri dish placed on the μG-SCD MEA chip was fulfilled again of Tyrode solution, and the output signals were collected, post-processed and plotted on MATLAB. The two comparisons can be observed in the figure 5.15. In this case, the signals

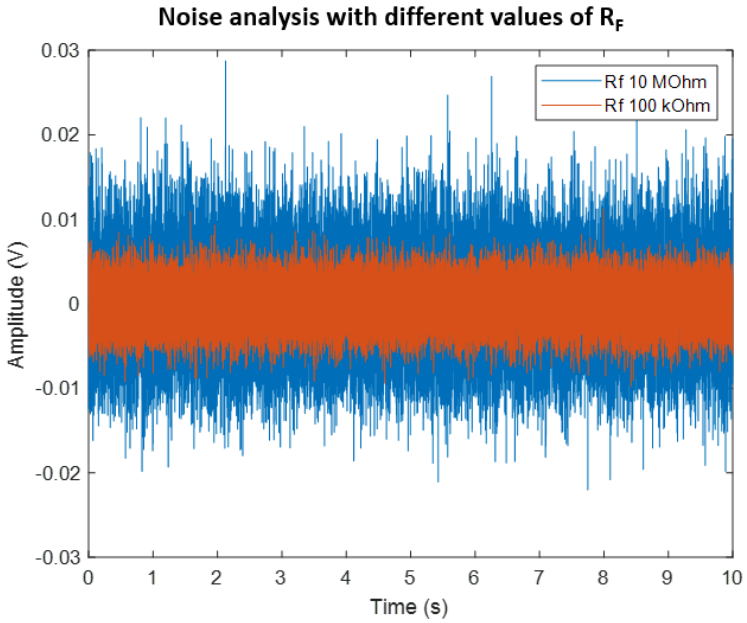

Figure 5.15: Noise analysis in an amperometric configuration. In blue, the TIA's output noise signal with a feedback resistor (R_F) of 10 MΩ. In red, the TIA's output noise signal with a feedback resistor (R_F) of 100 kΩ.

were not evaluated like the previous case, thus dividing their value to their nominal gain. In this way, it was possible to compare their effective amplitude at the output of the TIA. From the plots, the output signal related to the feedback resistor of 100 kΩ showed an amplitude which was more than half of the one of the designed R_F. As a result, the relative noise intensities calculated were:

- R_F of 10 MΩ: 5.33 mV_{rms} and around 34 mV_{pp}
- R_F of 100 kΩ: 2.50 mV_{rms} and around 14 mV_{pp}

From these results, it was possible to confirm the simulation's results on LTspice® reported in the table 5.1, thus a ratio between the two voltage noise of about 2.13. To sum up, the analysis of the noise due to the feedback resistor could help evaluating

in a future perspective if it is more convenient to implement two amplification stages. The first amplification stage might be implemented with a lower value of the feedback resistor (e.g., less than 100 kΩ) through the operational amplifier with more noise restraints—the second amplification stage with an operational amplifier with lower restrictions but with a higher gain.
In addition to analyzing the feedback resistor contribution to the noise, it was necessary to introduce a section about a possible filtering stage added to the preamplification one. For this purpose, the following section aims to find some solutions to improve the read-out system's general performances.

5.4 Analysis of the noise amplitude with an active filtering stage

Usually, a read-out system of extracellular signals requires, in addition to the designed preamplification stage, also active filters, which have to be precisely selected. Thus, this section introduces two different active filtering stages that could fit in this application. Remarkably, considering the observations done previously, also in this case, the results were performed on the most critical preamplifier's circuit, the TIA.
Active-filter circuits are built using operational amplifiers, which are the active elements, with the addition of resistors and capacitors that set the desired filter characteristics. As seen from the chapter 4, the operational amplifier specifications had to satisfy the noise requirements. Thus, the filtering amplifiers in this stage also had to be led by the constraint of low noise [41]. Mainly, two different kinds of active filters were implemented:

1. Multiple-feedback (MFB) active low-pass filter of the second order

2. Voltage-controlled voltage-source (VCVS) low-pass filter of the fourth order (devised by Sallen and Key).

These two kinds of active filters are the ones that are commonly used and advised in this kind of applications [3] [41]. The details are reported as following.

5.4.1 Multiple-feedback low-pass filter

This kind of active filter configures the operational amplifier as an integrator. Differently, to the VCVS configuration, at higher frequencies, the effect of the rising of the gain is less severe.
A low-pass filter of Butterworth of the second order was implemented. The Butterworth filter is known for being the one with the flattest pass-band response

but mediocre phase and transient properties. However, it was chosen because it could be a middle-way in terms of frequency- and time-domain performances compared to other typical filters (i.e., Chebyshev filters, etc.) [52].
A cutoff frequency of 1 kHz was selected. While each element was designed using the technical tables reported on the application report by *Texas Instruments* [53]. The resulted circuit scheme is shown in the figure 5.19. From the schematic above,

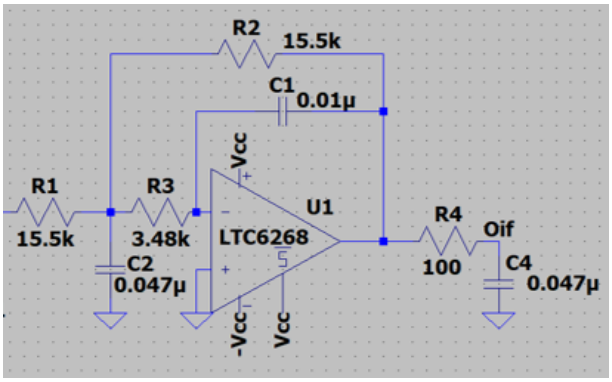

Figure 5.16: Butterworth filter of the 2^{nd} order with passive low-pass RC in series with the output.

it is possible to obtain the transfer function as:

$$H(f) = \frac{-\frac{R2}{R1}}{(j2\pi f)^2(R2R3C1C2) + (j2\pi f)\left(R3C1 + R2C1 + \frac{R2R3C1}{R1}\right) + 1} \tag{5.3}$$

Moreover, a passive low-pass filter, given by R4 and C4, was added in series with the output, for the same reason explained for designing the preamplifier's circuit. The passive pole at 40 kHz of these elements, in fact, helped to improve the high-frequency response. The total Bode plot of the preamplification stage in the amperometric configuration and the active filter was simulated in LTspice® and plotted in the figure 5.17. From the blue trace resulted, it was possible to observe that the low-pass filter transfer function, coupled with the amperometric configuration's one, reduced a bit the total gain. Particularly, from 10^7, it became 6×10^6. In the complex, the circuit also caused the inversion of the signal polarity [53].
The applicability of this active filter was verified by connecting the preamplification stage's output to its input on a breadboard. The same setup used in the section 5.1 with the means of the culture solution was then performed in the amperometric configuration.

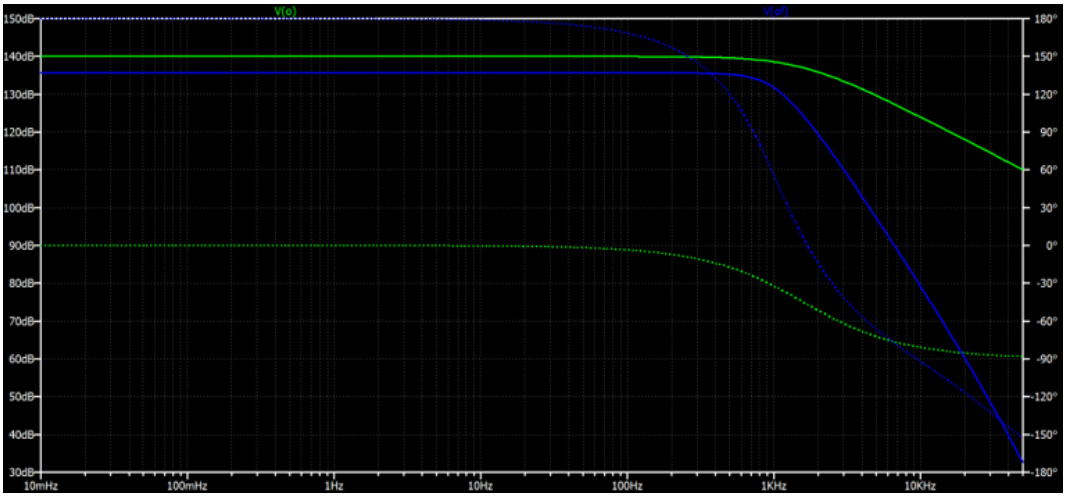

Figure 5.17: Bode plots. In green, the TIA's Bode plot. In blue, the total Bode plot (preamplifier + Butterworth filter of the second order).

Application on the amperometric configuration

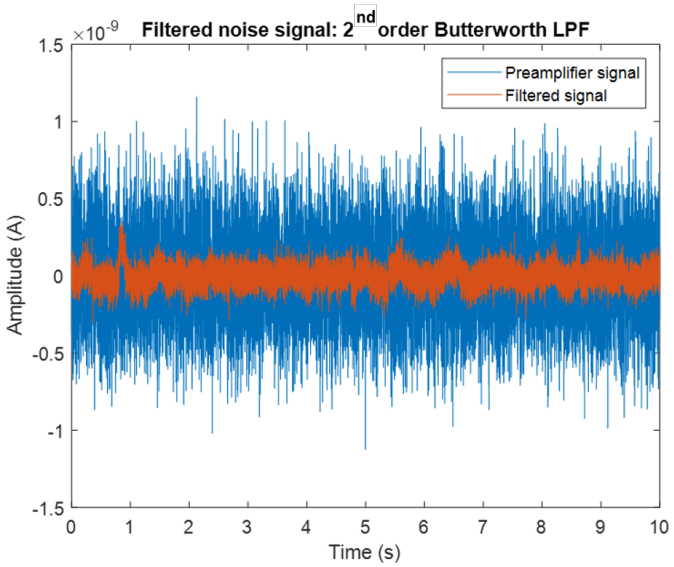

Figure 5.18: Noise analysis in an amperometric configuration. In blue, the output noise signal of the preamplification stage. In red, the output noise signal related to the output of the 2^{nd} order active filter, normalized for the nominal gain.

The active filtering stage was implemented on the breadboard and added in cascade to the preamplification stage.
Once implemented to the system, the noise bandwidth was studied again to check if it could improve the performance of the read-out device. As said previously, the most critical configuration is the amperometry; thus, it was performed just this configuration. In the NI DAQ were connected two analog inputs: one directly taken from the preamplifier's output, the other from the active filter's output. The signals were then digitally filtered (as explained in the section 4.5.4) and plotted again on MATLAB, dividing them for the nominal gains. The results can be seen from the figure 5.18.
The filtered signal (in red) was almost a quarter of the unfiltered signal. From the intensities calculated, it was found that:

1. Unfiltered signal: 0.27 nA_{rms} and around 2 nA_{pp}

2. Filtered signal: 68.6 pA_{rms} and around 0.25 nA_{pp}.

The simulation expressed that there could still be the necessity to reduce the noise amplitude for collecting good quality amperometric signals.
For this reason, it was tried to design a second active filter of a higher order to see if it would perform some improvements.

5.4.2 Voltage-controlled voltage-source low-pass filter

In this case, another kind of active filter was implemented: the voltage-controlled voltage source (VCVS). VCVS filters are the other also commonly used for active filtering stages. In contrast to the MFB, they are composed of operational amplifiers configured as voltage followers, depending on the order of the filter. Moreover, for this simulation, another type of filter was considered. In fact, the Butterworth filter has poor time-delay performances that can give rise to waveform distortion and overshoot. In these applications, it is essential to avoid the distortion of the shape of neuronal spikes.
According to this, many articles [41], [34] say that in extracellular signal processing, it is recommended to exploit Bessel filters to minimize the phase distortion. This characteristic can be reached thanks to their maximally flat time delay within the pass-band, thus a phase shift that varies linearly in the frequency domain. This property makes them adequately fitted for the processing of pulse signals [52]. In addition to this, to improve the phase linearity, it is suggested to use higher-order filters.
For these reasons, a Bessel filter of the fourth order was implemented.

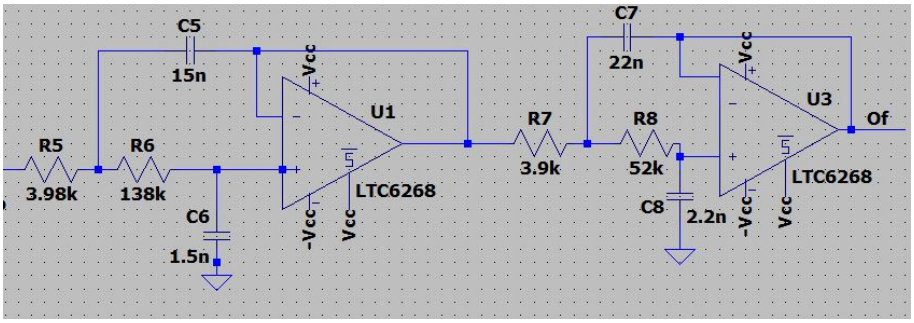

Figure 5.19: Bessel filter of the 4^{th} order.

Each component was designed throughout the online tool "Analog Filter Wizard" provided by *Analog Device*. The circuit selected is shown in the figure 5.19.
This circuit was implemented on the breadboard by cascading two second-order low-pass Sallen Key stages. In particular, each stage had the following characteristics.

Table 5.3: Second-order low-pass Sallen Key stages characteristics

# stage	**Gain (V/V)**	**Cut-off freq. (kHz)**	**Quality factor**
First stage	1	1.43	0.52
Second stage	1	1.61	0.80

The first stage had a gain of 1 V/V, a cut-off frequency of 1.43 kHz, and a quality factor Q of 0.522. While, the second stage: gain of 1 V/V, a cut-off frequency of 1.61 kHz, and a quality factor Q of 0.805. Thus, in this case, the total gain was not modified (10^7), and the input signal was not inverted at the output.
The resulting total Bode plot of the preamplification stage in the amperometric configuration with the added active filter was then simulated in LTspice®, and plotted in the figure 5.20.

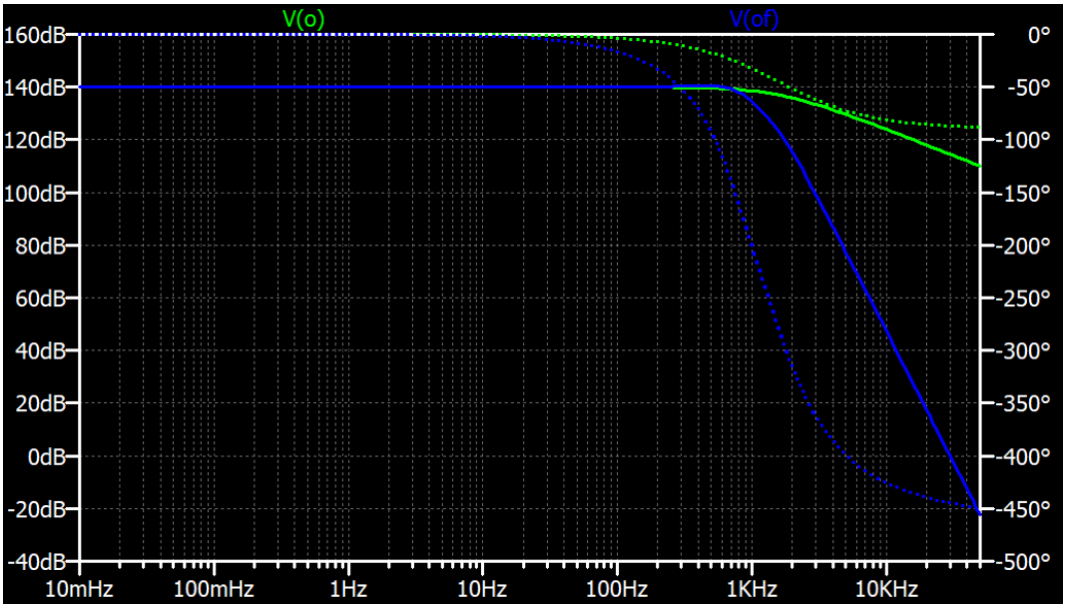

Figure 5.20: Bode plots. In green, the TIA's Bode plot. In blue, the total Bode plot (preamplifier + Bessel filter of the 4^{th} order).

Finally, the applicability of this active filter was verified by connecting the preamplification stage's output to its input on a breadboard.

Application on the amperometric configuration

Similarly to the previous test, the designed active filter was implemented on the breadboard and added in cascade to the preamplification stage.
Once implemented to the system, the noise amplitude was studied again to check if there was any improvement. The signals were then digitally filtered (as explained in the section 4.5.4) and plotted on MATLAB, dividing the amplitudes for the nominal gain of 10^7. As a result:

- Unfiltered signal: 0.4 nA_{rms} and around 2 nA_{pp}.
- Filtered signal: 39.7 pA_{rms} and around 0.16 nA_{pp}.

By comparing the two active filters implemented, the resulted voltage noise was slightly improved than the previous case.

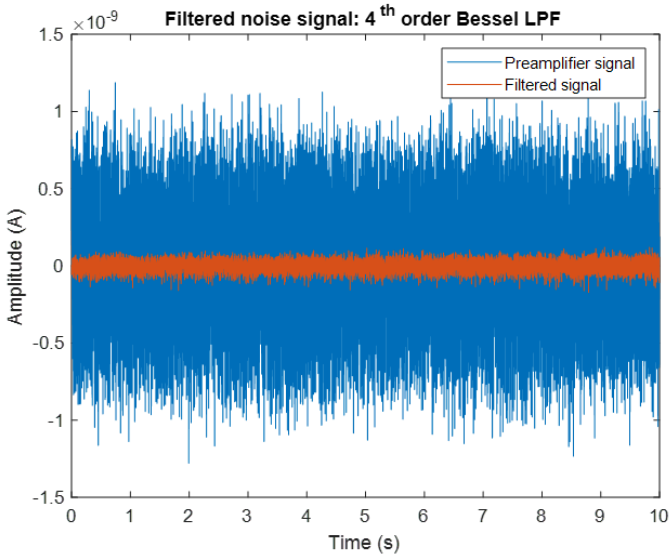

Figure 5.21: Noise analysis in an amperometric configuration. In blue, the output noise signal of the preamplification stage. In red, the output noise signal related to the output of the 4^{th} order active filter, normalized for the nominal gain.

To sum up, these sections gave a general idea of the performances and critical issues of the designed read-out device. Moreover, the results obtained by the noise analysis on the feedback resistor and the two active stages could be a useful tool for the future optimization of the device (read the section 6.1). However, just a real application with a cell culture could show the concrete performances of the designed read-out device with those additional circuits. Further tests on neuronal cells were so not possible to be planned.
The last section describes the final considerations and sums up the tools for a future perspective of this work.

Chapter 6

Conclusions

This work gave the main tools for designing a read-out device to detect the extracellular signals of dopaminergic neuronal cells. In particular, it showed how to arrange a front-end preamplification stage to be interfaced with a MEA. The first steps involved the selection of a suitable operational amplifier to fulfill noise constraints. After this choice, two different circuits were selected to allow the relatively simultaneous switching between two electroanalytical methods. The trans-impedance configuration (TIA) of the operational amplifier allowed the amperometric measurements, thus the study of the single quantal exocytosis events in the cell culture. While the inverting configuration (IOA), the potentiometric ones, hence the study of the spontaneous electrical activity of the neuronal net. These two different circuits were designed with proper passive components to achieve the desired gain and frequency bandwidth for the expected extracellular signals.
Auxiliary tests helped to have a general idea of the working principle of the preamplifier before proceeding with the design of the printed circuit board.
The device was then realized through Altium Designer® and additional expedients were considered to limit the leakage effects and noise coupling, such as the operational amplifier package (i.e., SOIC), the selection of the switch (i.e., the reed relay), and the guard ring technique. A LabVIEW interface was then implemented to select the electroanalytical configuration, post-process, and export the recorded data to the MATLAB's workspace.
Finally, the results highlighted the read-out device's general performances on a physiological solution and an amperometric experiment with PC12 cell lines. In general, it was found that the preamplification circuit works, can detect amperometric peaks, but it has still to be optimized and tested in both the electroanalytical methods (i.e., potentiometry). According to these considerations, the sections 5.3 and 5.4 gave some tools and suggestions for improving the performances. The simulation results obtained on LTspice® and the application with a physiological solution highlighted the high-gain feedback resistor's influence on the noise contribution in

the trans-impedance circuit. In addition to these, two examples of active filtering stages were implemented and tested just on a physiological solution to suggest a way to improve the device's general performances further.
Regarding these observations, it was fundamental to see the impact of the noise amplitude, which is essential to distinguish well the noise background from the small extracellular peaks. At the same time, they underlined the importance of testing the whole circuit in a real experimental application, which is the only useful way to predict the authentic performances of the designed read-out device.
The last section of this work finally describes and sums up the main tools for the future perspectives of this device.

6.1 Tools for future perspectives

Two main steps have to be integrated into a future perspective of the read-out device. The first one concerns the optimization of the designed single-channel read-out device. The second one discusses extending the single-channel to all the available electrodes of the μG-SCD MEA.

Optimization of the single-channel read-out device

The system has to be further optimized. Thus, it is advised to:

- Consider the introduction of two-amplification stages in the preamplifier circuit. As suggested through the study on the section 5.3, it is advised to replace the 10^7 MΩ feedback resistor with a lower value ($\leq$ 100 kΩ). This can be implemented in the first amplification stage, with the LTC6268, thus the operational amplifier with the strict specifications. A second amplification stage should be added to reach the desired gain for reading the extracellular signals. In the latter case, an operational amplifier with less strict specifications could be implemented.

- Add an active filtering stage. The section 5.4 introduced two active filters that have to be adequately tested on extracellular measurements. If they are not enough for the application, it is suggested to implement filters with a higher-order (e.g., sixth orders active filters [34]). Moreover, it is advised to combine the second amplification stage with the active filtering one.

- Introduce other shielding measures (in addition to the guard ring) for connecting the working electrode input to the preamplifier. For instance, introducing Altium via stitching and shielding techniques to maintain a constant ground (low impedance and short return loops), distributing heat, and reduce capacitive coupling [54].

16-channels read-out device

The future perspective of this work aims to implement the single-channel read-out device to all the available electrodes of the given μG-SCD MEA. In this manner, it would be possible to verify the concrete application of the device to the study of dopaminergic neuronal cells. For this purpose, it is advised to:

- Reduce as much as possible the track between the working electrodes and the preamplification stages. For instance, it is common practice to implement spring connectors that directly attach to the conductive pads of the MEA chip. Consequently, the MEA can be inserted directly in the center of the printed circuit board, as shown in the figure 6.1.

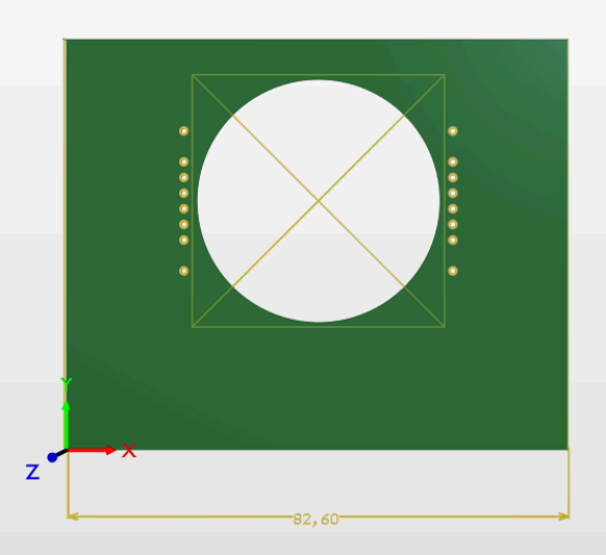

Figure 6.1: Future perspective of a printed circuit board realized through the software Altium Designer®. The green board implements on the center the original geometry of the μG-SCD MEA chip.

- Extend the single-channel read-out device to all the 16 electrodes. It is suggested to use a minimal number of components. Thus, if two-amplification stages are added to the system, the first should use the LTC6269 dual input operational amplifier. In contrast, the second one should implement operational amplifiers whose packages contain two or more inputs (e.g., better with four inputs).
- Set the electroanalytical measurement. It is important to be able from the LabVIEW interface to change on each electrode the electroanalytical

configuration in amperometry or potentiometry. Consequently, a single digital output containing each electrode configuration should be sent from the NI-DAQ to the preamplifier. At this point, a shift register should be implemented to read back out in parallel. Finally, the information should be sent to proper reed relays with multiple switches (minimizing the total number of components) to interchange the internal circuits from the amperometric to the potentiometric one.

- Set the stimulation mode measurement. It is advised to consider, at the last point, if it is more convenient to leave the stimulation from the external reference electrode (as done in this work) or implement it on each working electrode. Consequently, another switch should be implemented to connect the input electrodes to the stimulation signal in the latter case. As suggested in the section 3, it could be useful to implement a blanking circuit (digital or analog) to avoid the saturation of each channel or cross-talking effects between the near electrodes (in the case of the stimulation on each electrode).

- Add a D-Sub connector. It is recommended to use a single I/O connector with multiple parallel rows of pins and a metal cover for communicating with the NI DAQ, thus with the external communication system. The D-shaped metal shield can ensure good protection from EMI/RFI and provide good mechanical support. In this way, it is possible to fully protect the device inside the Faraday cage, allowing the passage of the cables outside and the complete isolation of the system.

Bibliography

[1] Jun Wang, Chengxiong Wu, Ning Hu, Jie Zhou, Liping Du, and Ping Wang. «Microfabricated electrochemical cell-based biosensors for analysis of living cells in vitro». In: *Biosensors* 2.2 (2012), pp. 127–170 (cit. on pp. 1, 9, 16–18).

[2] Jaime Punter Villagrasa, Jordi Colomer-Farrarons, and Pere Ll Miribel. «Bioelectronics for amperometric biosensors». In: *State of the Art in Biosensors Toonika Rinken [online]. IntechOpen* (2013), pp. 241–247 (cit. on pp. 1, 39, 40).

[3] Federico Picollo et al. «All-carbon multi-electrode array for real-time in vitro measurements of oxidizable neurotransmitters». In: *Scientific reports* 6.1 (2016), pp. 1–8 (cit. on pp. 2, 82, 91).

[4] Stephen Lower. *Chem1 virtual textbook*. 1999 (cit. on pp. 3, 5).

[5] Demar Larsen. «Reimaging the Future of Chemistry Textbooks with LibreTexts». In: (2020) (cit. on p. 4).

[6] Paul Flowers, Klaus Theopold, Richard Langley, William R Robinson, et al. «Chemistry: OpenStax». In: (2018) (cit. on p. 4).

[7] Daniel R Thevenot, Klara Toth, Richard A Durst, and George S Wilson. «Electrochemical biosensors: recommended definitions and classification». In: *Pure and applied chemistry* 71.12 (1999), pp. 2333–2348 (cit. on p. 5).

[8] EM Gross, RS Kelly, and DM Cannon. «Analytical Electrochemistry: Potentiometry». In: (2008) (cit. on p. 6).

[9] Junqiao Lee. «Electrochemical Sensing of Oxygen Gas in Ionic Liquids on Screen Printed Electrodes». PhD thesis. June 2014 (cit. on pp. 6, 7).

[10] Paul Worsfold, Alan Townshend, Colin F Poole, and Manuel Miró. *Encyclopedia of analytical science*. Elsevier, 2019 (cit. on p. 7).

[11] Juan Bernardo Cano, Katia Buonasera, and Gianni Pezzotti. «Transduction methods used on biosensors: amperometry and fluorescence». en. In: *Revista Facultad de IngenierÃa Universidad de Antioquia* (Sept. 2014), pp. 104–115. ISSN: 0120-6230. URL: `http://www.scielo.org.co/scielo.php?script=sci_arttext&pid=S0120-62302014000300009&nrm=iso` (cit. on p. 7).

[12] D Indruk. «Palmsens: Potentiostats for corrosion research». In: (2019) (cit. on pp. 7, 8).

[13] PM Biesheuvel, S Porada, and JE Dykstra. «The difference between Faradaic and non-Faradaic electrode processes». In: () (cit. on pp. 7, 8).

[14] Fritz Scholz. «Voltammetric techniques of analysis: the essentials». In: *ChemTexts* 1.4 (2015), p. 17 (cit. on p. 8).

[15] Genetic Engineering Biotechnology News. *CRISPR Screening IDs Factors for Turning Stem Cells into Neurons*. [Online; accessed October 2, 2020]. 2020. URL: https://www.genengnews.com/news/crispr-screening-ids-factors-for-turning-stem-cells-into-neurons (cit. on p. 9).

[16] Michael V Accardi, Michael K Pugsley, Roy Forster, Eric Troncy, Hai Huang, and Simon Authier. «The emerging role of in vitro electrophysiological methods in CNS safety pharmacology». In: *Journal of pharmacological and toxicological methods* 81 (2016), pp. 47–59 (cit. on p. 9).

[17] Pinterest. *Multi-Electrode Array (MEA): Neuronal Networks Electrophysiology*. [Online; accessed November 10, 2020]. 2020. URL: https://www.neuroservice.com/mea/ (cit. on p. 10).

[18] Mark W Barnett and Philip M Larkman. «The action potential». In: *Practical neurology* 7.3 (2007), pp. 192–197 (cit. on p. 11).

[19] Università degli Studi di Perugia. *Sinapsi centrali ed Integrazione sinaptica*. [Online; 2020]. 2019. URL: http://www.med.unipg.it/ccl/Materiale/20Didattico/Fisiologia%20(Grassi)/Sinapsi%20centrali%20ed%20Integrazione%20sinaptica.pdf (cit. on p. 11).

[20] Sarah X Luo and Eric J Huang. «Dopaminergic neurons and brain reward pathways: from neurogenesis to circuit assembly». In: *The American journal of pathology* 186.3 (2016), pp. 478–488 (cit. on p. 12).

[21] Tesi di Dottorato di Antonella Bacciu. «Sviluppo di un nuovo sistema microfluidico-amperometrico per lo studio della secrezione di dopamina in cellule PC12 utilizzando un microsensore nanostrutturato». In: () (cit. on p. 12).

[22] John H Byrne. «Introduction to neurons and neuronal networks». In: *Textbook for the Neurosciences* (2013) (cit. on p. 12).

[23] NMI Natural and Medical Sciences Institute at the University of Tübingen. *Microelectrode arrays for extracellular electrophysiology*. [Online]. URL: https://www.nmi-tt.de (cit. on pp. 13, 26, 32).

[24] Richard F Thompson. *Bioelectric recording techniques*. Vol. 1. Academic Press, 1973 (cit. on p. 14).

[25] Neuroservice. *Neuron model with neurotransmitters*. [Online; accessed December 2, 2020]. 2020. URL: https://i.pinimg.com/originals/33/04/98/3304986417dade7a2db66b87eeda29fc.jpg (cit. on p. 15).

[26] Ian L Jones, Paolo Livi, Marta K Lewandowska, Michele Fiscella, Branka Roscic, and Andreas Hierlemann. «The potential of microelectrode arrays and microelectronics for biomedical research and diagnostics». In: *Analytical and bioanalytical chemistry* 399.7 (2011), pp. 2313–2329 (cit. on p. 16).

[27] Giulia Meinero. *Attività elettrica spontanea di neuroni mesencefalici in coltura misurata tramite multielettrodi planari (MEA)*. Tesi di laurea. 2018/2019 (cit. on pp. 17, 22, 24).

[28] Jolien Pas. «Flexible neural probes with a fast bioresorbable shuttle: From in vitro to in vivo electrophysiological recordings». PhD thesis. Lyon, 2017 (cit. on p. 18).

[29] LGJ Tertoolen, SR Braam, BJ Van Meer, R Passier, and CL Mummery. «Interpretation of field potentials measured on a multi electrode array in pharmacological toxicity screening on primary and human pluripotent stem cell-derived cardiomyocytes». In: *Biochemical and biophysical research communications* 497.4 (2018), pp. 1135–1141 (cit. on p. 19).

[30] Adrian C Michael and Laura Borland. *Electrochemical methods for neuroscience*. CRC press, 2006 (cit. on p. 20).

[31] the free encyclopedia Wikipedia. *Microelectrode array*. [Online; 5-January-2021]. 2021. URL: https://en.wikipedia.org/wiki/Microelectrode_array#cite_note-21 (cit. on p. 20).

[32] Giulia Tomagra, Alfio Battiato, Ettore Bernardi, Alberto Pasquarelli, Emilio Carbone, Paolo Olivero, Valentina Carabelli, and Federico Picollo. «Diamond-based multi electrode arrays for monitoring neurotransmitter release». In: *Convegno Nazionale Sensori*. Springer. 2018, pp. 125–134 (cit. on pp. 21, 79).

[33] Federico Picollo, Alfio Battiato, Ettore Bernardi, Andrea Marcantoni, Alberto Pasquarelli, Emilio Carbone, Paolo Olivero, and Valentina Carabelli. «Microelectrode arrays of diamond-insulated graphitic channels for real-time detection of exocytotic events from cultured chromaffin cells and slices of adrenal glands». In: *Analytical chemistry* 88.15 (2016), pp. 7493–7499 (cit. on pp. 22, 37, 40).

[34] Giulia Tomagra, Claudio Franchino, Alberto Pasquarelli, Emilio Carbone, Paolo Olivero, Valentina Carabelli, and Federico Picollo. «Simultaneous multi-site detection of quantal release from PC12 cells using micro graphitic-diamond multi electrode arrays». In: *Biophysical chemistry* 253 (2019), p. 106241 (cit. on pp. 22, 78, 94, 99).

[35] Giulia Tomagra et al. «Quantal release of dopamine and action potential firing detected in midbrain neurons by multifunctional diamond-based microarrays». In: *Frontiers in neuroscience* 13 (2019), p. 288 (cit. on pp. 22, 23, 37, 38, 82).

[36] *MEA 1060-Inv-BC*. Multi Channel Systems MCS GmbH. 2019 (cit. on pp. 27, 29).

[37] *60SquareMEA200/50iR-Ti*. Multi Channel Systems MCS GmbH. 2019 (cit. on pp. 28, 29).

[38] Steve M Potter, Daniel A Wagenaar, and Thomas B DeMarse. «Closing the loop: stimulation feedback systems for embodied MEA cultures». In: *Advances in network electrophysiology*. Springer, 2006, pp. 215–242 (cit. on p. 32).

[39] Marco Crescentini, Marco Bennati, Marco Carminati, and Marco Tartagni. «Noise limits of CMOS current interfaces for biosensors: A review». In: *IEEE transactions on biomedical circuits and systems* 8.2 (2013), pp. 278–292 (cit. on pp. 41, 42, 52).

[40] Keithley Instruments. «Low Level Measurements Handbook». In: *Precision DC Current, Voltage and Resistance Measurements, 7th ed.; Keithley Instruments Inc.: Cleveland, OH, USA* (2013), p. 245 (cit. on p. 41).

[41] Giulia Regalia, Emilia Biffi, Giancarlo Ferrigno, and Alessandra Pedrocchi. «A low-noise, modular, and versatile analog front-end intended for processing in vitro neuronal signals detected by microelectrode arrays». In: *Computational intelligence and neuroscience* 2015 (2015) (cit. on pp. 42, 70, 91, 94).

[42] Wayne Storr. «Electronics-Tutorials. ws». In: *Inverting Operational Amplifier* (2012) (cit. on p. 43).

[43] Texas Instruments. «Inverting amplifier circuit». In: *Texas Instruments SBOS051B Oct* (2018) (cit. on p. 44).

[44] *500MHz Ultra-Low Bias Current FET Input Op Amp*. LTC6268/LTC6269. Linear Technology. 2014 (cit. on pp. 49, 50, 66, 67).

[45] Akshay Bhat. «Stabilize your transimpedance amplifier». In: (2012) (cit. on p. 50).

[46] Mohit Sharma, Avery Gardner, Hunter Strathman, David Warren, Jason Silver, and Ross Walker. «Acquisition of Neural Action Potentials Using Rapid Multiplexing Directly at the Electrodes». In: *Micromachines* 9 (Sept. 2018), p. 477. DOI: 10.3390/mi9100477 (cit. on pp. 50, 51).

[47] Yang Zhen. «Using MCP6491 Op Amps for Photodetection Applications». In: (2013) (cit. on p. 57).

[48] *Femtoampere Input Bias Current Electrometer Amplifier*. ADA4530-1. Analog Devices. 2017 (cit. on p. 67).

[49] Hernan Gonzalo Rey, Carlos Pedreira, and Rodrigo Quian Quiroga. «Past, present and future of spike sorting techniques». In: *Brain research bulletin* 119 (2015), pp. 106–117 (cit. on p. 70).

[50] Juan Martinez, Carlos Pedreira, Matias J Ison, and Rodrigo Quian Quiroga. «Realistic simulation of extracellular recordings». In: *Journal of neuroscience methods* 184.2 (2009), pp. 285–293 (cit. on pp. 70, 71).

[51] Analog Devices. *LTspice: Noise Simulations*. [Online; 15-January-2021]. 2021. URL: `https://www.analog.com/en/education/education-library/videos/5579265856001.html` (cit. on p. 86).

[52] Paul Horowitz and Winfield Hill. *The art of electronics*. Cambridge Univ. Press, 1989 (cit. on pp. 92, 94).

[53] Jim Karki. «Active low-pass filter design». In: *Texas Instruments application report* (2000) (cit. on p. 92).

[54] B. Curran, I. Ndip, S. Guttovski, and H. Reichl. «Managing Losses in Through Silicon Vias with Different Return Current Path Configurations». In: *2008 10th Electronics Packaging Technology Conference*. 2008, pp. 206–211. DOI: `10.1109/EPTC.2008.4763435` (cit. on p. 99).